

Fall 2007

Nanoparticle mediated oral delivery of insulin

Etienne Cabane

University of New Hampshire, Durham

Follow this and additional works at: <https://scholars.unh.edu/thesis>

Recommended Citation

Cabane, Etienne, "Nanoparticle mediated oral delivery of insulin" (2007). *Master's Theses and Capstones*. 291.
<https://scholars.unh.edu/thesis/291>

This Thesis is brought to you for free and open access by the Student Scholarship at University of New Hampshire Scholars' Repository. It has been accepted for inclusion in Master's Theses and Capstones by an authorized administrator of University of New Hampshire Scholars' Repository. For more information, please contact nicole.hentz@unh.edu.

NANOPARTICLE MEDIATED ORAL DELIVERY OF INSULIN

BY

ETIENNE CABANE

Engineering diploma, ESCPE Lyon (France), 2006

THESIS

Submitted to the University of New Hampshire

In Partial Fulfillment of

The Requirement for the Degree of

Master of Science

In

Materials Science

September, 2007

UMI Number: 1447878

INFORMATION TO USERS

The quality of this reproduction is dependent upon the quality of the copy submitted. Broken or indistinct print, colored or poor quality illustrations and photographs, print bleed-through, substandard margins, and improper alignment can adversely affect reproduction.

In the unlikely event that the author did not send a complete manuscript and there are missing pages, these will be noted. Also, if unauthorized copyright material had to be removed, a note will indicate the deletion.

UMI[®]

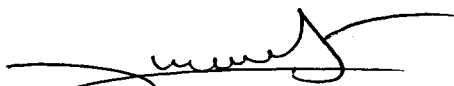
UMI Microform 1447878

Copyright 2007 by ProQuest Information and Learning Company.


All rights reserved. This microform edition is protected against unauthorized copying under Title 17, United States Code.

ProQuest Information and Learning Company
300 North Zeeb Road
P.O. Box 1346
Ann Arbor, MI 48106-1346

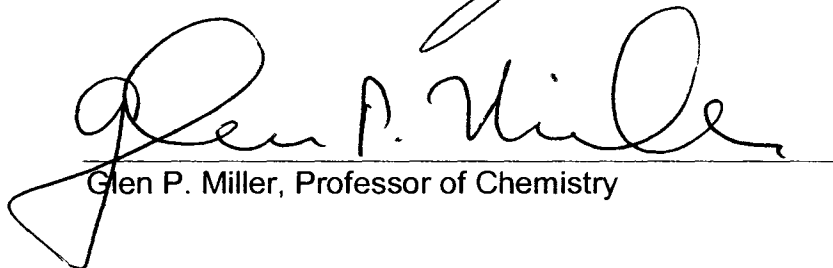
This thesis has been examined and approved.



Thesis Director, Yvon G. Durant, Associate research
professor of Materials Science



Donald C. Sundberg, Professor of Materials Science



Glen P. Miller, Professor of Chemistry

7.30.07

Date

ACKNOWLEDGEMENTS

First I would like to thank my advisors Yvon Durant and Jerome Claverie for their exceptional guidance, help and support during the time I spent at the NPRC on different research projects. I greatly appreciated their indefectible enthusiasm and they provided me with the most exciting and challenging opportunities, always improving the quality of my graduate experience. In their own very different ways, they taught me about everything I know about research.

Also I would like to especially thank Don Sundberg, for he has been one of the greatest teachers I had, from polymers to my first golf lesson.

I want to thank all the NPRC faculty members, Zac and John in particular, as well as my fellow graduate students Diane, Jon, Pooja, Brian, Ming, Sayantan, Mousoumi, Diana and the French contingent, Marine, Amelie, Anne, Romuald, Zakaria, Thomas, and Thibault. Their friendship and advice has made my work here enjoyable.

There are many others within the department that have been very helpful to me in many different ways. I will simply say a general thank you to all of them.

Finally I would like to thank Bentley Pharmaceuticals Inc. for funding this project and in particular Robert Gyurik and Zhengmao Li for their important collaboration to the project.

FORWARD

« Quand nous avons soif, il nous semble que nous pourrions boire tout un océan : c'est la foi. Et quand nous nous mettons à boire, nous buvons un verre ou deux : c'est la science. »

Anton Tchekhov

TABLE OF CONTENTS

ACKNOWLEDGEMENTS	iii
FORWORD	iv
TABLE OF CONTENTS	v
LIST OF TABLES.....	vii
LIST OF FIGURES	viii
ABSTRACT.....	xii
INTRODUCTION	1
I. REVIEW.....	5
1. 1. Challenges in Oral Delivery of Proteins and Peptides	5
1. 2. Existing Oral Delivery Methods for Proteins	9
1. 2. 1. Chemical modification of the protein	9
1. 2. 2. Complex with enzyme inhibitors.....	10
1. 2. 3. Permeation/adsorption enhancers	11
1. 2. 4. Multifunctional bioadhesive Polymers	12
1. 2. 5. Liposomes and Niosomes.....	12
1. 2. 6. Colon targeted delivery	13
1. 2. 7. Nanoparticles/polymersomes.....	14
1. 3. Insulin as a model.....	15
1. 4. State of the art in vesicles	17
II. SYNTHESIS.....	23
2. 1. Synthesis of B block and AB Diblock.....	23
2. 1. 1. Evolution of the work inherited from Collette's thesis.....	23
2. 1. 2. Common catalysts for ROP of Poly(lactic acid).....	24
2. 1. 3. Organic catalyst for the ROP of lactones	26
2. 1. 4. mPEG-PCL	41
2. 2. PGluOH synthesis	49
2. 2. 1. PGluBn synthesis.....	49
2. 2. 2. Deprotection.....	52
2. 3. Coupling	58

2. 4. Second synthetic pathway: macro amine as initiator of NCA opening.....	66
2. 4. 1. Activation of COOH from Fmoc-Lys(Fmoc)-OH.....	68
2. 4. 2. Coupling PLA-OH with activated Fmoc-Lys(Fmoc)-OH.....	68
2. 4. 3. Fmoc deprotection.....	69
2. 4. 4. NCA polymerization with PLA-NH ₂	72
III. SELF ASSEMBLY OF THE COPOLYMERS AND INSULIN LOADING.....	77
3. 1. Purification and storage.....	77
3. 1. 1. Formation of the vesicles.....	77
3. 1. 2. Purification.....	78
3. 1. 3. Storage.....	80
3. 2. Characterization of the self assemblies.....	84
3. 2. 1. Morphology and size characterization of crude vesicles.....	84
3. 2. 2. Evaluation of the loaded system.....	98
3. 3. Discussion.....	101
3. 3. 1. Understanding the self assembly.....	101
3. 3. 2. Protein solubilization.....	119
3. 3. 3. Some considerations on the behavior of the polymer in the GIT ...	132
CONCLUSIONS.....	136
LIST OF ABBREVIATIONS.....	140
EXPERIMENTAL SECTION.....	141
BIBLIOGRAPHY.....	145
APPENDICES.....	154
APPENDIX A: ADMINISTRATION ROUTES.....	155
APPENDIX B: BIODEGRADABLE POLYMERS.....	157
APPENDIX C: SYNTHESIS PATHWAY USING MACROAMINE.....	159
APPENDICE E: AFM IMAGING – TRIBLOCK AT PH 10.....	160
APPENDICE F: AFM IMAGING - TRIBLOCK AT PH 3.....	162

LIST OF TABLES

Table 1: Enzymes secreted in the GI tract and their function (adapted from reference [5])	8
Table 2: Listing of synthesized PEG-PLAs.....	37
Table 3: Listing of synthesized PLAs.	38
Table 4: Listing of PEG-PCL.....	46
Table 5: Calculation of deprotection.....	55
Table 6: List of diblock and triblocks synthesized.	60
Table 7: NCA polymerizations with macroamine initiator PEG-PLA(NH ₂) ₂	72
Table 8: Size of self assemblies.....	90
Table 9: Constants for the Helmotz free energy calculation.....	105
Table 10: Amounts of insulin associated with the vesicles: experiment vs. theory.	129
Table 11: Synthesis of PEG-PLA.....	141
Table 12: NCA polymerization.	142
Table 13: PGLuBn deprotection.	143
Table 14: Coupling reaction.	143
Table B15: Properties of common biodegradable polymers.....	157

LIST OF FIGURES

Figure 1: Self assembly of amphiphilic diblock PLA-PGluONa into vesicles.	2
Figure 2: Self assembly of triblock copolymer PEG-PLA-PGluONa into vesicles. 2	2
Figure 3: Digestive or gastrointestinal tract. ³	5
Figure 4: scheme of the small intestine wall. ⁴	6
Figure 5: Absorption pathways of drugs across intestinal epithelium.	7
Figure 6: Computer-generated image of insulin hexamers highlighting the threefold symmetry, the zinc ions holding it together, and the histidine residues involved in zinc binding. ¹⁸	16
Figure 7: an overview of supramolecular self assemblies of the block copolymer poly(isoprene-co-styrene). ¹⁹	17
Figure 8: a) Schematic of block copolymer morphologies. b) Schematic of membrane thickness scaling with MW. ²⁰	20
Figure 9: Lactides.	24
Figure 10: ROP of lactide using DMAP as a catalyst, adapted from [44].	27
Figure 11: ¹ H NMR spectrum of decanol initiated PLA in CDCl ₃	30
Figure 12: ¹ H NMR of the methine proton during lactide polymerization from 0 to 40 minutes (in CDCl ₃).	31
Figure 13: Conversion as a function of time for polymerization of lactide; (♦)bulk polymerization initiated by DMAP at 135°C; (■) solvent polymerization initiated by Zn(Et) ₂ at 60°C (data from F. Collette's thesis, ref. 41).	32
Figure 14: Kinetics of bulk PLA polymerization: first and second order approximations.	34
Figure 15: GPC of bulk PLA polymerization with DMAP.	35
Figure 16: Polydispersity index and number average molecular weight as a function of conversion. Bulk polymerization of lactide using DMAP and Decanol as initiator.	36
Figure 17: DSC spectrum of a PLA block.	38
Figure 18: ¹ H NMR of mPEG-PLA in CDCl ₃	40
Figure 19: DSC spectrum of polycaprolactone.	41
Figure 20: ε-caprolactone.	42
Figure 21. ROP of ε-caprolactone with tin ethyl hexanoate: A) formation of stannous alkoxide initiator, B) coordination/insertion of monomer, C) chain extension. ⁵²	44
Figure 22: Aluminum isopropoxide and triethyl aluminum.	45
Figure 23: ROP of ε-caprolactone using an aluminum alkoxide. ⁵³	45
Figure 24: GPC traces of PEG 2000 and PEG-PCL copolymer.	47
Figure 25: ¹ H NMR of PEG-PCL in CDCl ₃	48
Figure 26: N-CarboxyAnhydride (NCA).	49
Figure 27: Ring Opening Polymerization initiated by primary amines.	50
Figure 28: Termination by formation of pyroglutamic groups.	51
Figure 29: Benzyl deprotection mechanism using Methane Sulfonic Acid. ⁵⁸	52
Figure 30: 1H NMR spectrum in of PGluBn in d-TFA.	53

Figure 31: Kinetics of deprotection of PGluBn followed by 1H NMR.....	54
Figure 32: HPLC-MALS kinetic study on PGluBn deprotection.....	56
Figure 33: HPLC-MALS plot of a PGluOH deprotected for 45 minutes.....	57
Figure 34: Coupling agents.....	58
Figure 35: CDI coupling: reaction of N, N'-carbodiimidazole with carboxylic acid to form imidazolid followed by transacylation reaction of imidazolid to form esters. ⁶⁰	59
Figure 36: ¹ H NMR spectrum of PEG-PLA-PGlu in d-TFA.....	61
Figure 37: Synthesis of amides using imidazolid. ⁶¹	62
Figure 38: Formation of anhydrides of carboxylic acids.....	62
Figure 39: Stabilization of imidazole with trifluoroacetic acid,	63
Figure 40: Possible structures of PGluOH resulting from side reactions. A: coupling of a backbone tertiary amine with a COOH; B: back-biting coupling of a terminal NH ₂ with a COOH; C: Intermolecular coupling between terminal amine and COOH; D: intermolecular anhydride formation between two COOH.	63
Figure 41: Example of structures displaying 2 PLA chains (in blue) for one PGluOH chain.....	64
Figure 42: linear and branched structures of the copolymer using CDI coupling according to site of coupling.	65
Figure 43: NCA polymerization with macroamine.....	67
Figure 44: Coupling of poly(lactic acid) with Fmoc-Lys(Fmoc)-OH using CDI as coupling agent.	69
Figure 45: Scheme for Fmoc cleavage.....	70
Figure 46: 1, 8-Diazabicyclo[5. 4. 0]undec-7ene.....	71
Figure 47: GPC traces of PEG-PLA-(NH ₂) ₂ macroamine initiator (EC177) and PEG-PLA-PGluBn copolymers.	73
Figure 48: d-TFA ¹ H NMR of PEG-PLA-PGluBn initiated by PEG-PLA(NH ₂) ₂ macroamine.....	74
Figure 49: Initiation of NCA polymerization with tertiary amine. ⁶⁴	75
Figure 50: Ultrafiltration of the vesicles.....	79
Figure 51: Stability of polymer redispersed in water after liophilization.....	81
Figure 52: Freeze-thaw study on EC160, PLA ₁₃₇ PGlu ₇₂	82
Figure 53: Diameter of vesicles from the self assembly of PLA-PGlu diblock in water.....	85
Figure 54: Diameter of diblock and triblock self assembly as a function of pH....	86
Figure 55: Influence of ionic strength on triblock vesicles diameter at constant pH (7.4).	87
Figure 56: diameter of vesicles as a function of temperature.....	88
Figure 57: Evolution of vesicles diameter with increasing solvent concentration.	89
Figure 58: AFM 3D imaging of PEG-PLA-PGlu self-assembled vesicles at pH 10.	91
Figure 59: Field-flow fractionation channel showing laminar flow profile and field perpendicular to flow. ⁶⁷	93

Figure 60: Root Mean Square radius (RMS radius) as a function of the molar mass.	94
Figure 61: Thickness of membrane as a function of vesicle mass (number of chains).	95
Figure 62: SEM picture of triblock copolymer PEG ₄₅ PLA ₁₁₂ PGLuOH ₁₀₀	96
Figure 63: Cryo-TEM picture of nanoobjects formed by self-assembly of linear PEG ₄₅ PLA ₄₇ PGLu ₁₀₀	97
Figure 64: Chromatogram of insulin.	98
Figure 65: Separation of free insulin from loaded vesicles.	99
Figure 66: Typical data for the evaluation of encapsulation efficiency.	100
Figure 67: Bending of a flat bilayer into a spherical shape.	101
Figure 68: The Helmholtz surface free energy for bending a flat bilayer into a spherical membrane.	105
Figure 69: Favored critical radius as a function of membrane thickness.	106
Figure 70: Preferred radius R_c as a function of the interfacial tension between water and the hydrophobic block. k_c and R_0 from Table 9, $d = 10\text{nm}$	107
Figure 71: Influence of the bending modulus on the preferred size of vesicles. R_0 and γ from Table 9, $d = 10\text{nm}$	108
Figure 72: Preferred vesicle's size as a function of spontaneous curvature, γ and k_c from Table 9, and $d = 10\text{nm}$	108
Figure 73: Well defined versus interdigitated organization. a) a phosphatidylcholine lipid; b) a diblock copolymer of poly(acrylic acid– polystyrene) (PAA-PS); c) PS–poly(isocyno-L-alanine-L-alanine); and d) poly(ethyleneoxide-polybutadiene) (PEO-PBD). ²¹	111
Figure 74: two possible configurations of triblock membranes.	112
Figure 75: DSC trace of PEG-PLA-PGLu in water.	113
Figure 76: Self assembly of diblock and triblock copolymers, curvature is influenced by space filling.	115
Figure 77: Representation of the helix to extended equilibrium structures of PGLu under acid or base titration. ⁷⁶	116
Figure 78: Hydrogen bonds between COOH at acidic pH. Formation of aggregates, and colloidal instability.	117
Figure 79: Electrostatic repulsion between vesicles in basic water.	118
Figure 80: Insulin loading in vesicles.	120
Figure 81: A schematic of bilayer perturbation by nonincorporated transmembrane proteins. ⁷⁹	121
Figure 82: Insulin loading of triblock vesicles for different polymer concentration and insulin concentration.	122
Figure 83: Insulin loading of triblock PEG ₄₅ PLA ₁₁₂ PGLu ₉₅ at pH 9.	123
Figure 84: Diblock PLA ₁₃₇ PGLu ₇₂ copolymer at different concentration loaded with insulin (pH 9).	124
Figure 85: Insulin loading, triblock vs. diblock and pH study.	125
Figure 86: Theoretical encapsulation of insulin as a function of: a) vesicle diameter and membrane thickness (calculations made for [polym] = 1%), and b) vesicle diameter and polymer concentration (calculations made with a 15 nm membrane thickness).	127

Figure 87: Schematic of triblock and diblock vesicles showing scaled membrane thickness and diameters.	131
Figure 88: Evolution of Ca^{2+} concentration upon addition of triblock copolymer.	133
Figure 89: Structure of Heparin. ⁸¹	134
Figure 90: molecular model of the unbound carboxypeptidase A enzyme. ⁸²	134
Figure 91: Number of publications on controlled drug delivery published since 1970. ⁸⁶	155

ABSTRACT

NANOPARTICLE MEDIATED ORAL DELIVERY OF INSULIN

by

Etienne Cabane

University of New Hampshire, September, 2007

The oral delivery of therapeutic compounds, from small molecules to proteins is one of the most desirable routes of administration. Its advantages reside in low cost, patient compliance and ease of use. The major challenge associated to such a delivery route is the transport through the gastrointestinal tract (GIT). In the case of complex and fragile molecules such as proteins, this particular step is the source of multiple challenges. Among the approaches developed to protect the therapeutic compound, the use of polymeric carriers is the most promising. We developed biocompatible and biodegradable polymersomes formed by the self assembly of amphiphilic copolymers in water. The copolymers we used are a combination of the following homopolymers: poly(ethylene glycol), poly(lactic acid), poly(caprolactone) and poly(glutamic acid). The PEG-PLA or PLA blocks were prepared by ring opening bulk polymerization (ROP) using an organic catalyst, and an alcohol as initiator. The poly(glutamic acid) was prepared aside by ROP of the benzyl glutamate N-CarboxyAnhydride (NCA), followed by the deprotection of the benzyl group. The final copolymer was obtained by coupling a PEG-PLA (or PLA) to a PGLuOH. Another synthesis route was explored. It consists in the preparation of a macro

amine, namely PEG-PLA-(NH₂)_x, used to ring open the benzyl glutamate NCA. The PEG-PLA-PGluBn is then deprotected. The polymer chains obtained by one of these two synthesis routes self assemble in basic water into well defined vesicles with diameter ranging from 70 to 160 nm. They can be loaded with insulin and orally delivered. The vesicles are progressively degraded along the GIT before transport through intestine wall and insulin is released. A full characterization of the polymers and a study of the morphology of self assemblies constitute the bulk of this work.

INTRODUCTION

The objective of our study is to design a polymeric carrier capable of protecting a protein such as insulin from the action of enzymes in the gastrointestinal tract, therefore facilitating its oral delivery in the human body. We focused our work on the synthesis of amphiphilic block copolymers with the ability to self-assemble in aqueous media, encapsulating or adsorbing the protein, and releasing it in the blood stream after crossing the GIT.

We investigated several architectures and compositions of amphiphilic block copolymers and studied their potential to form vesicles, and potentially micelles, in water. The hydrophobic block (B) of the polymer is constituted by a polyester (PLA or PCL), the hydrophilic blocks being poly(ethylene glycol) (or PEG) (A) in the case of the triblock and poly(glutamic acid) or $\text{PGluO}^-\text{Na}^+$ (C). The copolymers we are proposing to use, PLA-PGlu, PEG-PLA-PGlu and PEG-PCL-PGlu are entirely biocompatible and biodegradable.

Figures 1 and 2 provide a simplistic view of the self assemblies with respect to the copolymer used. The BC diblocks in water behave like lipids and form the bilayer membrane of the vesicles.

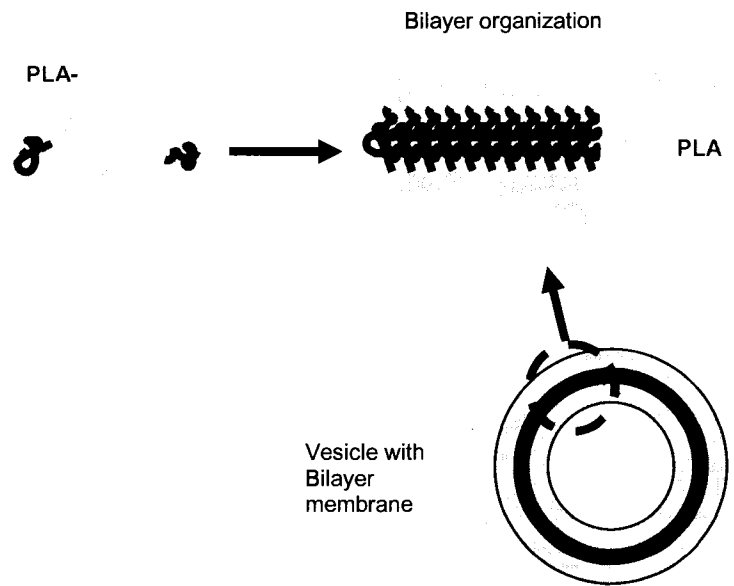


Figure 1: Self assembly of amphiphilic diblock PLA-PGluONa into vesicles.

The asymmetric ABC triblock is assembling into a monolayer membrane due to its two hydrophilic blocks.

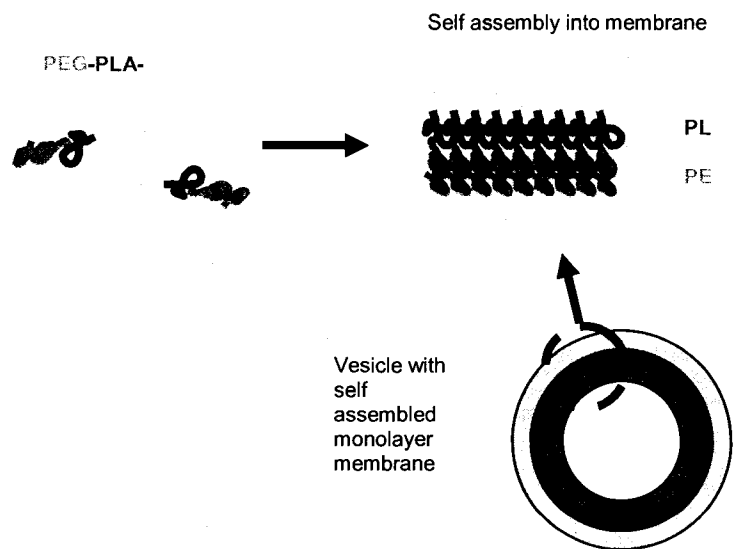


Figure 2: Self assembly of triblock copolymer PEG-PLA-PGluONa into vesicles.

Aside from being amphiphilic, allowing self assembly in water, the blocks have particular properties involved in different steps of the delivery process.

The polymer carriers obtained are loaded with insulin. The protein is associated with the vesicles in three different ways. Initially designed to encapsulate insulin in their inside volume, we believe that the vesicles are actually multifunctional. Most likely the major part is loaded by the association of the protein to the external charged PGLu layer. A second load corresponds to the fraction of insulin actually encapsulated, and the third load is due to entrapment of insulin in the membrane itself.

According to the hypothesis of three different loadings, the release of insulin in the GI tract is most probably the result of several mechanisms: dissociation of adsorbed insulin from the PGLu layer, release of the insulin trapped in membrane, and release of insulin encapsulated. This delivery is only possible upon degradation of the polymer carriers.

We believe that our system is not degrading immediately in the stomach, but slowly in the small intestine. The poly(amino acid) block gets digested by enzymes. The PGLu collapse is revealing the hydrophobic B block and therefore the vesicles eventually precipitate and are adsorbed by the hydrophobic environment of the intestine mucus. Transport through intestine membrane by endocytotic uptake follows: vesicles are invaginated in epithelial cells, where the PLA is hydrolyzed in acidic environment. Finally, insulin is released in the bloodstream.

In Chapter I, we debate the principal challenges encountered in the oral delivery of vulnerable compounds such as therapeutic proteins. The chapter is also dedicated to the overview of existing polymersomes systems for the oral delivery of proteins. In the second chapter we report the detailed synthesis and characterization of the various polymers involved in the formation of self assemblies. The third chapter is devoted to the self-assembly of the copolymers and their organization into different morphologies, and the insulin loading of the nanoobjects. The last section is dedicated to experimental work, where we report synthesis recipes and polymer formulation with insulin.

CHAPTER I

REVIEW

1. 1. Challenges in Oral Delivery of Proteins and Peptides

It is generally admitted that the difficulty for the oral administration of biomacromolecules is due to their high molecular weight, their hydrophilicity, and their susceptibility to enzymatic inactivation, the latest being the major issue.^{1, 2} The GI tract primary function is to digest and adsorb nutrients and exclude unwanted materials such as toxins.

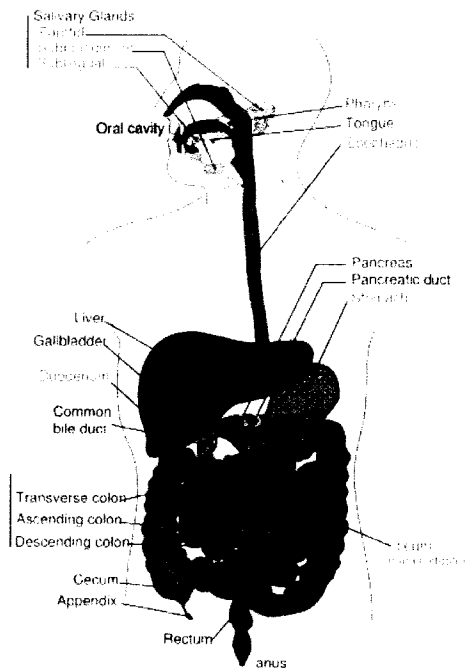


Figure 3: Digestive or gastrointestinal tract.³

In that respect, various challenges associated with oral drug delivery are directly related to the degradation of the protein/drug during transport through GIT and pathway to bloodstream.

Digested nutrients (nutritive proteins for instance) reach the surface of the intestine, the epithelium. This mucosa is constituted of epithelial cells, the membranes of which are covered by microvilli.

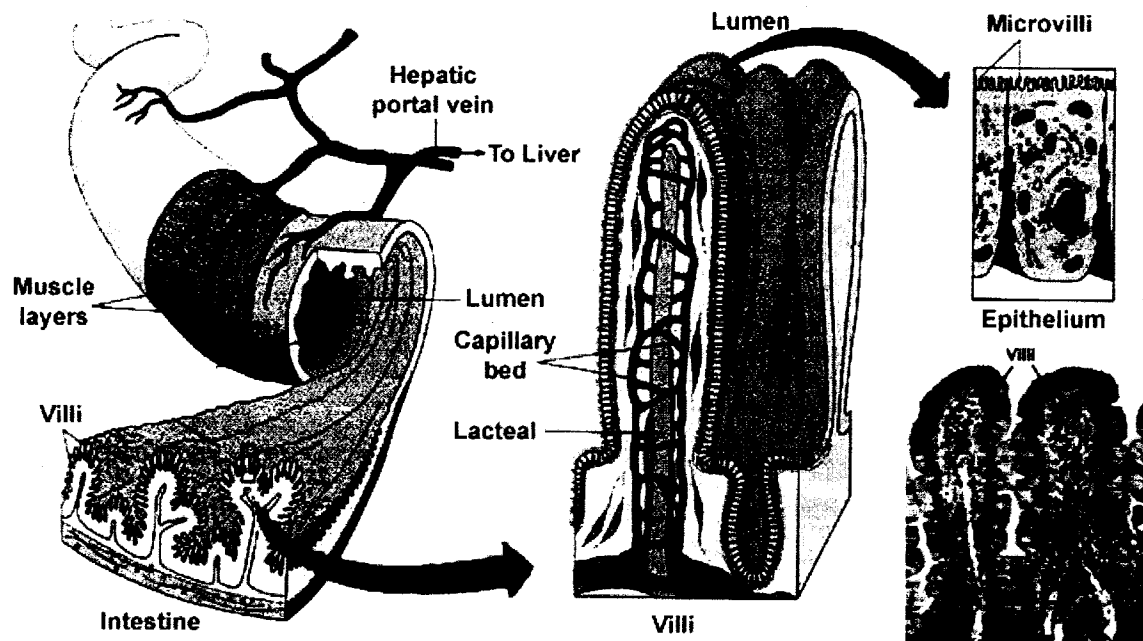


Figure 4: scheme of the small intestine wall.⁴

Once a nutrient reaches this hydrophobic area, it is transported through the epithelium by one of the following mechanism:

- Paracellular transport
- Transcellular transport
- Endocytotic uptake

A simplistic representation of these phenomena is given in Figure 5:

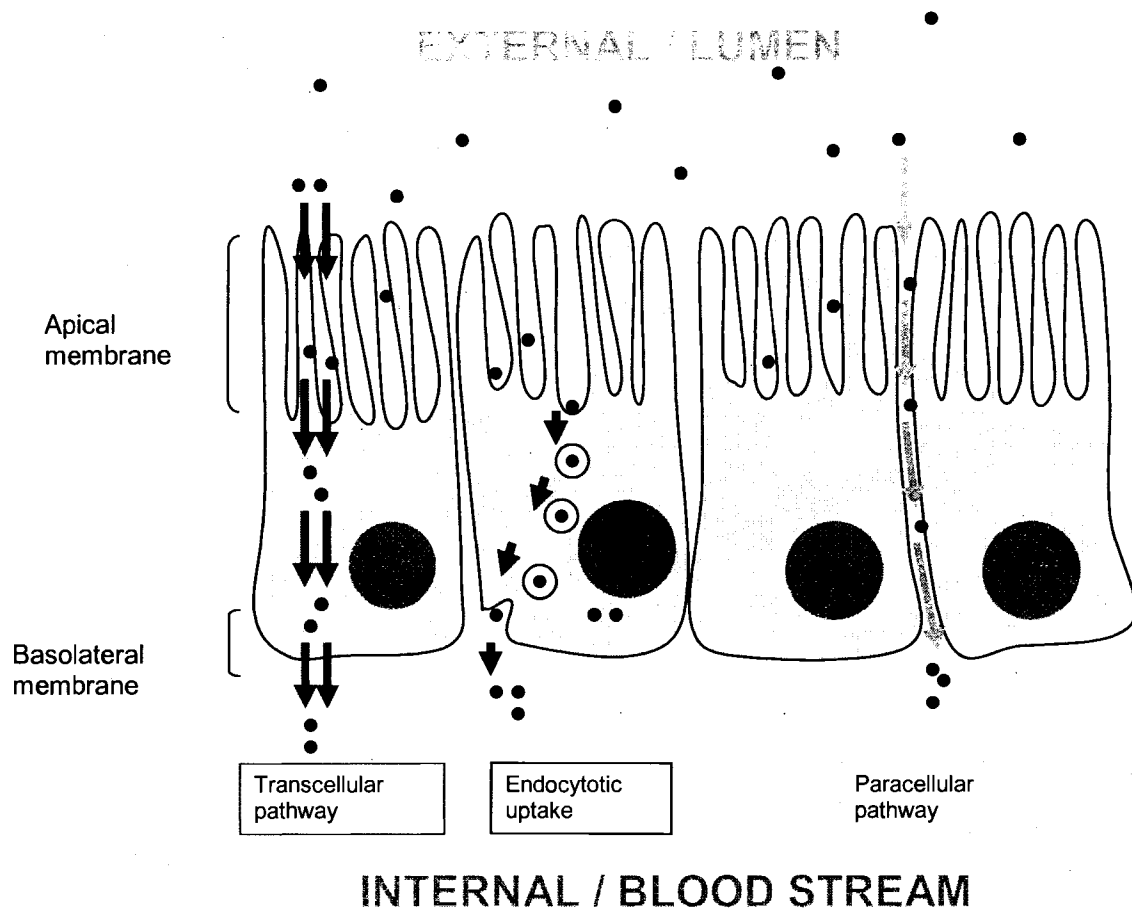


Figure 5: Absorption pathways of drugs across intestinal epithelium.

In addition to the diffusion and adsorption barrier (physical barriers) of the epithelial cells composing the surface of the small intestine, and the degradation in acidic pH of the stomach (physicochemical barrier), the enzymatic barrier is considered to be the major factor affecting the bioavailability of proteins after oral delivery. This barrier involves the degradation of peptide bonds by peptidases or proteases, as well as chemical modifications. Enzymes are found in almost every tissue in the human body. The GI tract produces a large amount of enzymes which are specific to different regions.

Table 1: Enzymes secreted in the GI tract and their function (adapted from reference [5])

Enzyme	Location	Function
Aspartic proteases (pepsin)	Stomach	Responsible for fragmentation of large proteins into smaller polypeptides
Pancreatic proteases (chymotrypsin, trypsin, elastase, carboxypeptidase A)	Small intestine	Catalyse degradation of polypeptides at specific amino residues
Proteases (aminopeptidase A and N, diaminopeptidase I, endopeptidase 24.11)	Brush border and cytosol of the enterocytes	Brush border proteases are mainly involved in hydrolysis of tri- and tetrapeptides. Cytosolic proteases preferentially digest dipeptides.

If degradation in the intestinal lumen cannot be suppressed, the problem can be minimized to some extent by protection against enzymes. Several attempts to overcome this barrier include the design of enzyme inhibitors, chemical modifications of the therapeutic macromolecules, use of absorption/permeation enhancers, mucoadhesive polymers, polymersomes, and drug delivery systems targeting colon where enzymatic activity is lower.¹ A quick discussion of the pros and cons of these techniques is provided in the next paragraph.

1. 2. Existing Oral Delivery Methods for Proteins

1. 2. 1. Chemical modification of the protein

Chemical modifications can be made in order to inhibit enzyme attack on proteins. These modifications include two approaches: prodrugs and permanent modifications.⁵

In the first technique, the prodrug is a molecule converting to the active protein/drug after in situ activation. Typically a “promoiety” is attached to the active molecule with a loose linkage, easily cleaved in the body. This promoiety can enhance protection against enzymes or transfer through membranes for instance.

The second technique involves the covalent (i. e. permanent) attachment of a molecule on the protein. A wide range of molecules can be covalently attached, from small molecules (glycosilation as an example) to polymers (pegylation for instance). The added molecule can have several actions:

- Increasing stability of the protein,
- blocking access to degradation sites,
- enhancing transport,
- targeting for selective cells.

Glycosilation consists in the addition of carbohydrates in order to increase protein stability.² For instance, glycosilated recombinant human granulocyte-macrophage colony-stimulating factor (GM-CSF) shows an increased half-life time in plasma compared to GM-CSF.⁶

Lipidization is another chemical modification that can increase the lipophilicity (i. e. hydrophobicity) of a given protein, helping both stability and transport through cellular membranes. For instance, caproic acid modified insulin was found to be more hydrophobic, and its uptake by gut mucus was increased.⁷

The most used polymer for chemical modification of proteins is poly(ethylene glycol) (PEG), by a process called pegylation. Several other polymers and oligomers are used, such as poly(sialic acid) and poly(hydroxyalkyl acrylate)s.² Polymers are found to mask parts of the proteins they are conjugated to and their hydrophilic nature is helping “hiding” the proteins from enzymatic attacks.

In all cases, the main concern with chemical modification of proteins is to keep biological activity of the therapeutic molecule. Also, the obtained conjugate is a new compound, and its properties in terms of toxicity for instance, need to be screened through the long preclinical studies used for pharmaceuticals.

1. 2. 2. Complex with enzyme inhibitors

Researchers have been investigating the use of protease inhibitors with the aim to slow the degradation rate of a given protein in the GI tract, enhancing its bioavailability. In the case of insulin, trypsin and α -chymotrypsin being the most important intestinal enzymes, the use of inhibitors such as aprotinin, pancreatic inhibitor or soybean trypsin inhibitor were found to affect the intestinal adsorption and degradation of insulin.^{1, 5, 8} However, there are major drawbacks associated with this method. The activity of the inhibitors generally lasts much

longer than the desired effect, and leads to several side effects, including systemic intoxications and disturbance in nutritive proteins digestion.^{1, 8}

Efforts are being done in this area, in order to have the inhibitor activity coinciding more accurately with the release of the protein.

1. 2. 3. Permeation/adsorption enhancers

The idea behind permeation and adsorption enhancers is to improve transcellular and paracellular transport of proteins through the intestine wall. Transcellular transport is improved by fluidization of the cell's lipid membrane, and paracellular transport is increased by the loosening of the tight junctions between epithelial cells.

Paracellular permeation enhancers include chelators of Ca^{2+} . The depletion in Ca^{2+} disrupts cell organization and helps loosening the tight junctions. Interestingly enough, several mucoadhesive polymers (such as polyanions) were found to chelate Ca^{2+} and therefore can be used as absorption promoters.^{1, 5}

Transcellular permeation enhancers are usually surfactants, lipids and bile salts. They help solubilizing phospholipids, compromising the integrity of cell membranes.⁸

These permeation enhancers are limited in use, since they are modifying the membrane functionality, allowing all sorts of macromolecules, i. e. also the toxic ones, to be absorbed.¹

1. 2. 4. Multifunctional bioadhesive Polymers

Bioadhesive polymers were initially designed to promote absorption of proteins by a prolonged contact between protein formulation and mucosa. Several polymers have been tested in the last few years, such as polyacrylates, polycarbophil (polyacrylic acid crosslinked with divinyl glycol),^{9, 10} chitosan based polymers,¹¹ as well as heparin based polymers.¹² These systems were proven efficient in increasing pharmacological efficacy, and they showed another promising capability in shielding enzymatic attacks. This latter functionality was further explored and a significant correlation between protease inhibition and polyanions was demonstrated. The most accepted explanation is the binding of metal cations by the polyanion, which deactivates metalloproteases present in the lumen, such as carboxypeptidase A.

Pharmaceutical companies are working on these promising multifunctional polymers, which are generally used in the form of gastrointestinal patches.⁶

1. 2. 5. Liposomes and Niosomes

In the last decades, liposomes were proven useful as drug carriers for peptides and proteins. They can encapsulate both hydrophobic and hydrophilic molecules, they are entirely biocompatible and provide good protection against enzymatic attacks along with poor immune recognition.

Liposomes are made of concentric lipid bilayers. The most studied phospholipid used in liposomes is phosphatidylcholine (or lecithin). Cholesterol and phosphatidylethanolamine are used with lecithin in order to tune the fluidity

of the bilayer.⁵ The major drawbacks of liposomes are their poor chemical and physical stability and rapid clearance from the blood.

Currently, research focuses on coated liposomes. The idea is to improve the bioavailability of the drug by prolonging its contact with the mucosal surface of small intestine. This is achieved by coating the liposomes with a mucoadhesive polymer, such as chitosan.^{5, 13} Therapeutic efficiency was demonstrated by Wu *et al.* using insulin delivered to mice.¹⁴

Similarly, niosomes or nonionic surfactant vesicles can be used as drug carriers. Niosomes are vesicles resulting from the self assembly of nonionic surfactant molecules, such as polyglyceryl alkyl ethers or fatty acid esters. Varshosaz *et al.* reported their good stability and protection from enzymatic attacks when encapsulating insulin.¹⁵

1. 2. 6. Colon targeted delivery

Colon targeted delivery has gained interest recently, due to the less hostile environment than stomach and small intestine. The enzymes are less numerous and less active in this region, and the retention time is higher. Technologies used to target colon involve pH dependent polymers and biodegradable swellable polymers. Common issues encountered with colon targeted delivery include protection during transport in the upper GI tract and poor solubility in the colon, where less fluid is available.¹³

1. 2. 7. Nanoparticles/polymersomes

Nanoparticles/polymersomes are polymeric particles with size ranging from 100 to 1000 nm. They are widely used for the delivery of therapeutic proteins because they have a low toxicity, they can protect proteins from enzymatic attacks and they are adsorbed by endocytotic pathway. The active protein can be encapsulated, dissolved, entrapped or adsorbed in the system. The polymer can be natural or synthetic, biodegradable or inert, hydrophobic or hydrophilic.

It is well accepted that nanoparticles having a small size (100 nm) show significantly higher uptake due to the limits imposed by endocytosis.¹ Literature also shows evidence that the efficiency of these systems is strongly dependent on the total charge of the objects, as well as the hydrophilicity.

A more detailed bibliography on polymersomes is given in paragraph 1. 4.

1. 3. Insulin as a model

In our study, we used insulin as a model of therapeutic proteins. The need for an oral formulation of insulin is evident, since diabetes is affecting more than 180 millions of patients all over the world. According to the World Health Organization, this number is expected to double in the next 25 years.¹⁶

Though we use insulin as model, we think that if our polymersomes are proven efficient with insulin, they will have the potential to carry other therapeutic proteins and peptides.

Insulin has some advantages over other proteins. It is relatively cheap and is very well documented. If causes of diabetes are not fully understood yet, the production and the enzymatic degradation of insulin are known.

Like other proteins, insulin is degraded by enzymes upon digestion. The first protease encountered in the GI tract is pepsin, a zymogene activated in the stomach. Pepsin degrades large polypeptides such as proteins into smaller units, preferentially cleaving hydrophobic and aromatic residues, such as Phe and Tyr. As an example, the bonds in the B chain of insulin are cleaved as follows:¹⁷

Phe¹↓Val, Gln⁴↓His, Glu¹³↓Ala, Ala¹⁴↓Leu, Leu¹⁵↓Tyr, Tyr¹⁶↓Leu, Gly²³↓Phe, Phe²⁴↓Phe and Phe²⁵↓Tyr.



Figure 6: Computer-generated image of insulin hexamers highlighting the threefold symmetry, the zinc ions holding it together, and the histidine residues involved in zinc binding.¹⁸

Peptides that went through the stomach are eventually degraded by other peptidases. For instance, two enzymes that degrade insulin in the small intestine lumen are pancreatic enzymes, trypsin and α -chymotrypsin.⁸ Insulin is not subject to enzymatic degradation by brush-border enzymes.

1. 4. State of the art in vesicles

Amphiphilic species are composed of at least two parts. One or more hydrophilic part, and a hydrophobic part. In a selective solvent, such as water, the hydrophobic parts tend to associate together in order to minimize interaction with water molecules, when the hydrophilic parts tend to expand and be hydrated. It is well known that block copolymers can be designed to show amphiphilic properties. According to the nature of the blocks and the conditions (temperature, ionic strength, etc...), amphiphilic block copolymers can lead to several morphologies, such as lamellar structure (LAM), micelles, bicontinuous structures, nanotubes or vesicles.

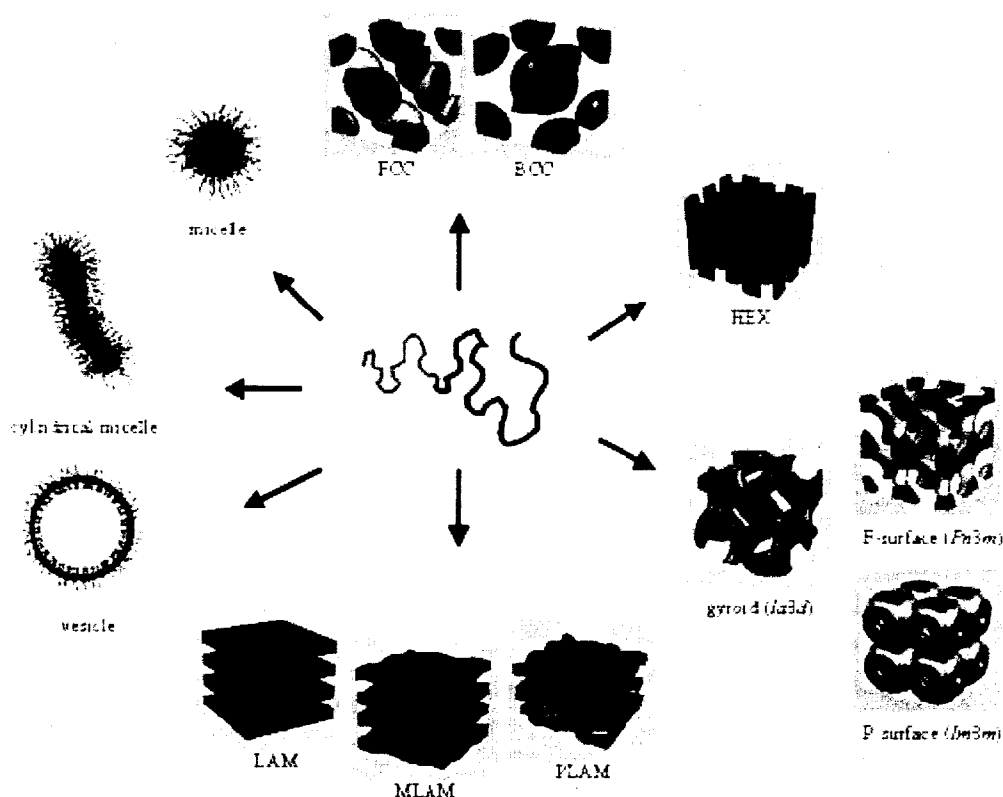


Figure 7: an overview of supramolecular self assemblies of the block copolymer poly(isoprene-co-styrene).¹⁹

Polymersomes are vesicles made from amphiphilic copolymers. Polymer chains can self assemble into spherical shells similar to liposomes. Due to much larger molecular weights, polymersomes have thicker membranes and different in vivo behaviors.²⁰

A wide range of synthetic and semi-synthetic copolymers is available, as well as a multitude of MW combinations. These are important choices to make and impart tunable properties to these carriers system.

Copolymers used to form polymersomes are very similar to lipids since they are amphiphiles. The hydrophilic blocks are delimiting two interfaces, the inner and outer faces of a bilayer membrane.

According to the literature there are three major parameters that can influence different characteristics of a self assembly, namely stability, morphology and size:

- the interaction energy ϵ between monomers and the bulk solution is related to stability
- the ratio (in mass) of the hydrophilic block over the total mass of the polymer chain called f , dictates morphology
- the total molecular weight of the chain MW scales with the membrane thickness of the assembly

In a review on polymersomes, Disher *et al.*^{20, 21} state that, in order to obtain vesicles, f should be around 35%. Under 25%, the chains are expected to form inverted structures, and molecules with $f > 45%$ are expected to yield

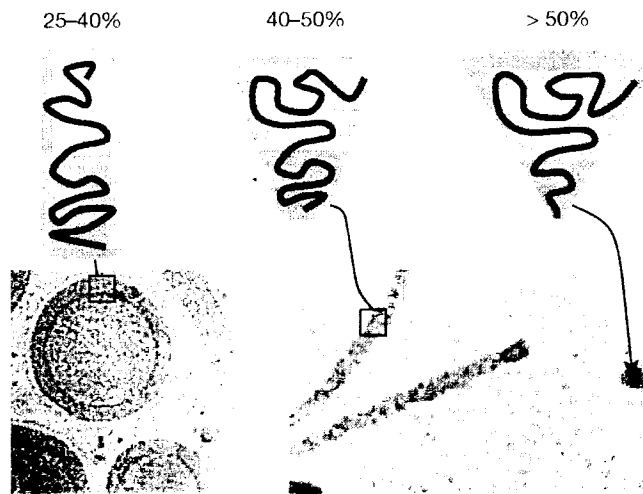
micelles (Figure 8a). In this hypothesis the arrangement of polymer chains is driven by the curvature imposed by the size of the hydrophilic block.

More generally, the curvature of the vesicles is a result of the segregation of the hydrophilic polymer in aqueous environment. Eisenberg *et al.*²² proposed that vesicles are stabilized due to intrinsic polydispersity of the copolymer chains: long chains segregate on the outside while small chains are oriented toward the inside.

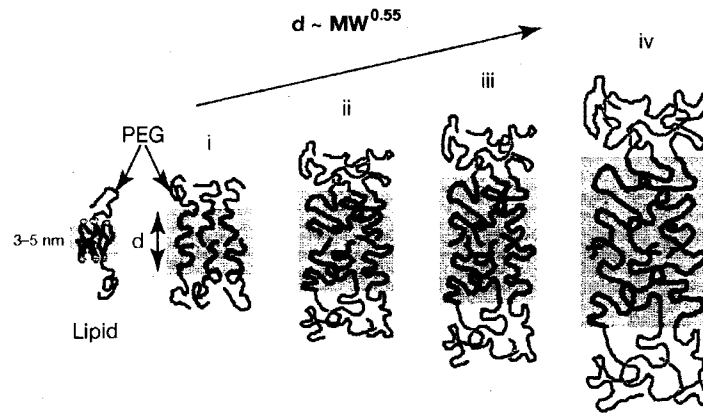
In our case, added to the polydispersity effect, another constraint might influence the morphology of the assembly. The external hydrophilic block is a polyanion with a potential “branched” structure. It is more likely to require a lot of space to arrange on the outside. When considering the assembly of ABC triblocks, there are no general rules on the object formed by self assembly.

The molecular weight of the chains dictates the thickness of the membrane. When liposomes have membrane thickness around 3-5 nm, polymersomes have membrane ranging from 8 to 20 nm, according to the size of the blocks (Figure 8b).

a f dictates aggregate morphology



b MW dictates aggregate dimension



AR Discher DE, Ahmed F. 2006.
Annu. Rev. Biomed. Eng. 8:323-41

Figure 8: a) Schematic of block copolymer morphologies. b) Schematic of membrane thickness scaling with MW.²⁰

The third parameter concerns the stability of the aggregates in aqueous media. Stability of vesicle can be measured by critical micelle concentration (CMC). The CMC is given by the following equation:

$$C_{CMC} \sim \exp(-n\varepsilon_h / k_B T) \quad (1)$$

where $k_B T$ is the thermal energy, n is the number of repeat units and ϵ_h is the monomer's effective interaction energy. Aggregates such as vesicles are only formed when concentration is above the CMC. Using this equation, amphiphiles concentration should range from micromolar to picomolar (i. e. stability is obtained at high dilution).

Several groups have reported the fabrication of polymersomes using many polymer systems. Vesicles have been prepared from amphiphilic diblocks, such as PS-PEO and PS-PAA studied by Eisenberg and coworkers,²³ PEO-PEE and PEO-PBD by Discher *et al.*²⁴ There are numerous reports of polymersomes based on PEO, including PEO-PLA (or PEG-PLA),^{25, 26} PEO-PCL,^{25, 27, 28} and poly(fumaric acid/sebacic acid)-PEG.²⁹

Another approach to diblock copolymer based vesicles involves peptide based copolymers. Diblocks including one or two different amino acids such as PEG-poly(glycolic acid-valine),³⁰ PLA-poly(aspartic acid),³¹ PBD-PGlu.^{32, 33} Jeong *et al.* reported encapsulation of Nifedipine in PGluBn-*b*-PEG nanoparticles.³⁴ Poly(Glc-Lys)-*b*-PLA and poly(Glc-Asp)-*b*-PLA have been reported by Ouchi and coworkers,^{35, 36} and though self assembly was not studied, it seemed possible to obtain vesicles.

A few studies reported the formation of vesicles with triblock copolymers. Symmetric ABA triblocks have been investigated, for instance Floudas *et al.* studied the self assembly of PBLG-PEG-PBLG,³⁷ vesicular structures where reported using PMOXA-PDMS-PMOXA,³⁸ and a commercial triblock PEO-

poly(propylene oxide)-PEO sold by BASF as Pluronic ®. We found only two examples of asymmetric ABC triblocks forming vesicles so far, PMOXA-PDMS-PEO synthesized by Meier's group,³⁹ and PDMAI-PS-PMA reported by Bieringer *et al.*⁴⁰

CHAPTER II

SYNTHESIS

2. 1. Synthesis of B block and AB Diblock

The first step in the formation of the triblock is the synthesis of the diblock copolymer, mPEG-PLA or mPEG-PCL, or a PLA alone. mPEG-PLA/PCL and PLA can be synthesized by ring opening polymerization of the corresponding lactones. The advantage of ring opening polymerization over other techniques is the livingness of the polymerization allowing good control of molecular weight and low polydispersity.

ROP of lactones are typically initiated with alcohols. In our work, we used methoxy poly(ethylene glycol). The use of poly(ethylene glycol) would form a triblock copolymer PEG-*b*-PLA-*b*-PEG for instance. Other alcohols can be used to obtain simple PLA or PCL blocks. Several catalysts system can be used for these reactions, metal based catalysts being the most widely used systems, such as Stannous Octanoate, SnOct₂.

2. 1. 1. Evolution of the work inherited from Collette's thesis

The work presented in this thesis is the continuation of F. Collette's master thesis, reference 41. Several modifications have been performed on the initial synthesis scheme proposed in her work, as well as the final formulation itself

(this part of the work is described later). Particularly, we were interested in modifications of the process. If we were to sell our product, the need for a safe and affordable preparation would be highly desirable. Therefore, the idea behind these changes was to simplify the whole synthesis process by eliminating the use of dangerous compounds as well as compounds needing special handling, elimination of solvents when possible, and eventually shortening of reaction times.

2. 1. 2. Common catalysts for ROP of Poly(lactic acid)

Poly(lactic acid) is a polyester obtained by ROP of lactide. Lactide is a cyclic dimer of lactic acid.

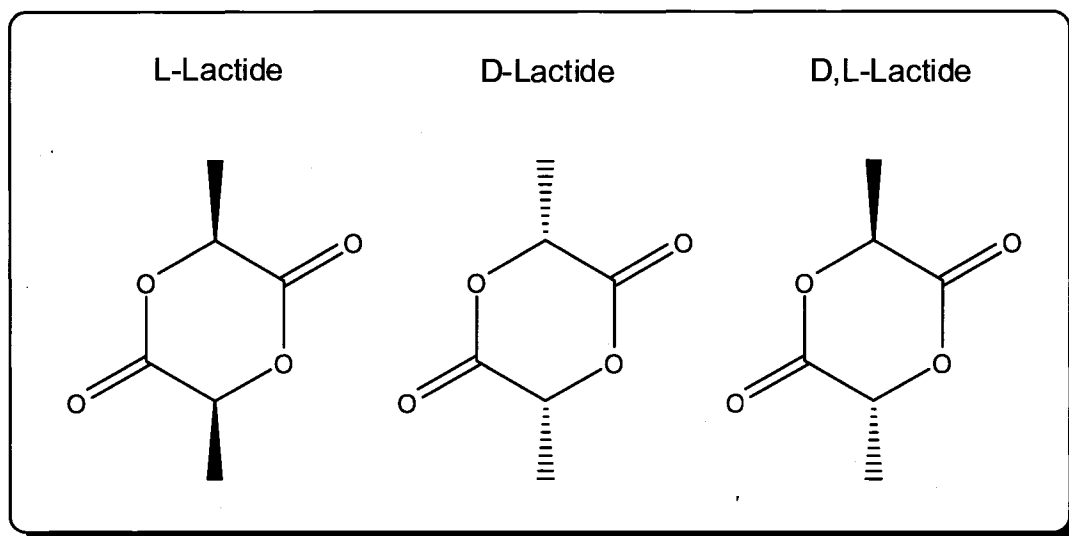


Figure 9: Lactides.

Most frequently, ROP is initiated with metal based catalysts. Typically, an alcohol is used as initiator and the metal is the catalyst. Any covalent metal

alkoxide with free p or d orbital is susceptible to react as a coordination initiator. The first step is the complexation of the monomer on the carbonyl oxygen of the lactide. It is followed by the insertion of the monomer into the metal-oxygen bond. According to Kricheldorf *et al.* various metal alkoxides, including aluminum isopropoxide, tributyltin methoxide, titanium or zinc n-butoxide, were able to ring open lactide.⁴² Among these systems Dubois *et al.* reported that $Zn(OR)_2$ and $Al(OR)_3$ were the ones that limited severely intra- and intermolecular transesterification.⁴³ These metal alkoxides yield lactic acid homopolymer or copolymers with controlled MW and low polydispersity (i. e. very few transesterification events).

According to the dimmer used to obtain PLA, it is possible to get different levels of crystallinity. Typically, L-Lactide and D-Lactide yield isotactic polymers whereas D,L-lactide yields mostly atactic structure. For the purpose of our work we are not interested in a crystalline polymer. The self-assembly of polymer chains would be disturbed by a high amount of crystallinity.

The first modifications were done on the PLA (mPEG(PLA) or mPEG(PCL)) synthesis. Using Et_2Zn as catalyst for the ROP of lactones imposes manipulations under dry nitrogen atmosphere, and eventually the use of a dry box. This step is quite prohibitive in terms of scaling up. In a first attempt to replace diethyl Zinc, several tests were done in bulk polymerization with $Sn(Oct)_2$.

Sn(Oct)₂ lead to mitigated results. First, Sn(Oct)₂ can be cautiously used under a hood, outside dry box. Second, we eliminated the need for a solvent. However the reaction times are extremely long even at very high temperature (160°C). Full conversion is reached after more than 24h at 160°C, leading to a large amount of termination and transfer reactions. Since we were not satisfied with this technique, we looked for another catalyst.

2. 1. 3. Organic catalyst for the ROP of lactones

2. 1. 3. 1. Literature

In our search of an alternative to traditional organometallic approaches for ROP of lactones, we looked for organocatalytic polymerizations. Nederberg *et al.*⁴⁴ first reported the ROP of lactide using organocatalysts. Their work was based on the use of strong bases commonly used as transesterification catalysts. 4-dimethylaminopyridine (DMAP) was found to be very efficient in transesterification reactions. It can be used in bulk or solution polymerization to ring open lactones. A plausible scheme was proposed by Nederberg *et al.*:

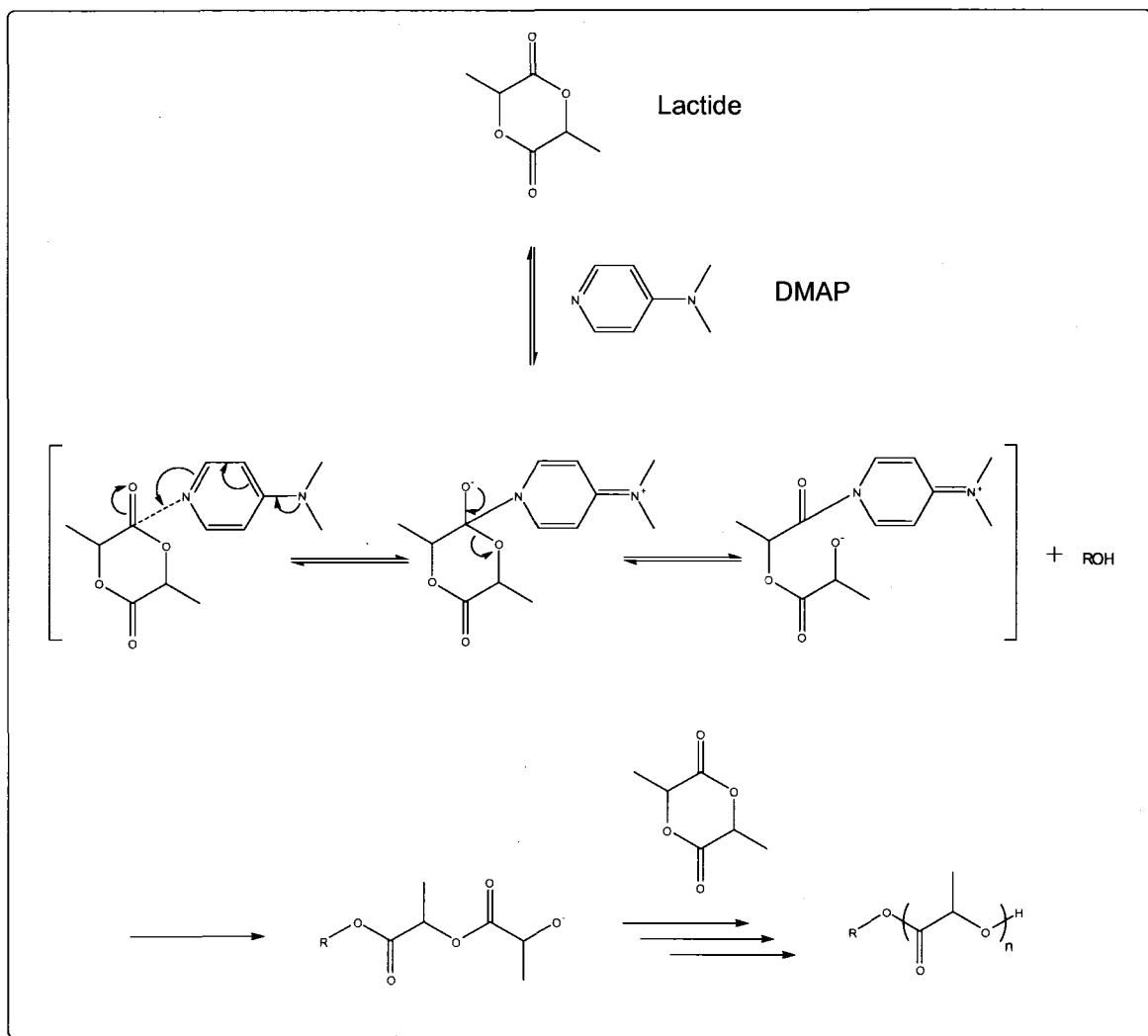


Figure 10: ROP of lactide using DMAP as a catalyst, adapted from [44].

DMAP activates the lactide, giving birth to a DMAP-lactide complex, which react with a nucleophile, such as an alcohol. The polymerization proceeds when the hydroxyl-terminated oligomer acts as a nucleophile and opens additional lactide. The polymers obtained had very low polydispersity, and had predictable molecular weights, both characteristics of living polymerizations. According to their work, in bulk conditions, times as low as 5 minutes were necessary to

achieve conversion and obtain the targeted MW at high reaction temperatures (135°C). A variety of alcohol can be used as the nucleophiles. According to the alcohol used it is possible to work in solvent polymerization (typically dichloromethane) with longer reaction times.

Since then, a few authors have reported the use of DMAP in several ROP of lactones. Feng *et al.* reported the synthesis of Chitosan-*graft*-poly(ϵ -caprolactone) with DMAP,⁴⁵ Trimaille *et al.* reported the polymerization of a variety of monoalkyl-substituted lactides using DMAP too.⁴⁶

2. 1. 3. 2. PLA and PEG-PLA synthesis using DMAP

Poly(lactic acid)

The PLA polymerization using DMAP as an activator was investigated using different alcohols as initiators, a variety of monomer to initiator ratios, as well as reaction conditions. Lactide is obtained by the cyclic dimerization of lactic acid. It can be contaminated by lactic acid and non-cyclic dimers of lactic acid. Lactide was recrystallized from hot toluene and washed with the same cold solvent prior to use in polymerization. The bulk polymerization of lactide at 135°C was followed by ^1H NMR and GPC (Gel Permeation Chromatography). A glass pipette was dip in the bulk, the embedded tip was broken and the polymer was dissolved in CDCl_3 , filtrated to remove the glass and immediately analyzed by ^1H NMR. The remaining fraction of the polymer was dried from CDCl_3 and dissolved in THF to be analyzed by GPC.

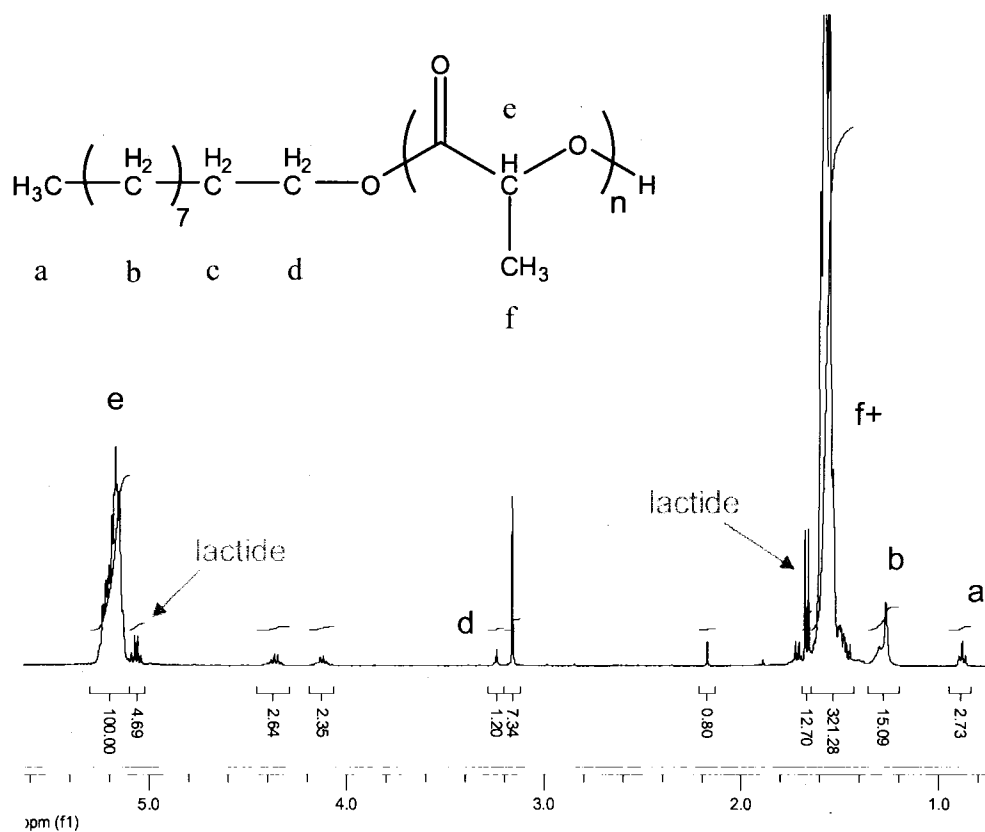


Figure 11: ^1H NMR spectrum of decanol initiated PLA in CDCl_3 .

In ^1H NMR, the conversion was evaluated by the ratio between the integrals of polymer and lactide. The signal of the methine proton C-H differs between the dimer and its polymerized form, shifted in the polymer (see figure 12). After 40 minutes, high conversion is reached and the reaction is quenched by instant freezing in liquid nitrogen.

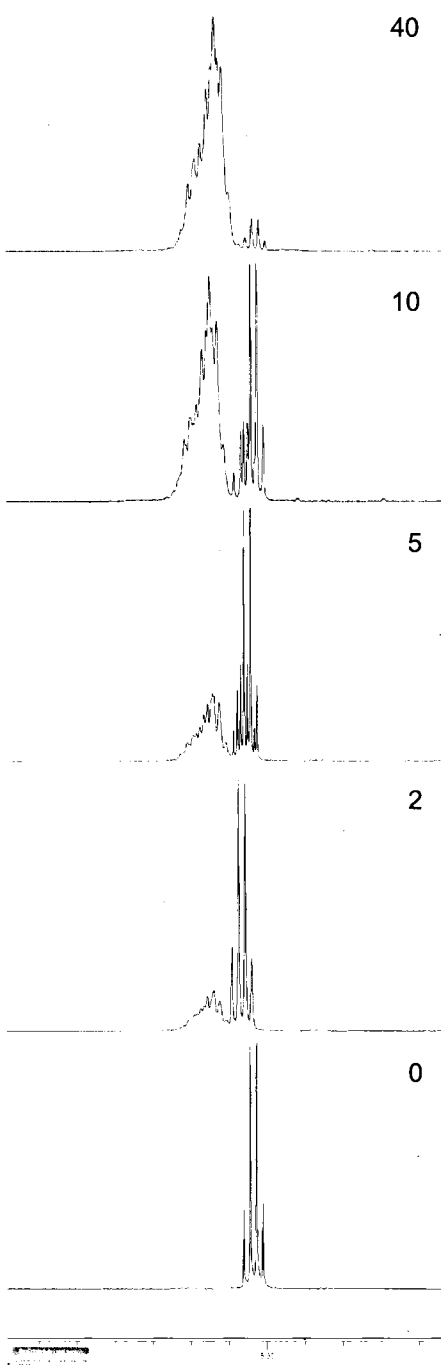


Figure 12: ¹H NMR of the methine proton during lactide polymerization from 0 to 40 minutes (in CDCl₃).

From the ¹H NMR spectra, it is possible to obtain the MW of the PLA, either by conversion or by taking an alcohol initiator of known structure as a

reference for the calculation. In the case of the PLA polymerization the alcohol signal is weak, and calculations were preferentially done with conversion. As an example, the calculation from spectrum of figure 11 is given here. The conversion is obtained by the ratio between the polymerized and the unpolymerized lactide: $100/(100+4.69) = 0.955$. The initial target being 140 units, we can say we have $0.955 \cdot 140 = 133.7 \Rightarrow 134$ units in our PLA.

As we shown on figure 10 the polymerization mechanism involves several steps: the activation of the lactide dimer with DMAP leading to the formation of the DMAP-lactate, followed by the ROP of lactide dimers. Depending on which step is rate determining, the polymerization is either zero or first order toward monomer, or a more complicated law, with an order for the initiator (which is here considered to have a constant concentration).

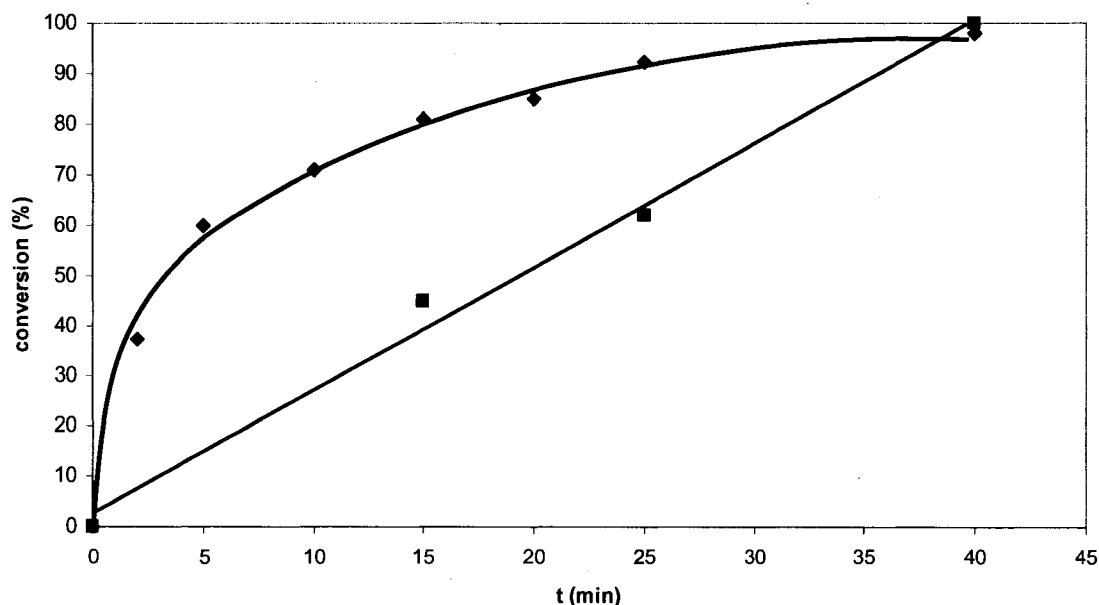


Figure 13: Conversion as a function of time for polymerization of lactide; (♦)bulk polymerization initiated by DMAP at 135°C; (■) solvent polymerization initiated by Zn(Et)₂ at 60°C (data from F. Collette's thesis, ref. 41).

From this plot, it is obvious that the DMAP polymerization is not a zero order law, as Collette reported when using $Zn(Et)_2$ as a catalyst. Apparently, higher conversions are reached more rapidly using DMAP. If a lot of literature is available on the polymerization kinetics using common catalysts (such as $Sn(Oct)_2$), there are very few studies on the kinetics of DMAP polymerization. We expect this polymerization to be first order in monomer. The kinetic law is given by the following equation:

$$R = -\frac{d[M]}{dt} = k[M]^n \quad (2)$$

R is the rate of polymerization, t is the time, [M] is the monomer concentration, k is the kinetic constant and n is the order toward monomer.

(2) can be rewritten as:

$$\frac{d[M]}{[M]^n} = -k dt \quad (3)$$

Equation (3) can be integrated, and according to the value of n, we obtain the following equations, respectively for n = 1 and n = 2:

$$\ln\left(\frac{[M]}{[M]_0}\right) = -kt \quad (4)$$

$$\left(\frac{1}{[M]} - \frac{1}{[M]_0}\right) = kt \quad (5)$$

In order to verify a first order law, consistent with the polymerization reaction, we plotted $\ln([M]/[M]_0)$ and $(1/[M]-1/[M]_0)$ as a function of t in Figure 14:

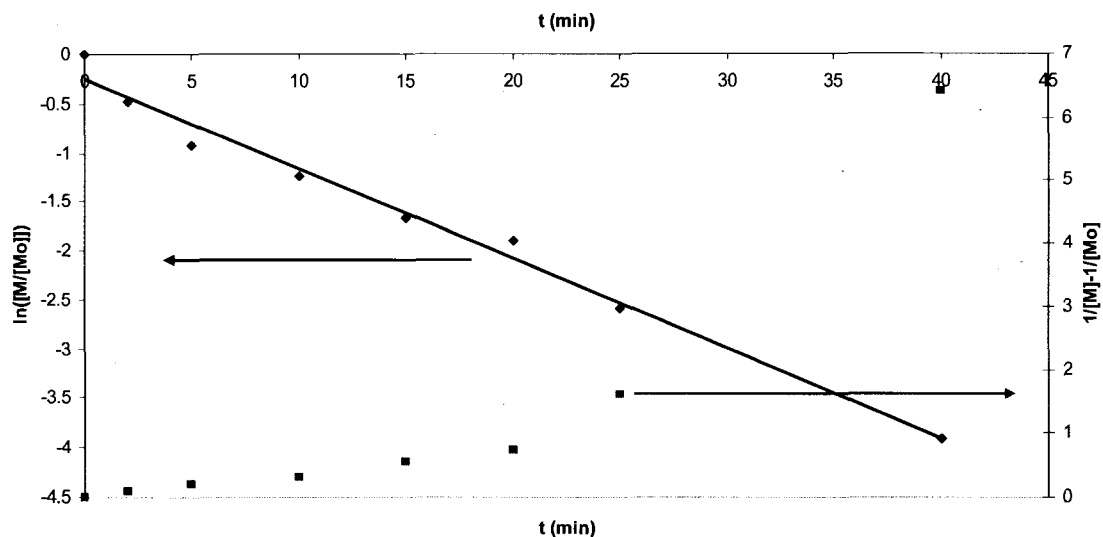


Figure 14: Kinetics of bulk PLA polymerization: first and second order approximations.

The initial concentration of monomer in bulk was simply calculated as the ratio between density and MW of the monomer. According to Figure 14, only the first order equation yields a linear relation versus time, indicating that $n=1$ is a good fit to our data. The second order law is not linear, therefore we can reasonably confirm a first order kinetics toward monomer.

Surprisingly, while we expected a dramatic slow down of the slope (in Figure 13) due to the fact that the polymerization becomes controlled by diffusion, i.e. the equilibrium toward polymer is not favored, we did not observe it. This effect should be dramatically increased in a bulk polymerization, while the viscosity is changing with time.

We measured the ability of the reaction to produce blocks with well defined MW and low polydispersity. These characteristics are consistent with a living polymerization profile. One activated monomer is initiated by one alcohol,

leading to one single chain. Chains MW grows linearly with conversion and ideally have the same length. GPC and ^1H NMR were used to follow the livingness of the polymerization. ^1H NMR was used to specifically follow conversion, by resonance shift of the methine proton as demonstrated previously.

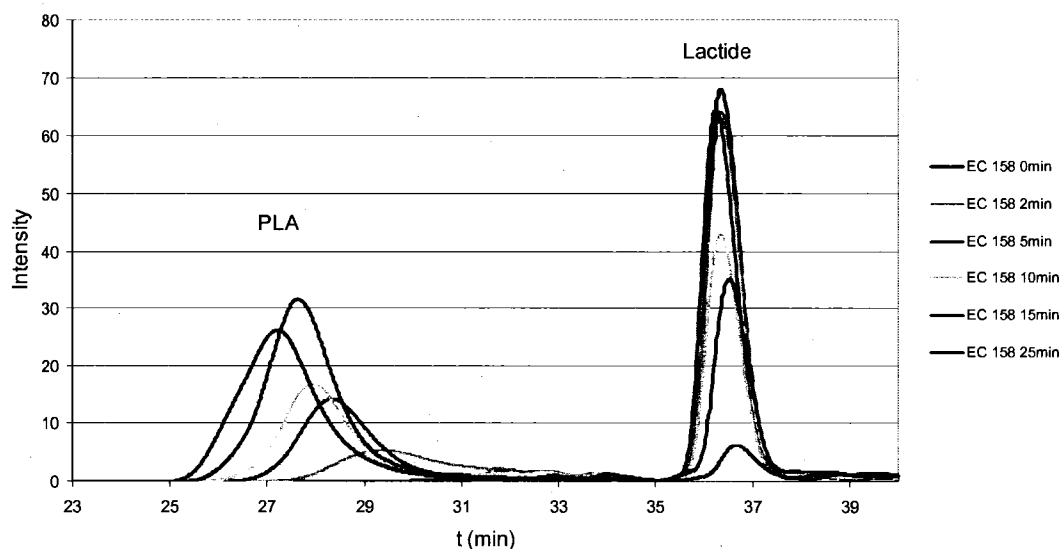


Figure 15: GPC of bulk PLA polymerization with DMAP.

We used the following set up for GPC analysis: a low molecular weight column, THF as the solvent, and temperature control at 35°C and pump rate = 1ml/min. Typically our polymer has no exploitable signal in UV, and we used an RI detector. The first peaks correspond to the distribution of high molecular weights, i. e. our polymer. GPC traces on figure 15 show the MW of the PLA fractions taken during polymerization at different times. The retention times of the peaks clearly show that MW is growing with time. On the same curve, we can see the intensity of the lactide peak dramatically decreasing with time. Though

this lactide peak could have been used for conversion calculations, we preferred considering the conversion values obtained from the ^1H NMR study. Using these conversion data, a plot of MW vs. conversion was drawn.

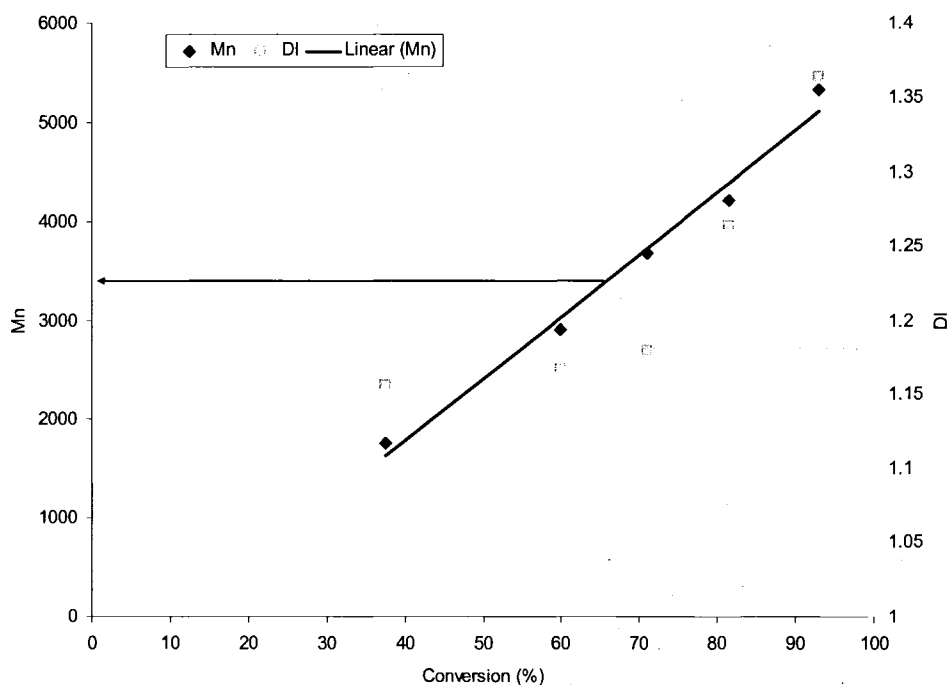


Figure 16. Polydispersity index and number average molecular weight as a function of conversion. Bulk polymerization of lactide using DMAP and Decanol as initiator.

Note that the number average molecular weight M_n of PLA is purely indicative: it is not an absolute MW since calculations are based on the GPC calibration made with poly(styrene) standards.

From this plot we can see that the molecular weight of PLA is growing linearly with conversion, indicating that the polymerization is living and can be controlled. The polydispersity index (PDI) is reasonably low for such a

polymerization. However, the value of 1.4 could be explained by side reactions occurring at the high polymerization temperature. Transfer and termination reactions as well as cross esterifications are the most plausible mechanism leading to polydispersity.

The initiators used were chosen for their high boiling point. The reaction in bulk taking place at 135°C requires fully melted initiator, monomer and catalyst.

Table 2: Listing of synthesized PEG-PLAs.

ID	Catalyst	Initiator	T	t	M/I	[catalyst] mol/L	MW PLA	PDI	Quencher
PEG-PLA									
EC29*	Zn(Et)2 (1 equiv)	PEG2000 (2 equiv)	60	1 h	139	0.0036	8900	1.24	HCl (in dioxane)
EC31*	Zn(Et)2 (1 equiv)	PEG2000 (2 equiv)	60	1 h	139	0.0036	9800	1.34	HCl (in dioxane)
EC34*	Zn(Et)2 (1 equiv)	PEG2000 (2 equiv)	60	1 h	139	0.0031	6800	1.33	HCl (in dioxane)
EC43*	Zn(Et)2 (1 equiv)	PEG2000 (2 equiv)	60	1 h	139	0.0031	4200	1.19	HCl (in dioxane)
EC44*	Zn(Et)2 (1 equiv)	PEG2000 (2 equiv)	60	1 h	139	0.0036	9900	1.57	HCl (in dioxane)
EC60*	Zn(Et)2 (1 equiv)	PEG2000 (2 equiv)	60	1 h	139	0.0042	9100	1.25	HCl (in dioxane)
EC61*	Zn(Et)2 (1 equiv)	PEG750 (2 equiv)	60	1 h	139	0.0032	NC	NC	HCl (in dioxane)
EC62*	Zn(Et)2 (1 equiv)	PEG5000 (2 equiv)	60	1 h	138	n/a	NC	NC	HCl (in dioxane)
EC92	Sn(Oct)2 (1 equiv)	PEG2000 (84 equiv)	140	19 h	238	n/a	26000	1.55	MeOH
EC92 ter	Sn(Oct)2 (1 equiv)	PEG2000 (84 equiv)	140	19 h	238	n/a	26000	1.53	Cyclohexane
EC99	Sn(Oct)2 (1 equiv)	PEG2000 (100 equiv)	160	5 h	100	n/a	6600	1.55	Cyclohexane
EC100	DMAP (1 equiv)	PEG2000 (1 equiv)	65	1 h	278	n/a	NC	NC	Cyclohexane
EC101	Sn(Oct)2 (1 equiv)	PEG2000 (100 equiv)	160	7 h	140	n/a	8600	1.55	Cyclohexane
EC102	Sn(Oct)2 (1 equiv)	PEG2000 (100 equiv)	130	10 h	140	n/a	8800	1.39	liquid Nitrogen
EC106	DMAP (2 equiv)	PEG2000 (2 equiv)	135	2 h	140	n/a	9400	1.42	liquid Nitrogen
EC109	DMAP (2 equiv)	PEG2000 (1 equiv)	135	2 h	280	n/a	18600	1.39	liquid Nitrogen
EC111	DMAP (2 equiv)	PEG2000 (1 equiv)	135	2 h	140	n/a	9400	1.5	liquid Nitrogen
EC112	DMAP (2 equiv)	PEG2000 (1 equiv)	135	20 min	140	n/a	7500	1.3	liquid Nitrogen
EC133	DMAP (2 equiv)	PEG2000 (1 equiv)	135	20 min	140	n/a	6200	1.34	liquid Nitrogen
EC134	DMAP (1 equiv)	PEG2000 (1 equiv)	135	20 min	140	n/a	3000	NC	liquid Nitrogen
EC135	DMAP (2 equiv)	PEG2000 (1 equiv)	135	40 min	140	n/a	8100	1.41	liquid Nitrogen
EC179	DMAP (2 equiv)	PEG2000 (1 equiv)	135	40 min	110	n/a	6500	1.24	liquid Nitrogen

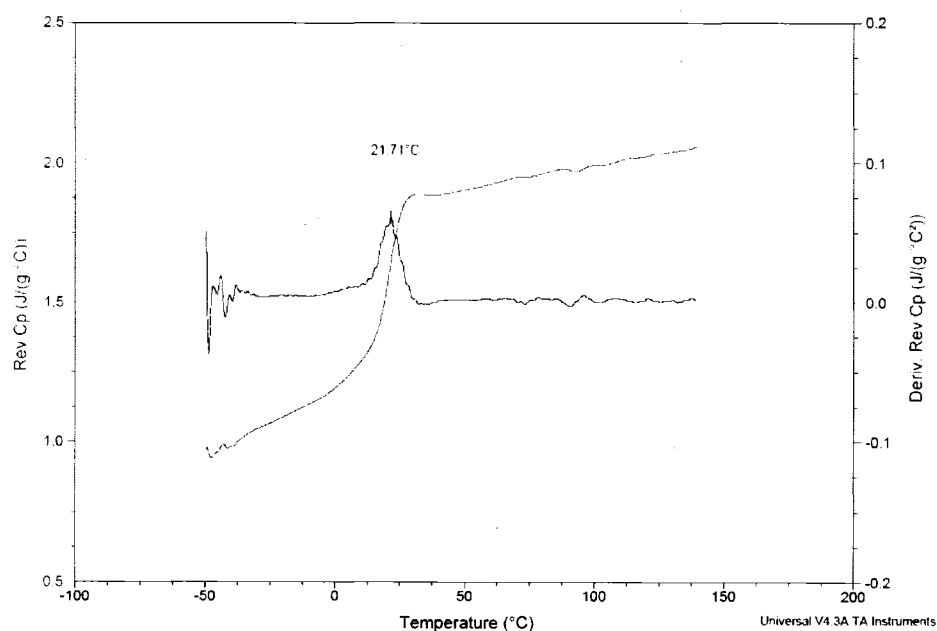
* Polymerization in toluene.

Table 3: Listing of synthesized PLAs.

ID	Catalyst	Initiator	T	t	M/I	[catalyst] mol/L	MW PLA	PDI	Quencher
PLA									
EC103*	DMAP (4 equiv)	Decanol (1 equiv)	60	20 h	140	0.08	NC	NC	Cyclohexane
EC105	DMAP (2 equiv)	Decanol (1 equiv)	135	75 min	140	n/a	9600	1.34	liquid Nitrogen
EC142	DMAP (2 equiv)	Decanol (1 equiv)	135	20 min	20	n/a	1100	1.5	liquid Nitrogen
EC143	DMAP (2 equiv)	Decanol (1 equiv)	135	20 min	25	n/a	1700	1.51	liquid Nitrogen
EC148	DMAP (2 equiv)	1-Pyrenemethanol	135	20 min	140	n/a	8100	NC	liquid Nitrogen
EC157	DMAP (2 equiv)	Decanol (1 equiv)	135	20 min	140	n/a	9100	1.66	liquid Nitrogen
EC158	DMAP (2 equiv)	Decanol (1 equiv)	135	40 min	140	n/a	9900	1.36	liquid Nitrogen

* Polymerization in toluene.

From the work of Collette,⁴⁷ we know that crystallinity of the PLA is a parameter we need to avoid, since it is detrimental to the formation of vesicles. Therefore, we used racemic lactide yielding an amorphous PLA in all our polymerizations. DSC was used to show the amorphous state of our polymers. As an example, a DSC trace for a PLA is shown in Figure 17.

**Figure 17: DSC spectrum of a PLA block.**

The T_g of our polymer is measured to be around 20°C, and no crystallization peak is observed. The low T_g found for this particular sample is most probably due to residual solvent.

Methoxy Poly(ethylene glycol-co-lactic acid)

The diblock mPEG-PLA was obtained using the same process, with a methoxyPEG OH-terminated instead of a simple alcohol. The use of PEG is no different from another alcohol in theory. However, we observed that the polymerization using PEG as initiator required extra time to reach high conversion. One explanation is due to the high viscosity of the reaction bulk at 135°C when using PEG, a low molecular weight macromolecular alcohol, versus the viscosity of the media when using a simple alcohol molecule such as decanol.

The molecular weight distribution was studied by GPC, and the MW value was calculated from ¹H NMR. A typical NMR of PEG-PLA is given below (figure 18).

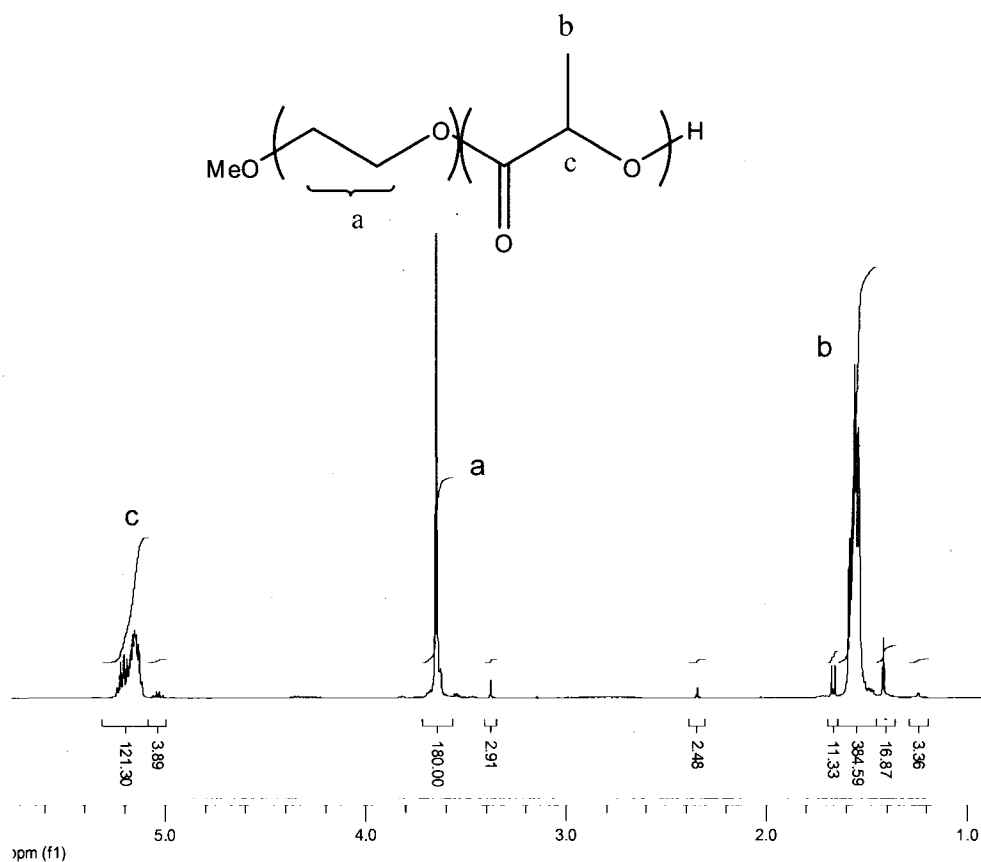


Figure 18: ^1H NMR of mPEG-PLA in CDCl_3 .

The calculation is particularly easy when the initiator has a strong ^1H NMR signal such as PEG 2000. As an example, the calculation is done on the spectrum represented above.

Since the initiator is PEG 2000 (corresponding to 45 repeat units), we know that the CH_2 signal represents $45 \times 4 = 180$ H. If we attribute an integral of 180 to this signal, then the signal of the H of the PLA, counting for one H per repeat unit, directly gives us the MW of the PLA. In this case, the integral is 121.30; therefore we can consider our diblock to be a $\text{PEG}_{45}\text{PLA}_{121}$. Note that the signal of the methyl of the PLA chain can also be used for the calculation: the

integral of 384.59 counts for 3 H, and the number of repeat unit is given by $384.59/3 = 128.19$, or 128, which is reasonably close to the value found with the methine proton.

2. 1. 4. mPEG-PCL

One of the tunable properties of our system is the degradability of the hydrophobic block. The purpose of exploring different diblocks was to have a variety of degradation time scales for the final system. As we have seen before, poly(ϵ -caprolactone) and poly(lactic acid-co-glycolic acid) have very different properties: PCL is more resistant to hydrolysis while PGLA is degrading faster.

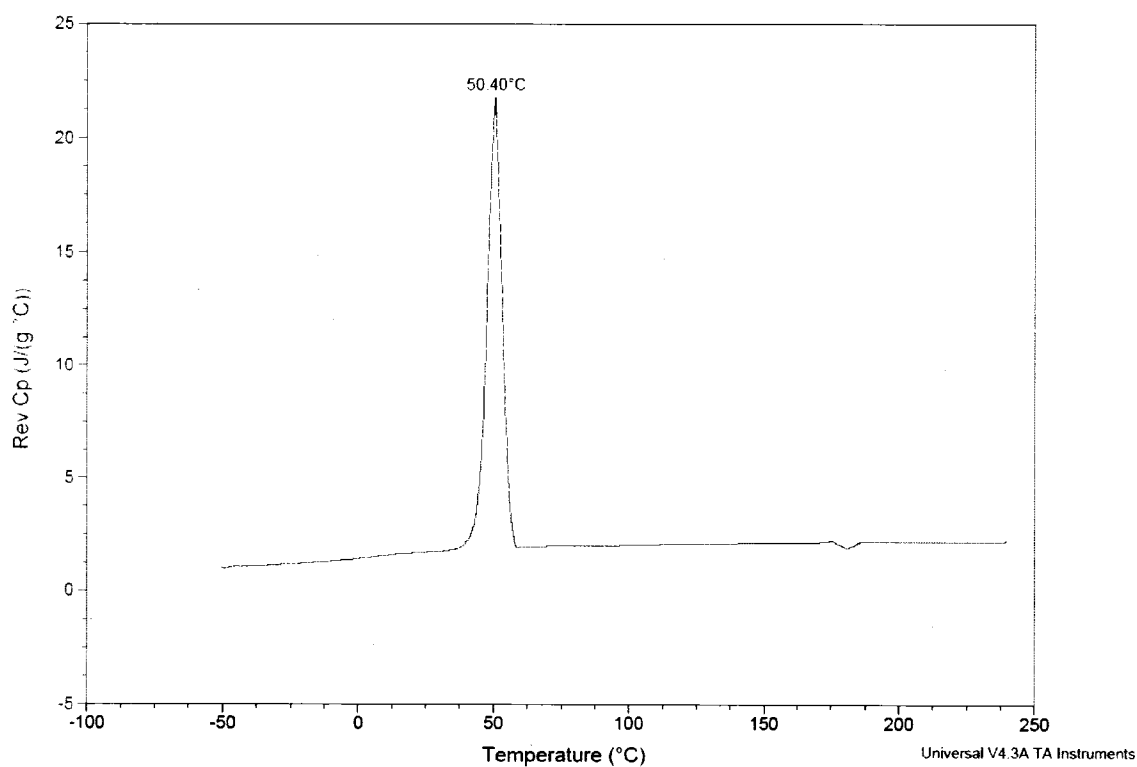


Figure 19: DSC spectrum of polycaprolactone.

PCL resistance to degradation is in part due to the high crystallinity of the polymer, excluding low molecular weight molecules from these domains. The DSC trace of PCL (figure 19) shows a crystallization peak around 50°C.

Poly(ϵ -caprolactone) is a polyester which can be obtained by ring-opening polymerization of its monomer, ϵ -caprolactone.

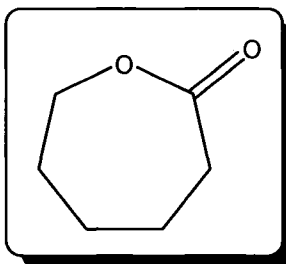


Figure 20: ϵ -caprolactone.

The ROP allows a controlled/living polymerization. Such a polymerization is desirable in order to avoid any termination or transfer reactions during the polymerization, leading to well controlled molecular weight and architecture for the final polymer.

A variety of catalysts have been described. Activated monomer cationic polymerization of ϵ -caprolactone has been reported using $\text{HCl}\cdot\text{Et}_2\text{O}$ as an activator.^{48, 49} Homopolymers (PLA, PCL) as well as copolymers mPEG-PCL were obtained, all with few chain transfer and good control of molecular weight. The use of cheap chemicals in this polymerization procedure is interesting, however, it requires up to 24 hours for ϵ -caprolactone to reach high conversions.

E-caprolactone polymerization can be initiated by metal alkoxides. Monomethoxy-PEG becomes a macromolecular initiator in the presence of the catalyst, and generates a copolymer diblock PEG-PCL. Deng *et al.*⁵⁰ reported the polymerization of PCL blocks by ROP using diethyl zinc as a catalyst. The polymerization was done at 130°C for 20 hours.

Ahmed *et al.*²⁵ reported the synthesis of mPEG-PCL diblocks by ROP using tin ethylhexanoate. In this method, reagents are dissolved in toluene, and the reaction is held at 100°C for 2 hours. Choi *et al.*⁵¹ reported the polymerization to be complete after 24 hours at 140°C in toluene.

Storey *et al.*⁵² used the same catalyst in bulk polymerization to produce poly(ϵ -caprolactone). The reaction scheme is given in figure 21:

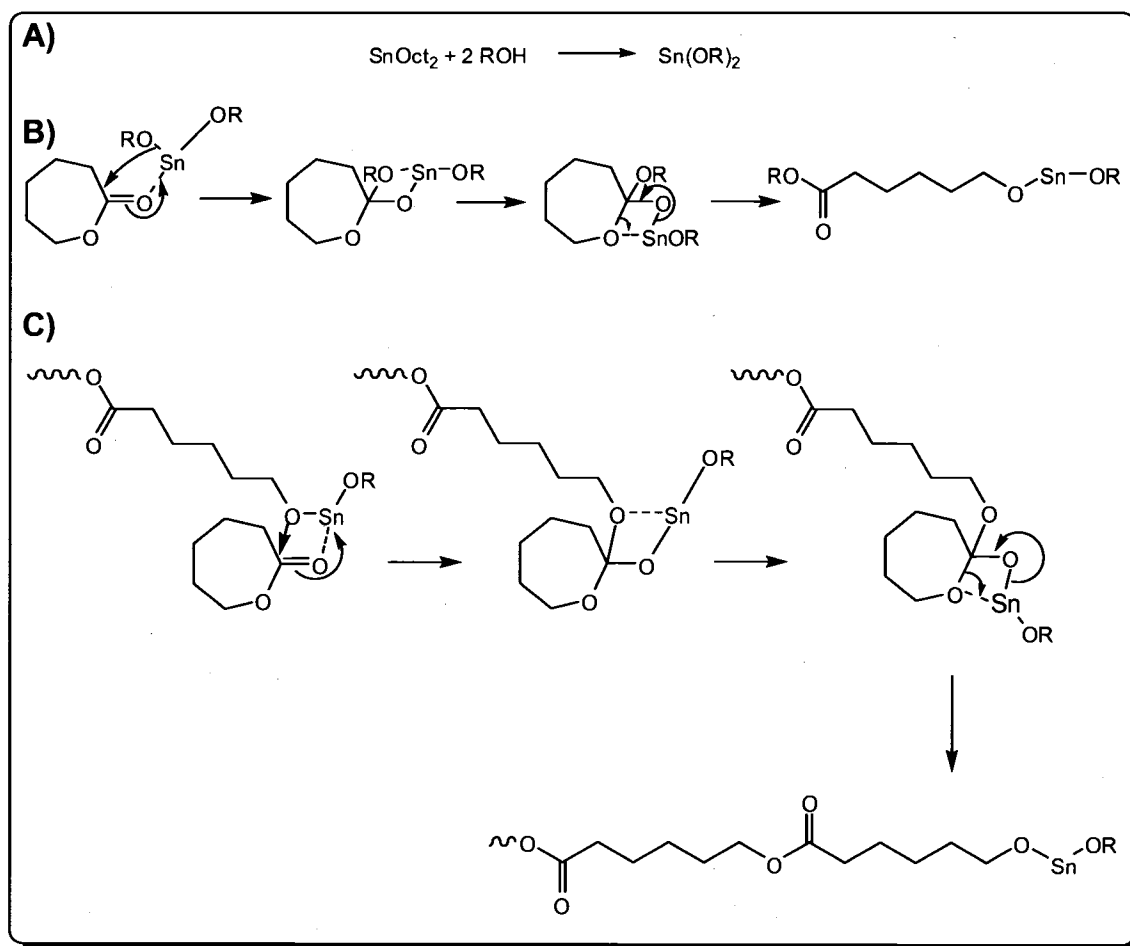


Figure 21. ROP of ϵ -caprolactone with tin ethyl hexanoate: A) formation of stannous alkoxide initiator, B) coordination/insertion of monomer, C) chain extension.⁵²

Other groups^{42, 53} investigated the polymerization of ϵ -caprolactone with aluminum based catalysts, the simplest ones being aluminum isopropoxide and triethyl aluminum. Aluminum complexes such as aluminum amine bis(phenolate)s,⁵⁴ or aluminum thiolates⁵⁵ could be used.

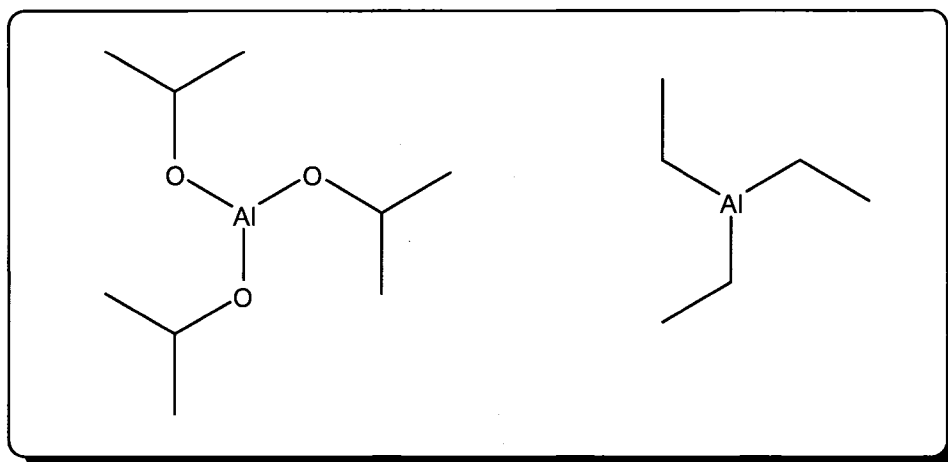


Figure 22: Aluminum isopropoxide and triethyl aluminum.

The following mechanism for ROP of ϵ -caprolactone with aluminum isopropoxide was proposed by Dubois *et al.*⁵³

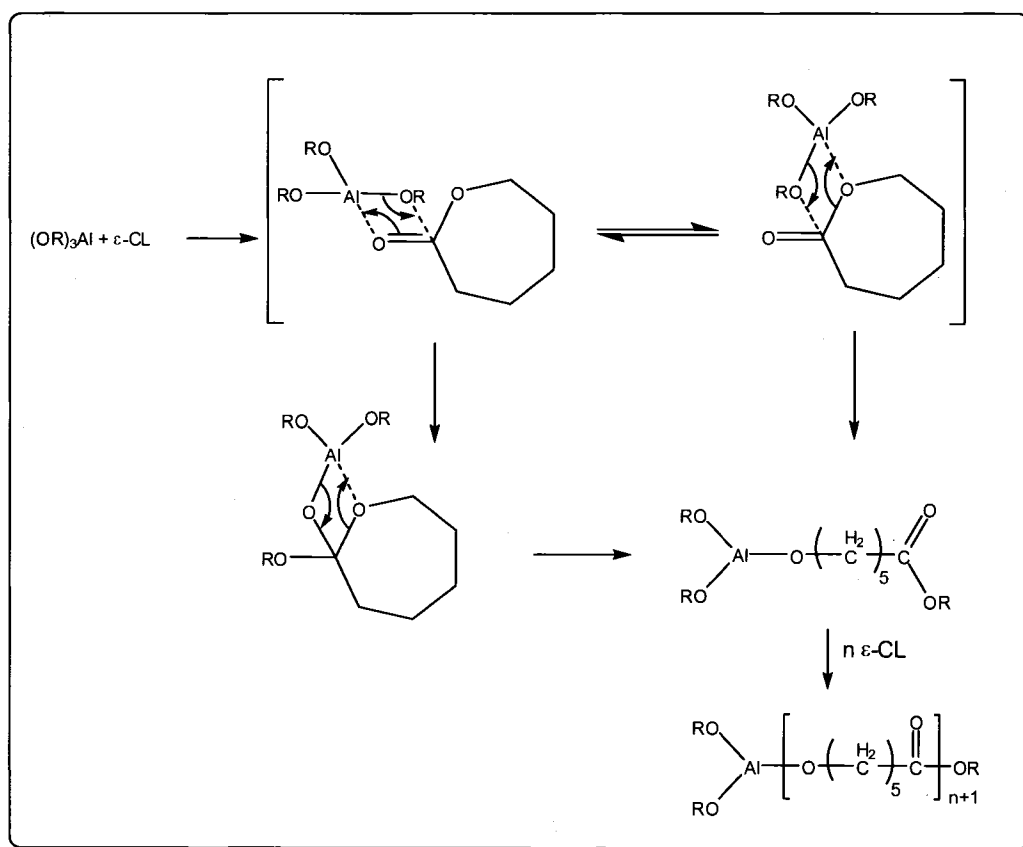


Figure 23: ROP of ϵ -caprolactone using an aluminum alkoxide.⁵³

Aluminum alkoxides have been found to be very efficient for the severe limitation of inter and intramolecular side reactions. Those polymerizations are typically done at room temperature. ϵ -Caprolactone polymerization can be initiated by alcohols such as PEG terminated by hydroxyl groups. With two –OH termination, a triblock PEG-b-PCL-b-PEG would be obtained. Using a mPEG, a diblock PEG-b-PCL is generated.

A few experiments were done on the polymerization of ϵ -caprolactone using metal catalysts. The most efficient catalyst was found to be triethyl aluminum ($\text{Al}(\text{Et})_3$).

Table 4: Listing of PEG-PCL.

ID	Catalyst	initiator	T	t	M/I	[catalyst] mol/L	MW PLA	PDI	Quencher
EC20	$\text{Zn}(\text{Et})_2$ (1 equiv)	PEG2000 (2 equiv)	60	1 h	44	0.017	4000	NC	HCl 35%
EC24	$\text{Al}(\text{Et})_3$ (1 equiv)	PEG2000 (3 equiv)	60	1 h	29	0.016	3300	NC	HCl 35%
EC26	$\text{Al}(\text{Et})_3$ (1 equiv)	PEG2000 (3 equiv)	0	1 h	29	0.01	3300	NC	HCl 35%
EC28	$\text{Al}(\text{Et})_3$ (1 equiv)	PEG2000 (2 equiv)	RT	75 min	44	0.016	5000	NC	HCl 35%
EC30	$\text{Al}(\text{Et})_3$ (1 equiv)	PEG2000 (2 equiv)	RT	2 h	44	0.01	7100	1.21	MeOH
EC32	$\text{Al}(\text{OiPr})_3$ (1 equiv)	PEG2000 (3 equiv)	RT	1 h	29	0.006	NC	NC	MeOH
EC36	$\text{Al}(\text{Et})_3$ (1 equiv)	PEG2000 (2 equiv)	RT	90 min	44	0.01	5000	1.26	MeOH
EC57	$\text{Al}(\text{Et})_3$ (1 equiv)	PEG2000 (2 equiv)	RT	1 h	22	0.016	2850	1.26	MeOH

All polymerizations in toluene.

No polymerization was observed using $\text{Al}(\text{OiPr})_3$. According to ^1H NMR, $\text{Zn}(\text{Et})_2$ was found to polymerize ϵ -caprolactone and yield very low MW block copolymers. The preparation of A-B diblock copolymers by stepwise addition successfully proceeds only if the active species remain at the chain end of the growing block. If the active species are transferred to the monomer, ideally we obtain a blend of A and B homopolymers. In the case of $\text{Zn}(\text{Et})_2$ polymerization, the active species were most likely transferred from the PEG chain to the ϵ -

caprolactone monomers. In the case of triethyl aluminum, we succeeded into synthesizing diblocks PEG-PCL with low PDI and controlled MW.

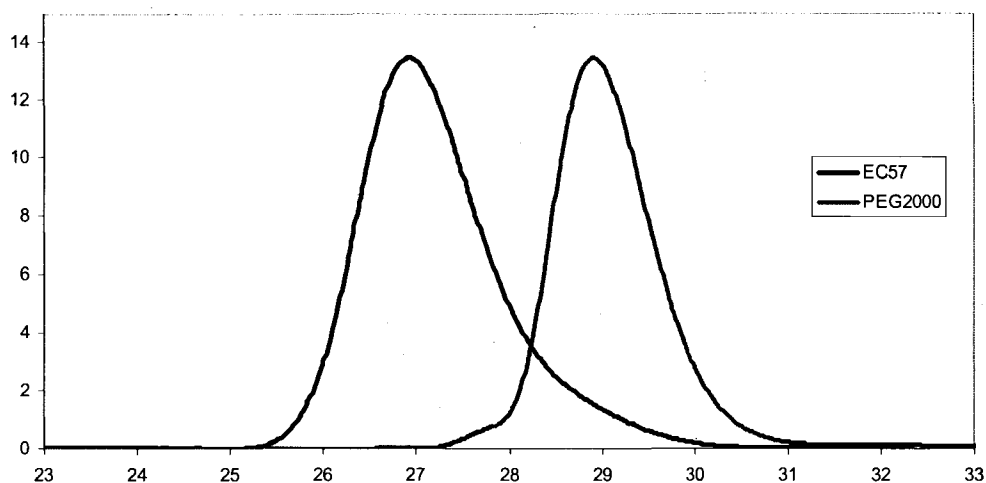


Figure 24: GPC traces of PEG 2000 and PEG-PCL copolymer.

From the GPC experiment we can see that the PEG chains have been extended with poly(caprolactone). The ^1H NMR confirmed this polymerization. Upon successful coupling of PEG to PCL, the signal of the CH_2 from a PEG unit attached to a caprolactone unit slightly shifted toward the high fields region. This is due to the contribution of the close $\text{O}=\text{C}-\text{O}$ of the PEG/PCL junction versus the $\text{C}-\text{O}$ in regular PEG. On the ^1H NMR spectrum given below, this signal is the triplet labeled c at 4.2 ppm. The presence of this peak is a proof that we did obtain a diblock and not two homopolymers.

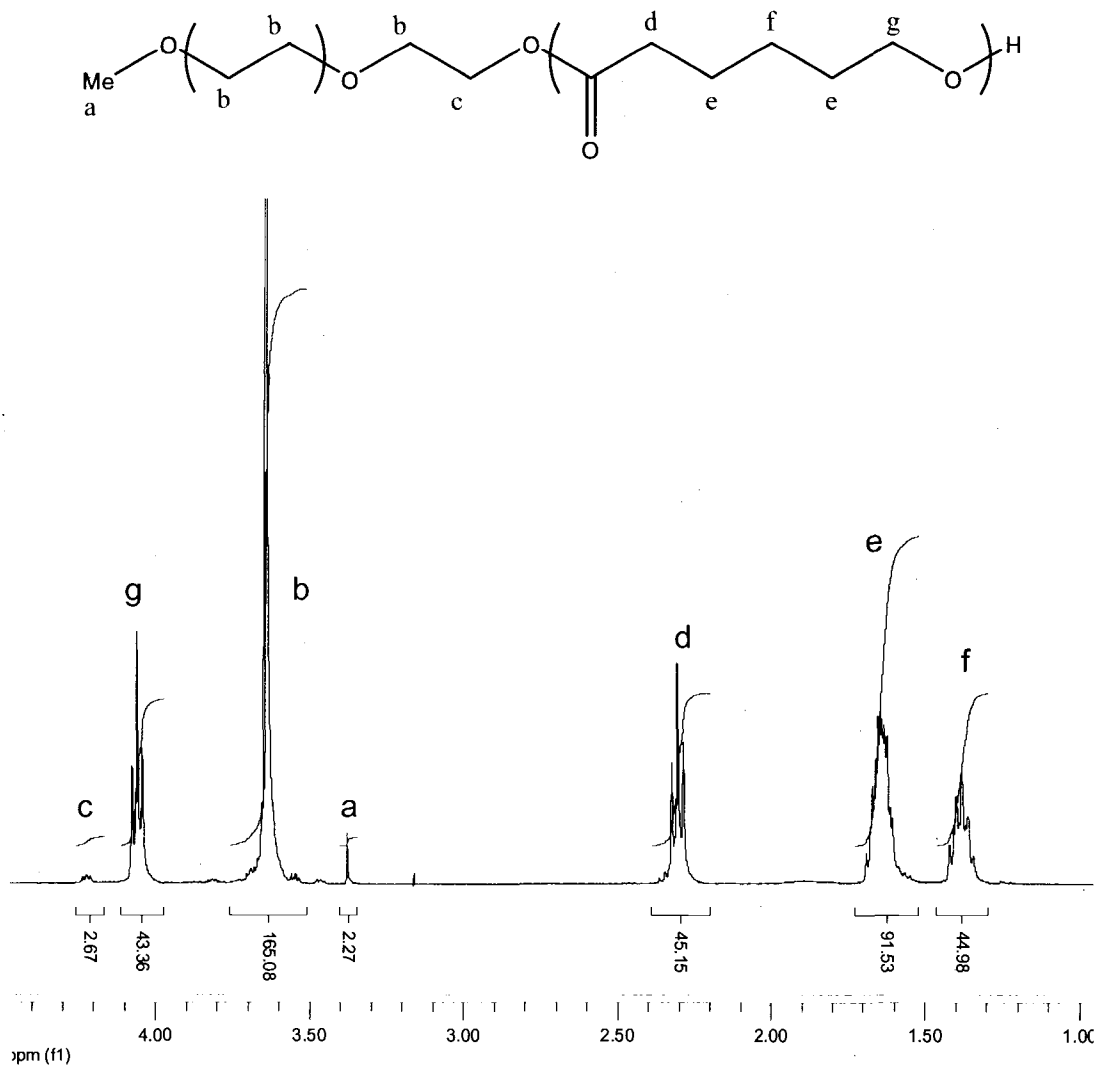


Figure 25: ^1H NMR of PEG-PCL in CDCl_3 .

Using the integrals of peaks b and e, which are counting for 2H each, we found a molecular weight of 2850 g/mol or 25 repeat units for the spectrum represented above.

2. 2. PGluOH synthesis

2. 2. 1. PGluBn synthesis

Controlled living anionic polymerization of N-Carboxyanhydrides (NCAs) allows the preparation of peptide block copolymers with a well defined architecture and composition. Poly(glutamic acid) is a polypeptide constituted with a single amino acid repeat unit, glutamic acid.

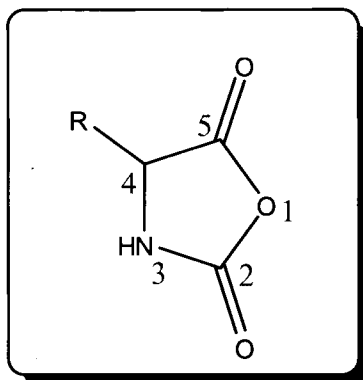


Figure 26: N-Carboxyanhydride (NCA).

It is prepared by ring opening polymerization of the NCA of glutamic acid potentially initiated with four classes of compounds: protic nucleophiles, aprotic nucleophiles, aprotic bases and organometallics. Among the protic nucleophiles, the most widely used compounds for NCA polymerization, we could use water, amines and alcohols.

We describe here the mechanism using a primary amine. Primary amines react with the C5 carbon atom, leading to a compound with a new primary amine function that can promote a nucleophilic attack on another NCA molecule and so on.

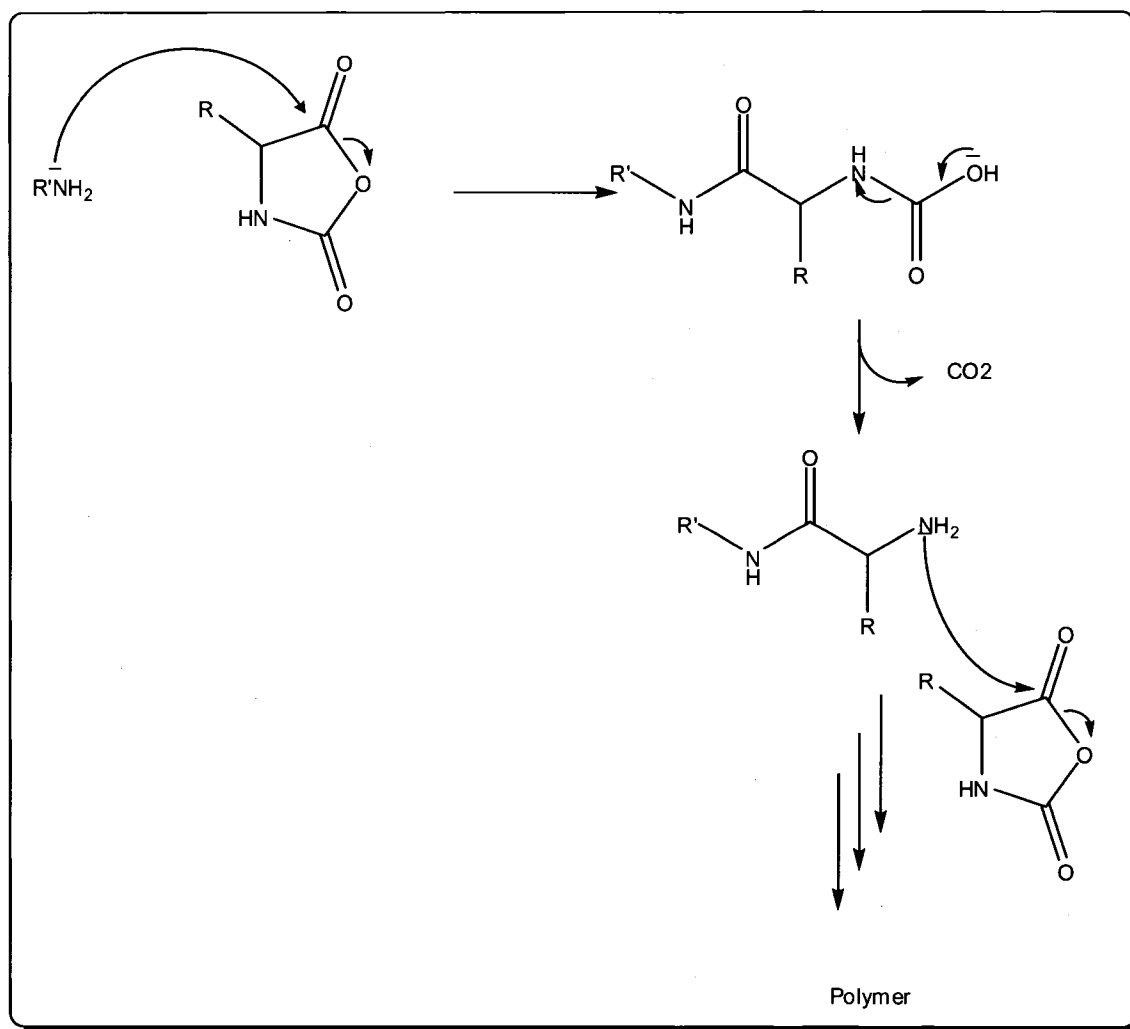


Figure 27: Ring Opening Polymerization initiated by primary amines.

The termination of the polymerization occurs when all the monomer is reacted, leading to NH_2 functionalized polymer chains. However, Hanby⁵⁶ was the first to report another termination mode. It is possible that the terminal primary amine function reacts with the carbonyl of the benzyl group protecting the acid. In this case, a five membered imide cycle is formed, called pyroglutamic group. This termination is ending the polymerization of a growing chain and is obviously detrimental to the control of MW and low polydispersity.

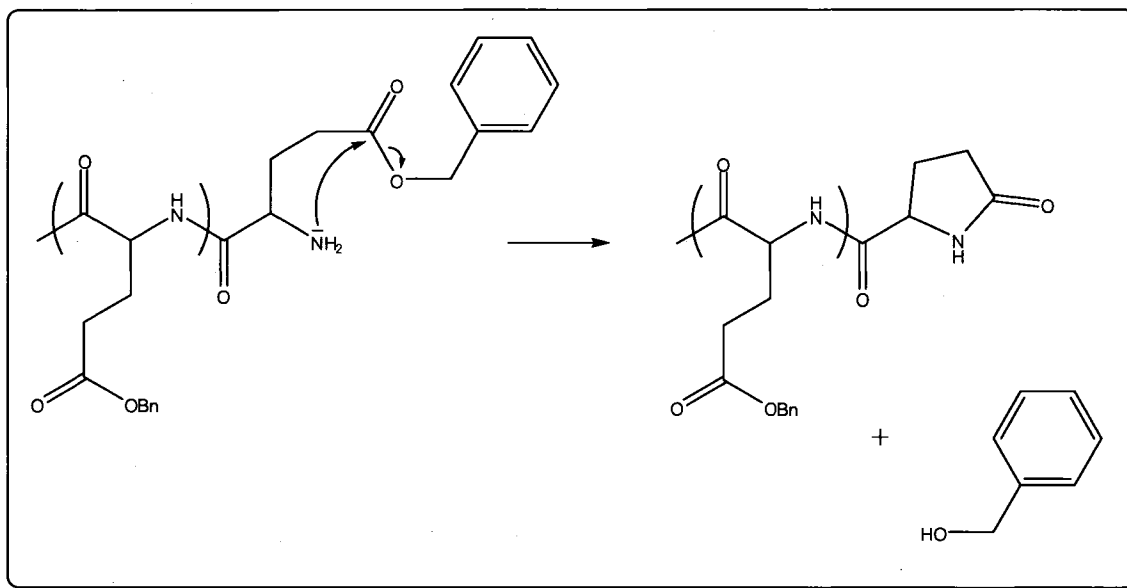


Figure 28: Termination by formation of pyroglutamic groups.

The synthesis of poly(benzyl glutamate) was done by ROP of the corresponding protected NCA. NCA of benzyl glutamate was purchased from Isochem (France) and used without further purification. The polymerization is well described by Collette.⁵⁷ It is polymerized in NMP at 40°C using an amine as initiator and no catalyst. The evolution of CO_2 is the major driving force and little side reactions are encountered. Collette used FT-IR and HPLC to follow the polymerization of PGluBn and we used her results and data. Polymerization times were inconsistent (from 3 hours to 48 hours) and we worked on refining the ideal polymerization conditions. In this study, we had issues with yields often found to be over 100%. We found out that the washes using water at different pHs were ineffective regarding non polymerized NCA. After several solubility tests, we decided to wash the polymer with a mixture of solvents,

THF/Isopropanol (2:1 volume ratio). This mixture elaborated considering polarity affinities helped selective solubilization of NCA.

2. 2. 2. Deprotection

A kinetic study was done in $^1\text{H-NMR}$ to follow the deprotection of the PGLuBn. PGLuBn was dissolved in TFA, and MSA and Anisole were added at 10°C . A sample was taken every 15 minutes, precipitated in a small volume of ether and washed with ether, then dissolved in d-TFA and analyzed. The mechanism of the reaction is given below:

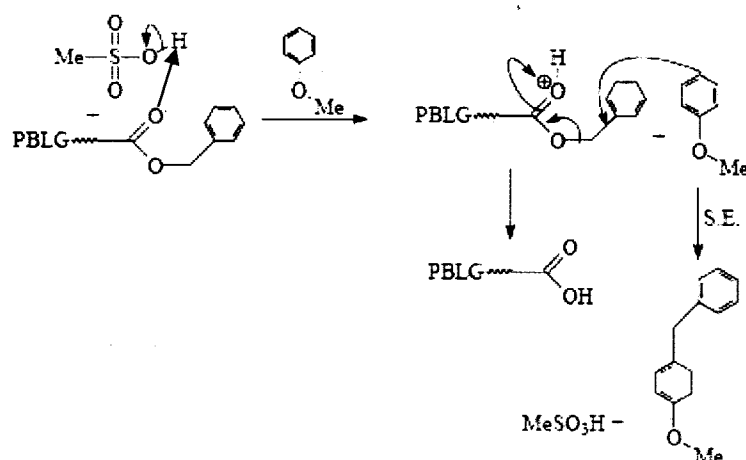


Figure 29: Benzyl deprotection mechanism using Methane Sulfonic Acid.⁵⁸

MSA protonates the carbonyl of the protected acid, then anisole is used as an ion scavenger trapping the leaving O-benzyl group. The NMR of PGLuBn is shown on Figure 30:

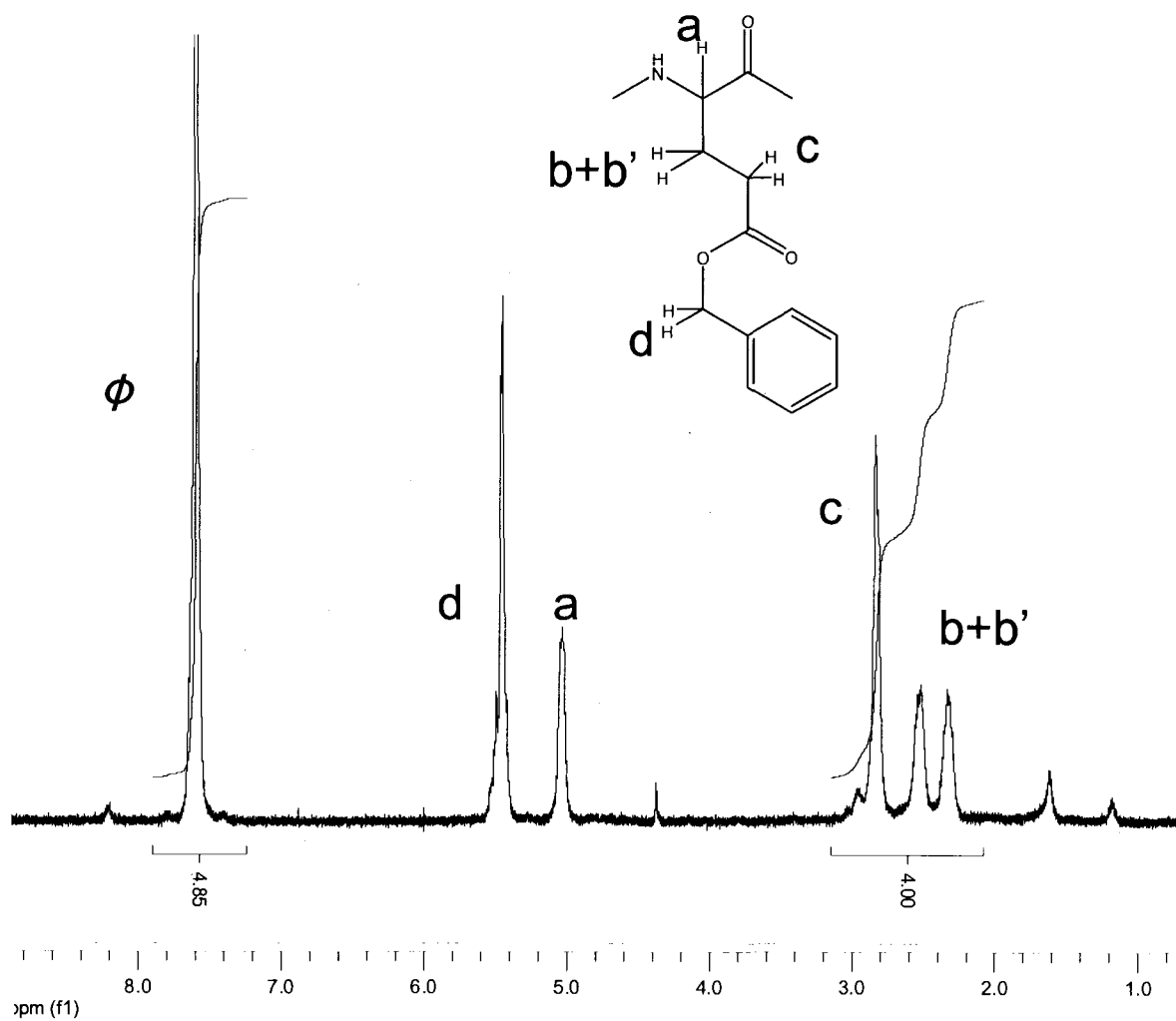


Figure 30: ^1H NMR spectrum in of PGluBn in $d\text{-TFA}$.

The disappearance of the aromatic signal was monitored. The ^1H NMR spectra are given below.

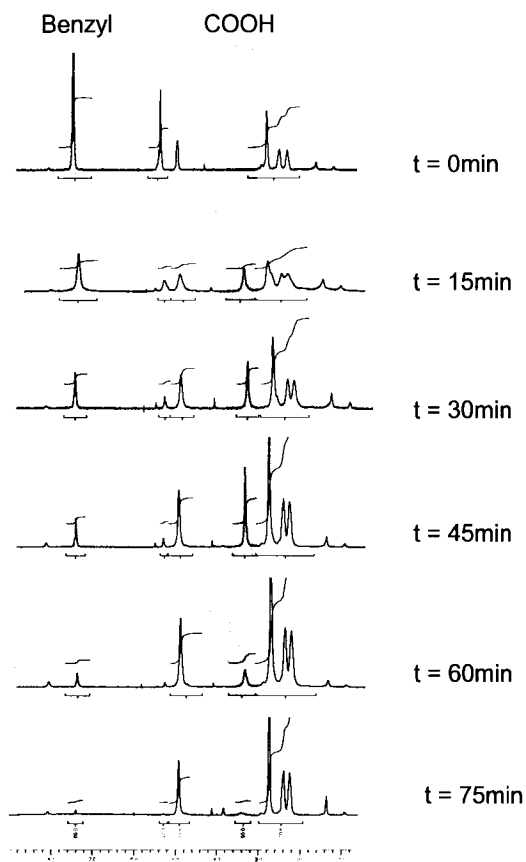


Figure 31: Kinetics of deprotection of PGluBn followed by ^1H NMR.

The percentage of deprotected PGlu is simply calculated from the ratio between the integral of the aromatics and the integral corresponding to the 2H b and b' of the PGlu (see Figure 30). Table 5 summarizes the calculations:

Table 5: Calculation of deprotection.

t (min)	Assigned Integral For b + b' + c	Integral of Bn	% deprotection	Integral of COOH
0	4	5	0	0
15	4	1.5	70	0.8
30	4	0.75	85	1
45	4	0.25	95	0.95
60	4	0.12	97.6	0.31
75	4	0.04	99.2	0.17

From this study we observe that the deprotection is fast and almost complete at 45 min of reaction, when about 95% of the benzyl group is cleaved. Another interesting change can be observed on the spectrums of Figure 31: the appearance of a peak at 3.5 ppm, corresponding to the COOH. This peak was expected to be seen and its intensity should grow, scaling with the disappearance of the benzyl signal. But what we observe is completely different. The COOH is growing until 45 minutes of reaction, and then starts to fade away before disappearing. One explanation is that the COOH are reacting together to form anhydrides, the reaction being catalyzed by the acidic environment.

One of the effects of such a reaction would result in a crosslinking of the PGLuOH chains. Two chains could be linked together by an anhydride formed by two COOH. This would yield high MW PGLuOH chains.

The hypothesis was indirectly verified by another analysis. MW analysis by HPLC-MALS was done on PGLuOH deprotected for 75 minutes. The advantage of using Multi Angle Light Scattering rather than GPC in this case is that MALS is giving us the absolute MW of the polymer, so we can actually compare the experimental MW to the targeted one. The targeted molecular

weight for PGLuOH was 12900 g/mol, and a HPLC-MALS experiment on kinetics ran by Zakaria Boukhal gave the following report:

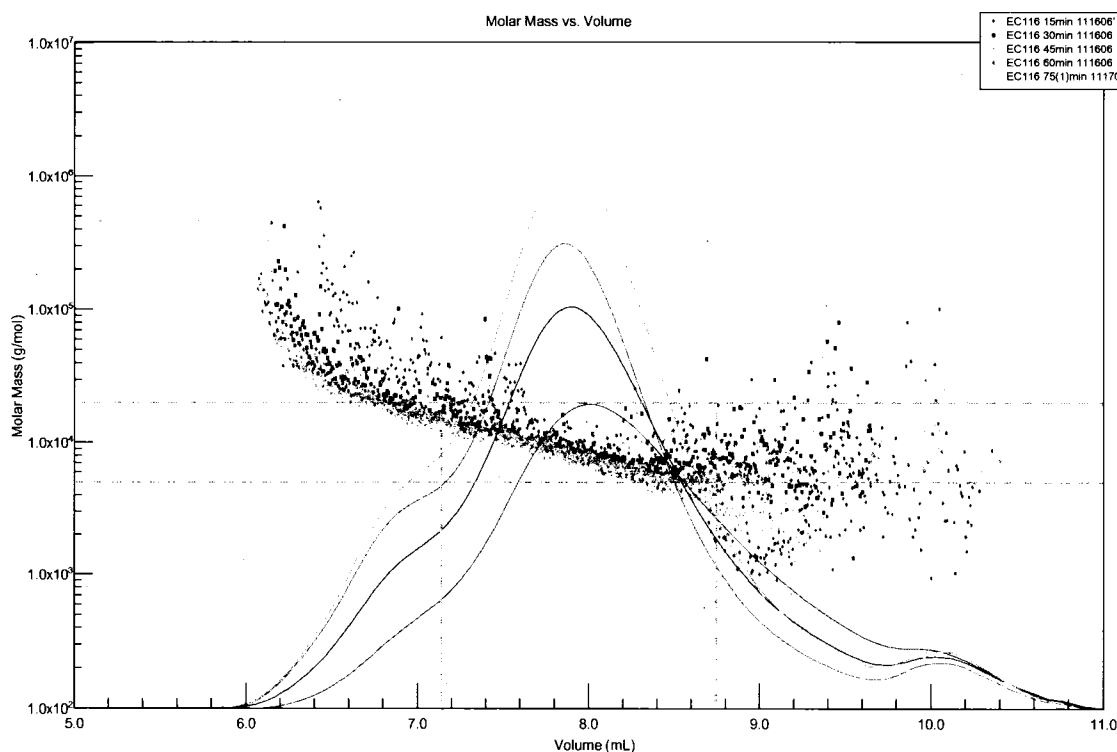


Figure 32: HPLC-MALS kinetic study on PGLuBn deprotection.

The PGLuOH was dissolved at 1% in basic water and injected in HPLC-MALS. According to the plot of MW versus volume fraction, about 80% of the polymer is found to have MW between 5000 to 20000 g/mol, and a significant fraction (20%) has a MW higher than 20000 g/mol. This fraction is most likely the result of crosslinking between chains through the formation of anhydride bonds. From this point we decided to stop the deprotection reaction at 45 minutes, in order to avoid such side reactions for all our deprotections. A new HPLC-MALS experiment gave us the following plot (Figure 33). This time, no fraction of high

MW was seen, proving that stopping the reaction at 45 minutes was effectively avoiding crosslinking.

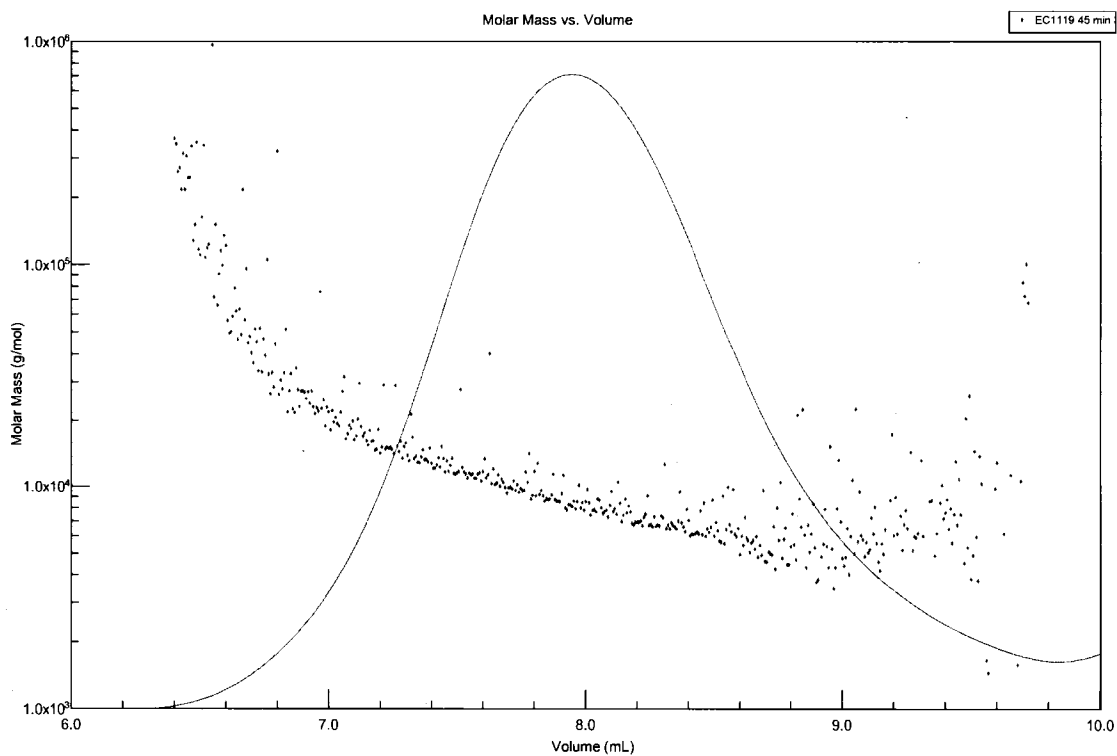


Figure 33: HPLC-MALS plot of a PGLuOH deprotected for 45 minutes.

2. 3. Coupling

In order to obtain our amphiphilic copolymer, PLA (or else) and PGluOH need to be coupled together. The coupling is achieved between the hydroxyl terminated PLA and one carboxylic acid of PGlu. Several coupling agents can be used to couple these two functions. Usually, the carboxylic acid is activated first by the coupling agent then, the activated species is reacted with the alcohol to form an ester linkage. Dicyclohexylcarbodiimide (DCC) and carbodiimidazole (CDI) are among the most widely used coupling agents in coupling reactions between amino group and carboxylic acid.

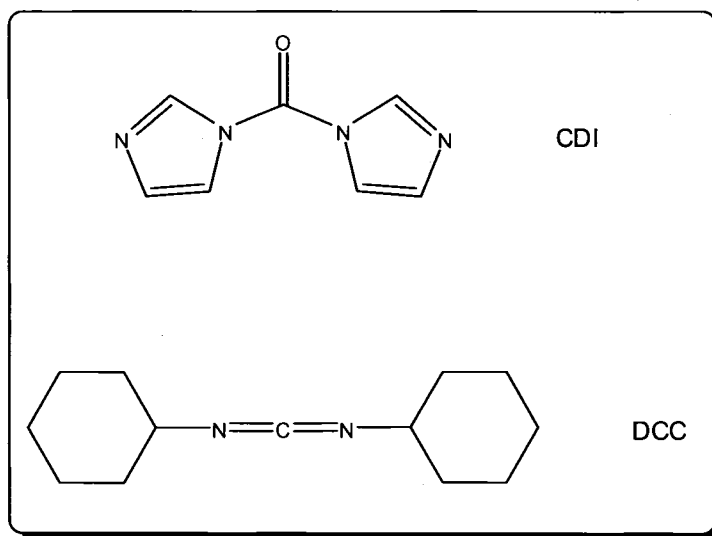


Figure 34: Coupling agents.

DCC is potentially a very toxic compound not suitable for pharmaceutical applications. The acute toxicity of CDI is significantly smaller and therefore, we investigated this compound to replace DCC. The work on coupling conditions and parameters is reported elsewhere by Roset.⁵⁹

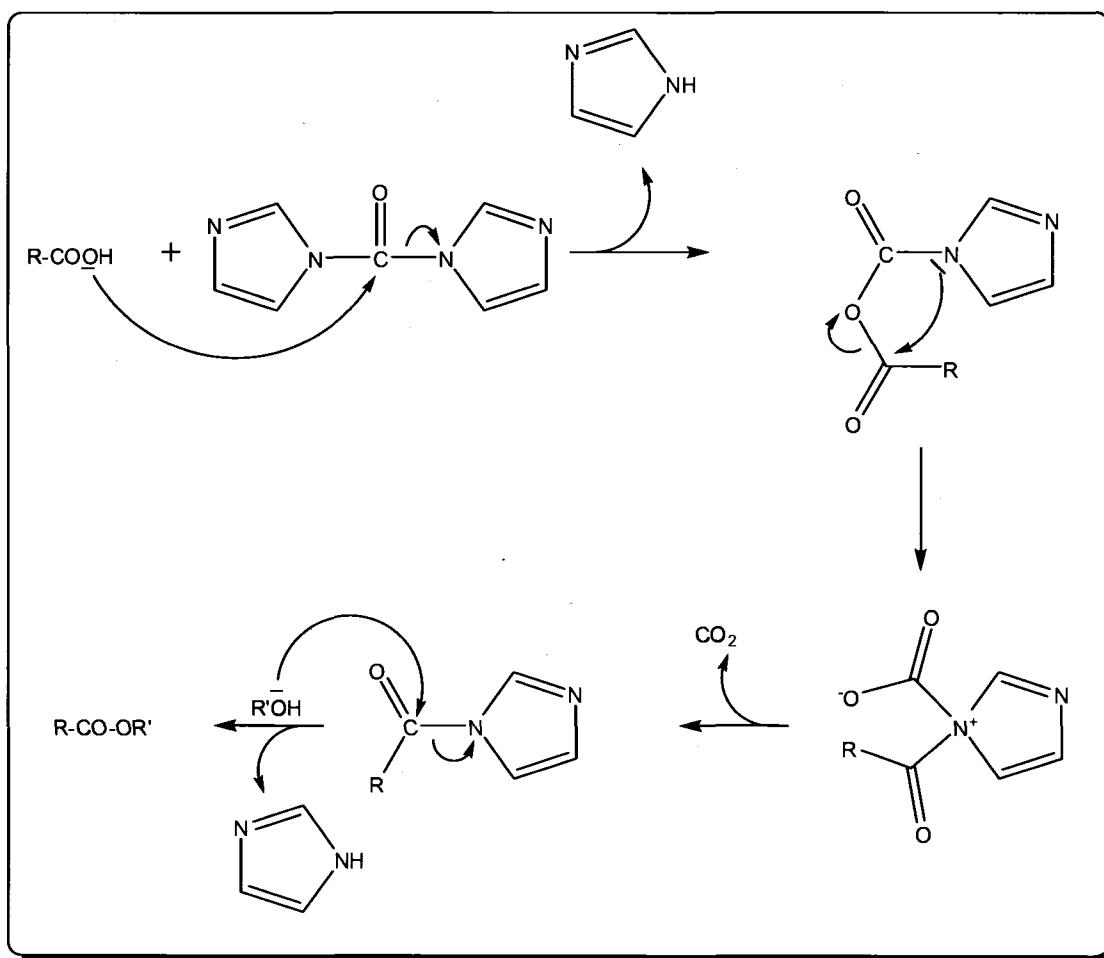


Figure 35: CDI coupling: reaction of N, N'-carbonyldiimidazole with carboxylic acid to form imidazolide followed by transacylation reaction of imidazolide to form esters.⁶⁰

Coupling with CDI starts with an activation reaction. CDI can activate several compounds such as amines for the formation of amide linkage, carboxylic acids or alcohols. When alcohols and carboxylic acids are present, the latter are activated first.⁶⁰ Then the activated $-\text{COOH}$ reacts with a nucleophile such as an alcohol, and an ester linkage is obtained between the carboxylic acid and the alcohol.

Coupling was done between the OH terminated PLA or PEG-PLA and a COOH of a poly(glutamic acid) chain. PGLuOH was first dissolved in NMP and

activated by the coupling agent CDI, then the macroalcohol is added, and the compounds are left reacting for an hour at 10°C; then the solution is precipitated in 5 volumes of water containing 1.1 equivalents of NaOH in order to have the carboxylic acids of the PGLu in their deprotonated form, PGLuO⁻Na⁺. The polymer is washed several times with basic water with the goal of removing non-coupled chains of PGLuOH.

Table 6: List of diblock and triblocks synthesized.

Triblocks PEG-PLA-Pglu			
ID	MW PEG (g/mol)	MW PLA (g/mol)	MW Pglu (g/mol)
EC11	2000	6850	12900
EC12	2000	6850	12900
EC15	2000	6850	12900
EC46	2000	10000	12900
EC47	2000	4000	12900
EC51	2000	6850	12900
EC88	2000	10000	12900
EC98	2000	28000	12900
EC120	2000	7500	12900
EC150	2000	7300	12900
EC183	2000	4500	9000
EC186	2000	7300	12300
Triblocks PEG-PCL-Pglu			
ID	MW PEG	MW PCL	MW Pglu (g/mol)
EC35	2000	6400	12900
EC42	2000	6300	12900
EC54	2000	6300	12900
EC58	2000	4700	12900
Diblocks PLA-Pglu			
ID		MW PLA	MW Pglu (g/mol)
EC126		10800	12900
EC149		8000	12900
EC151		1400	12900
EC160		9900	9300

The efficiency of coupling can be monitored by ^1H NMR by a calculation based on the known MW of the diblock PEG-PLA. A typical ^1H NMR spectrum of the triblock copolymer is given in figure 36.

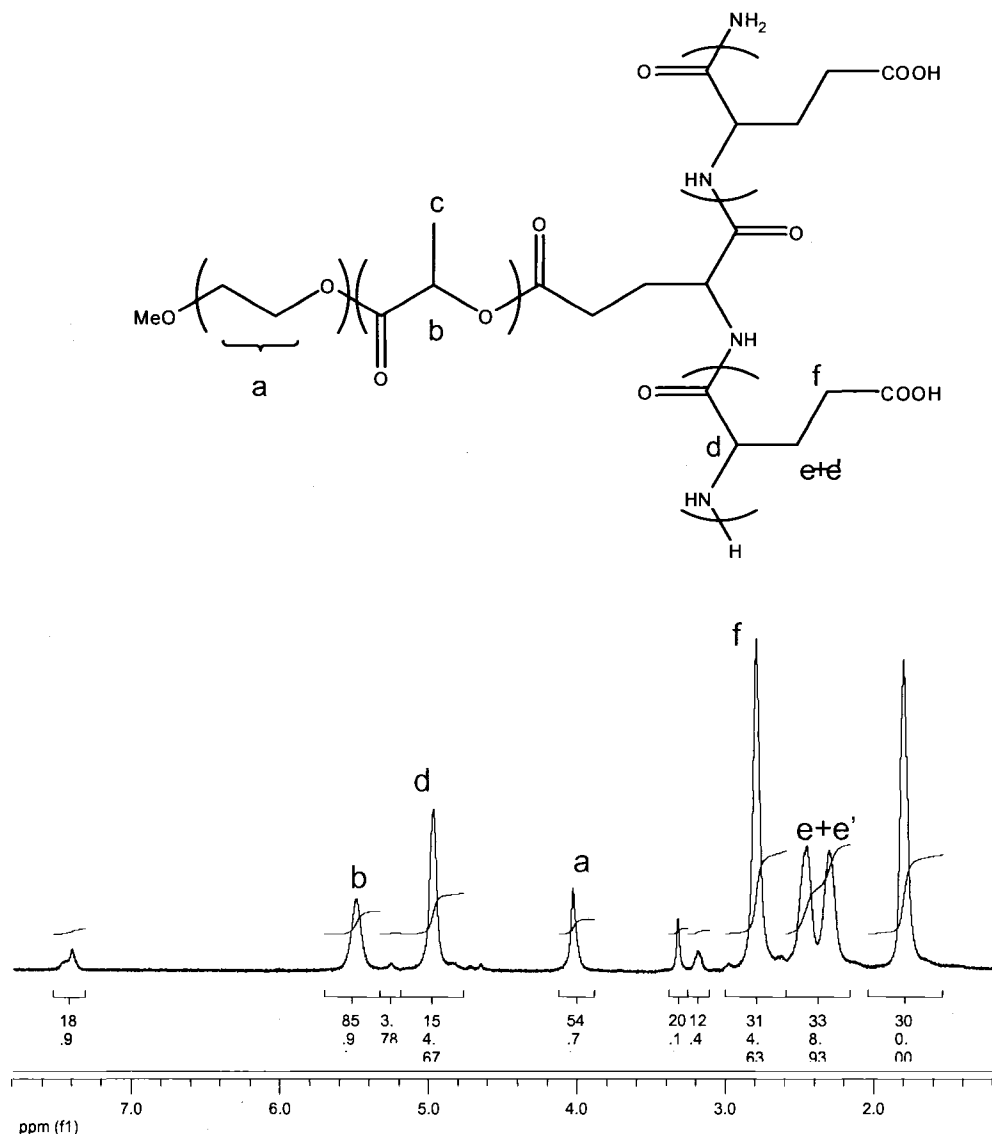


Figure 36: ^1H NMR spectrum of PEG-PLA-PGlu in d-TFA.

There are two major drawbacks when using such a method for coupling of diblock with PGLuOH. The first problem is due to low coupling yields, usually between 50 to 75%. The coupling yields could be improved by either a longer

reaction time or heating. However, this would lead to undesired side reactions in the mixture, such as the formation of amide bonds and possibly anhydrides.

Amides can be prepared by reacting a carboxylic acid with CDI to form imidazolides, followed by addition of an amine at room temperature (primary and secondary amines).⁶¹

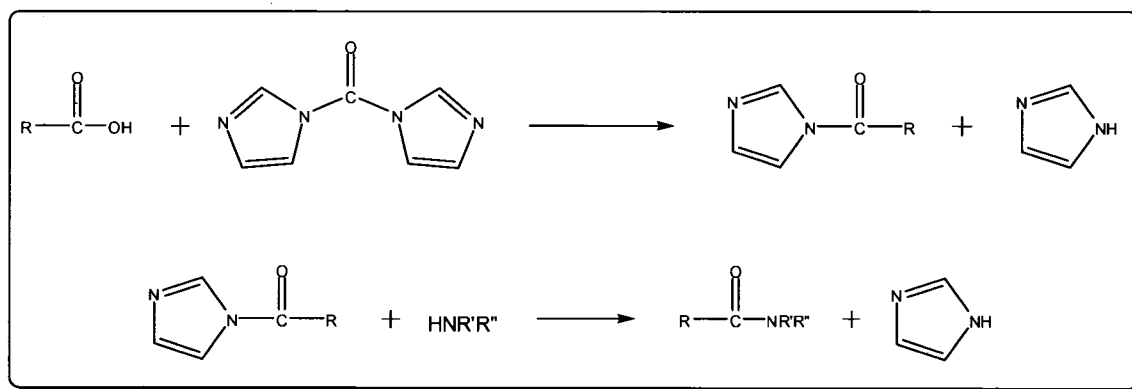


Figure 37: Synthesis of amides using imidazole.⁶¹

Such a reaction could produce intra and inter molecular amide bonds, changing the PGLu structure.

Staab⁶⁰ mentioned that anhydrides of carboxylic acids can be obtained at room temperature by reaction of an imidazolide with a carboxylic acid if the equilibrium is pulled toward anhydride formation. This is likely happening if the formation of an irreversible complex with imidazole is formed.

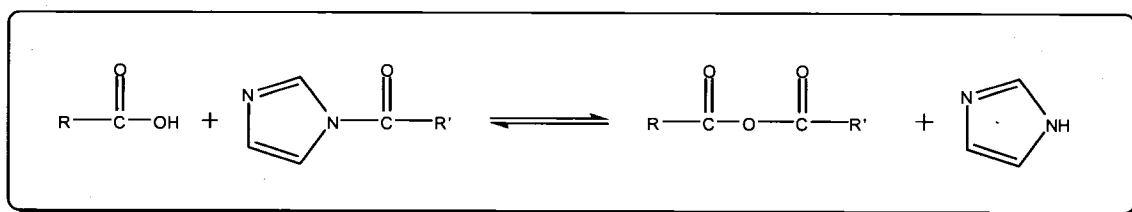


Figure 38: Formation of anhydrides of carboxylic acids.

In our synthesis, it is possible to have traces of trifluoroacetic acid (TFA) from the precedent step, the deprotection of the poly(benzyl glutamate). The carboxylic acid from TFA can form a complex with imidazole, allowing the formation of some anhydrides by stabilization of the imidazole product.

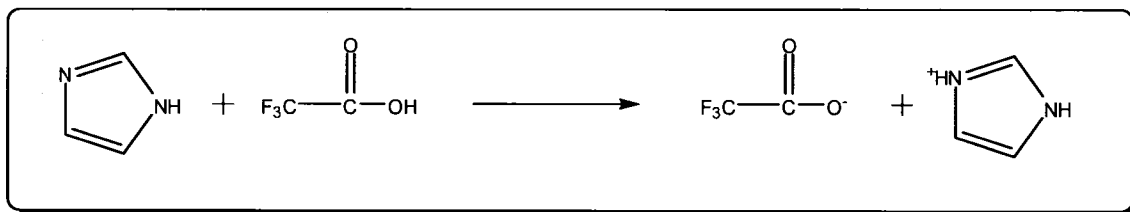


Figure 39: Stabilization of imidazole with trifluoroacetic acid.

Figure 40 is a non-exhaustive list where different structures obtained with such reactions are represented.

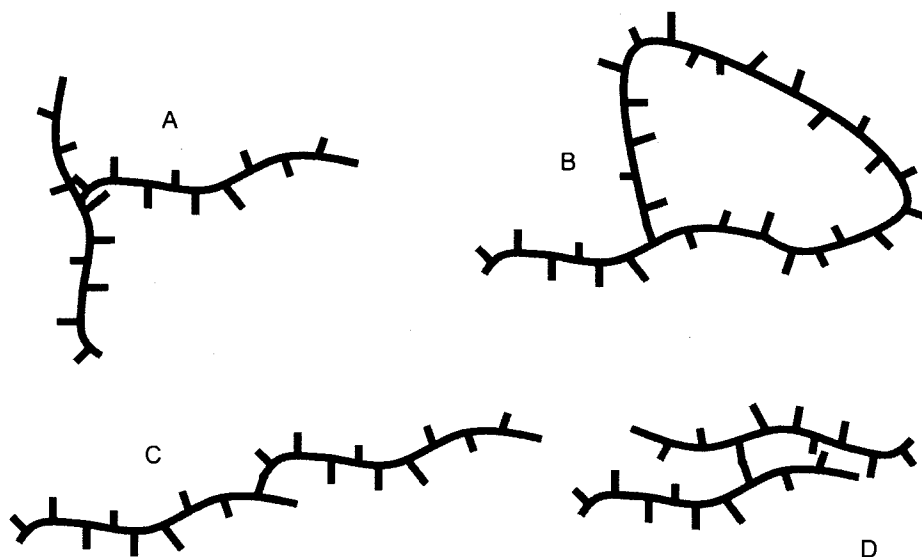


Figure 40: Possible structures of PGLuOH resulting from side reactions. A: coupling of a backbone tertiary amine with a COOH; B: back-biting coupling of a terminal NH₂ with a COOH; C: Intermolecular coupling between terminal amine and COOH; D: intermolecular anhydride formation between two COOH.

The second drawback associated with this method, is the lack of control over the architecture of the polymer. The stoichiometry of the coupling is calculated in such a way that, statistically, only one PLA is coupled per PGluOH chain. However it is likely that we can have two or even more PLA chains per PGluOH.

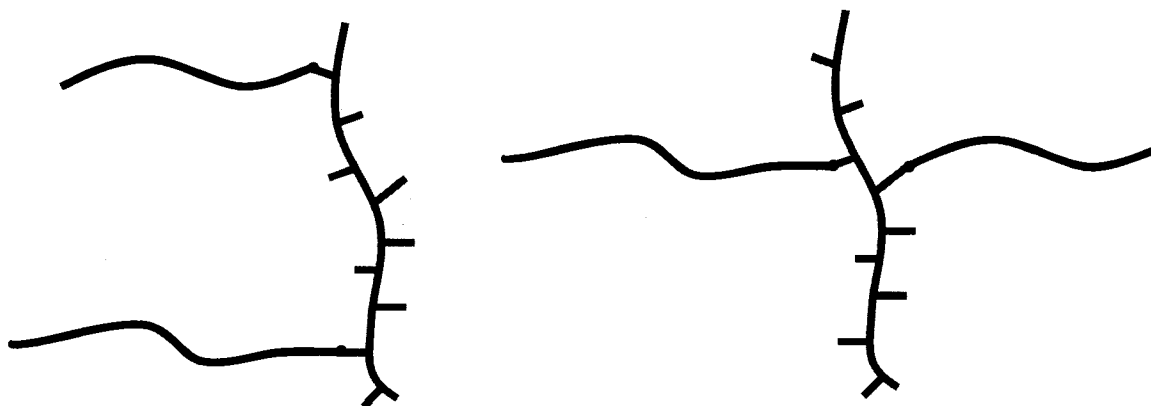


Figure 41: Example of structures displaying 2 PLA chains (in blue) for one PGluOH chain.

In addition, the coupling of a PLA chain on the carboxylic acids of PGluOH may happen in very different places. There is no preferential site for the attachment of the hydroxyl terminated function. It can be on the last unit of a PGlu chain, as well as in the center. This uncertainty leads to very different structures, potentially from linear copolymers to branched ones.

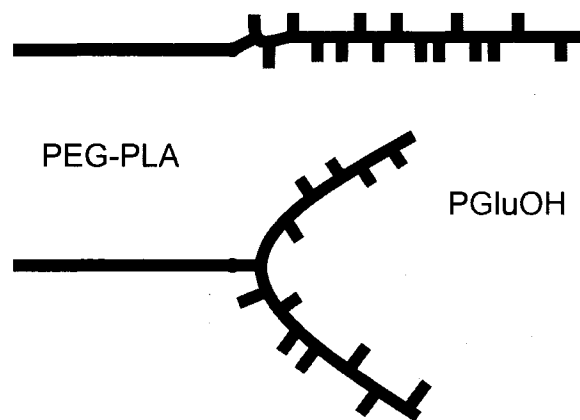


Figure 42: linear and branched structures of the copolymer using CDI coupling according to site of coupling.

In conclusion we believe that our copolymers might have a large variety of structures, obtained in a non-controlled manner, and yielding a mixture of different species. This structure disparity between the chains might be a potential obstacle to the formation of regular assemblies. This topic will be discussed later in Chapter III.

2. 4. Second synthetic pathway: macro amine as initiator of NCA opening

Another pathway for the synthesis of the copolymer was explored. The idea was to modify the PLA and use it as a macroamine for the ring-opening of the NCA monomer. Though this process requires one more step compared to the traditional coupling method described in the precedent paragraph, it would potentially allow a better control on polymer architecture and offers multiple synthetic modifications.

It is desirable to have a good control on the polymer architecture and molecular weight. It is one of the keys to obtain well defined self assemblies. The coupling method does not allow control of poly(glutamic acid) branching.

Several groups reported the ROP of NCA with macroamines. Gotsche synthesized a series of PLA-block-polyaminoacids with PLA-NH₂ macroinitiators prepared in two different ways: the first macroinitiator was obtained by ROP of lactide in presence of the in situ initiator formed by Zn and N-Boc-aminopropanol, followed by deprotection of the amine. The second PLA-NH₂ was prepared by endcapping PLA-OH with N-Boc-AA followed by deprotection of the amine.⁶² Other polymeric initiators were reported, such as a mono amine terminated PEG as the initiator to obtain poly(benzyl glutamate-co-ethylene glycol).³⁴

We used lysine(Fmoc)₂ to functionalize the PLA. When the deprotection of Fmoc is complete, we obtain a macrodiamine, PLA(NH₂)₂. This primary diamine will be used to ring open the NCA under classical conditions described before. There is no reason to believe that the two amines on the poly(lactic acid) present a significant difference in their ability to initiate the NCA opening.

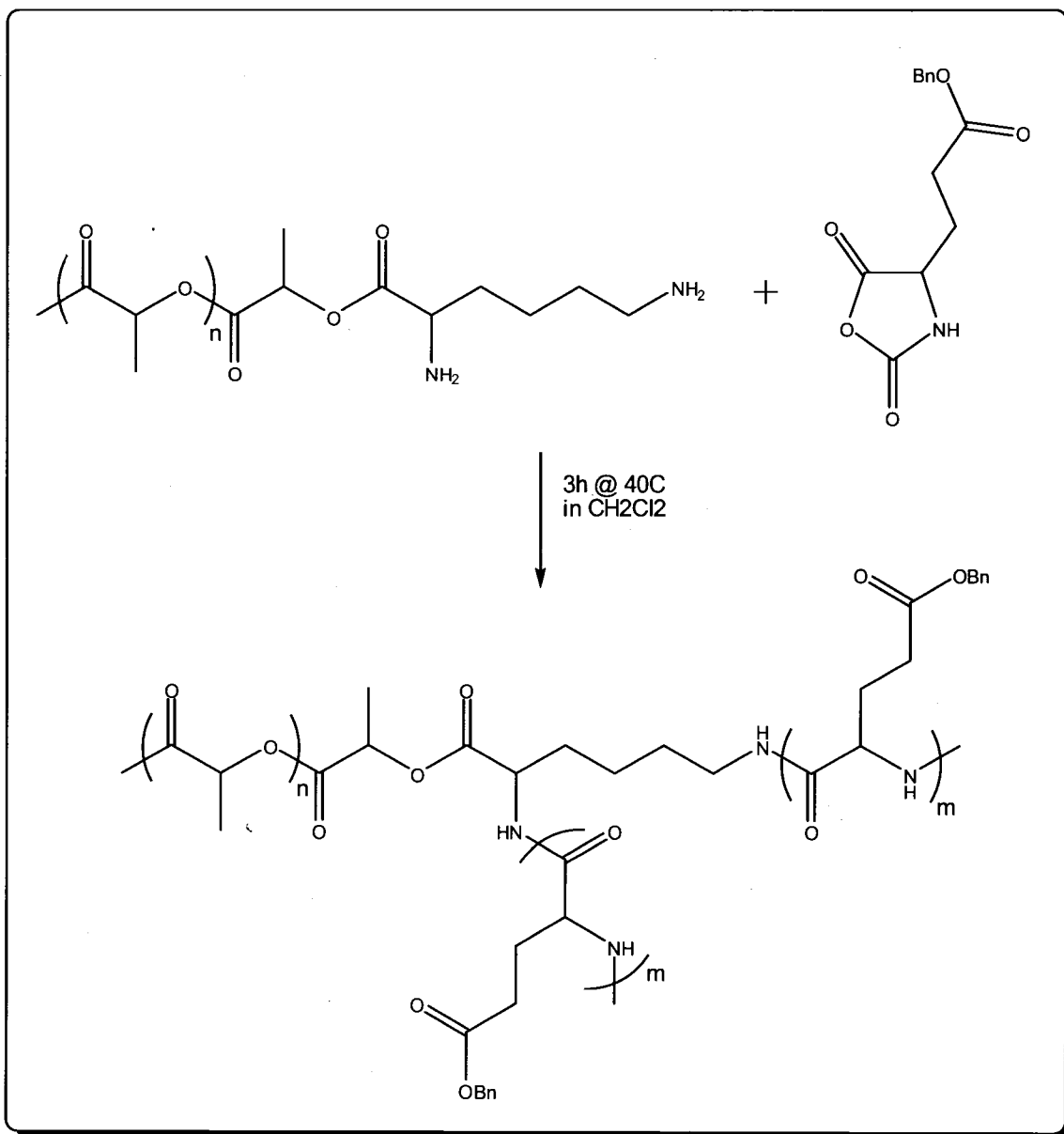


Figure 43: NCA polymerization with macroamine.

Therefore this macromamine is thought to initiate the growth of two PGLu branches of equal molecular weight, leading to a polymer with a controlled structure. By adjusting the ratio of monomer to PLA(NH₂)₂, it is possible to tune the length of the PGLu branches as needed.

After NCA polymerization is complete, the benzyl group is removed using a method described precedently to obtain the final polymer.

2. 4. 1. Activation of COOH from Fmoc-Lys(Fmoc)-OH

As we saw before, the coupling between a carboxylic acid and an alcohol is realized by activation of the COOH prior to reaction with OH. Here the activation of the protected lysine was done using CDI as the activator. The PLA-OH terminated reacted for 1 hour with CDI in chloroform. Lysine is added to the mixture in order to start the coupling.

2. 4. 2. Coupling PLA-OH with activated Fmoc-Lys(Fmoc)-OH

The first step in this synthesis is the coupling of PLA-OH terminated with a protected amine. Since we were interested in the synthesis of a branched architecture, we looked for a diamine having an available carboxylic group to be coupled with PLA. We chose lysine as the diamine. Lysine is commercially available with two Fmoc groups protecting the amines, and the COOH unprotected, as Fmoc-Lys(Fmoc)-OH.

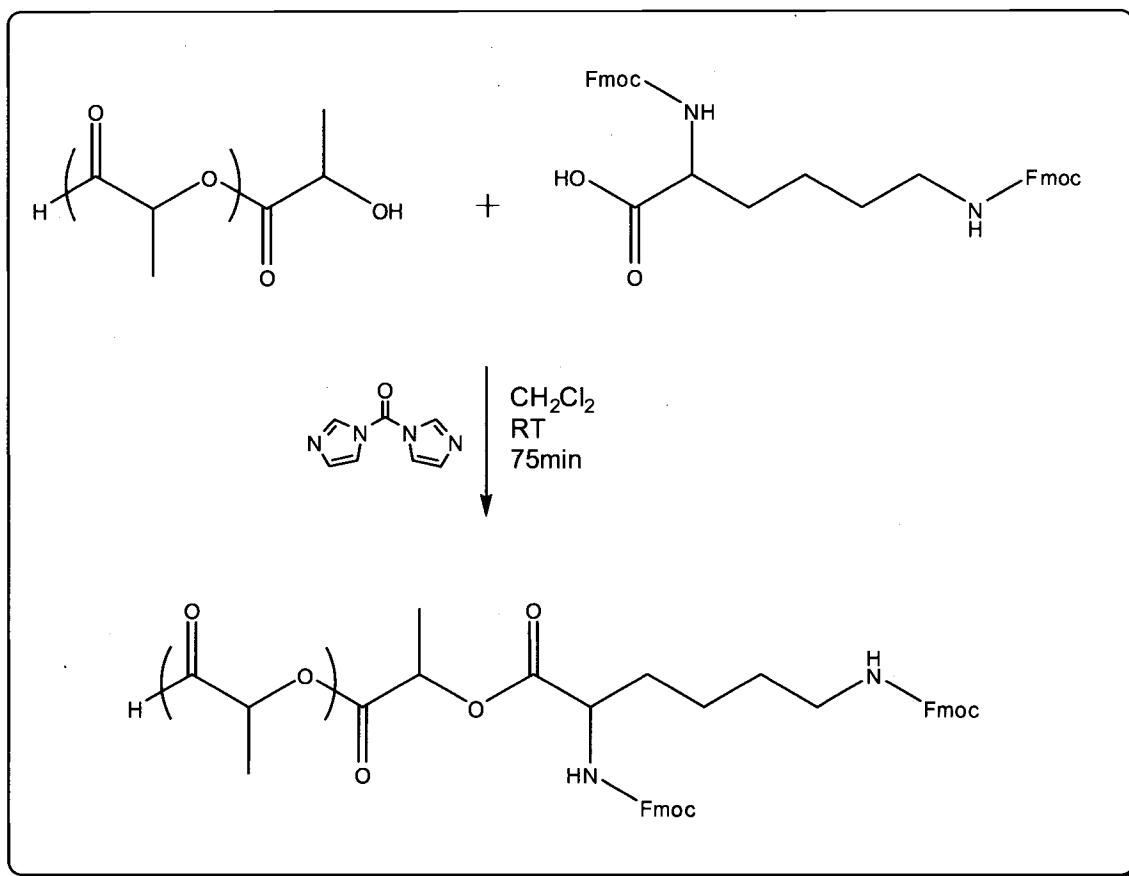


Figure 44: Coupling of poly(lactic acid) with Fmoc-Lys(Fmoc)-OH using CDI as coupling agent.

The coupling reaction was described previously. No specific characterization of this step was performed.

In fact, the most efficient proof of the functionalization of the PEG-PLA was the successful synthesis of PEG-PLA-PGluBn by ROP of NCA (see 2. 4. 4.).

2. 4. 3. Fmoc deprotection

After coupling, the Fmoc protecting groups are removed by a classical deprotection method,⁶³ using piperidine as a weak base to knock off the Fluorenyl group, producing CO₂ as a byproduct.

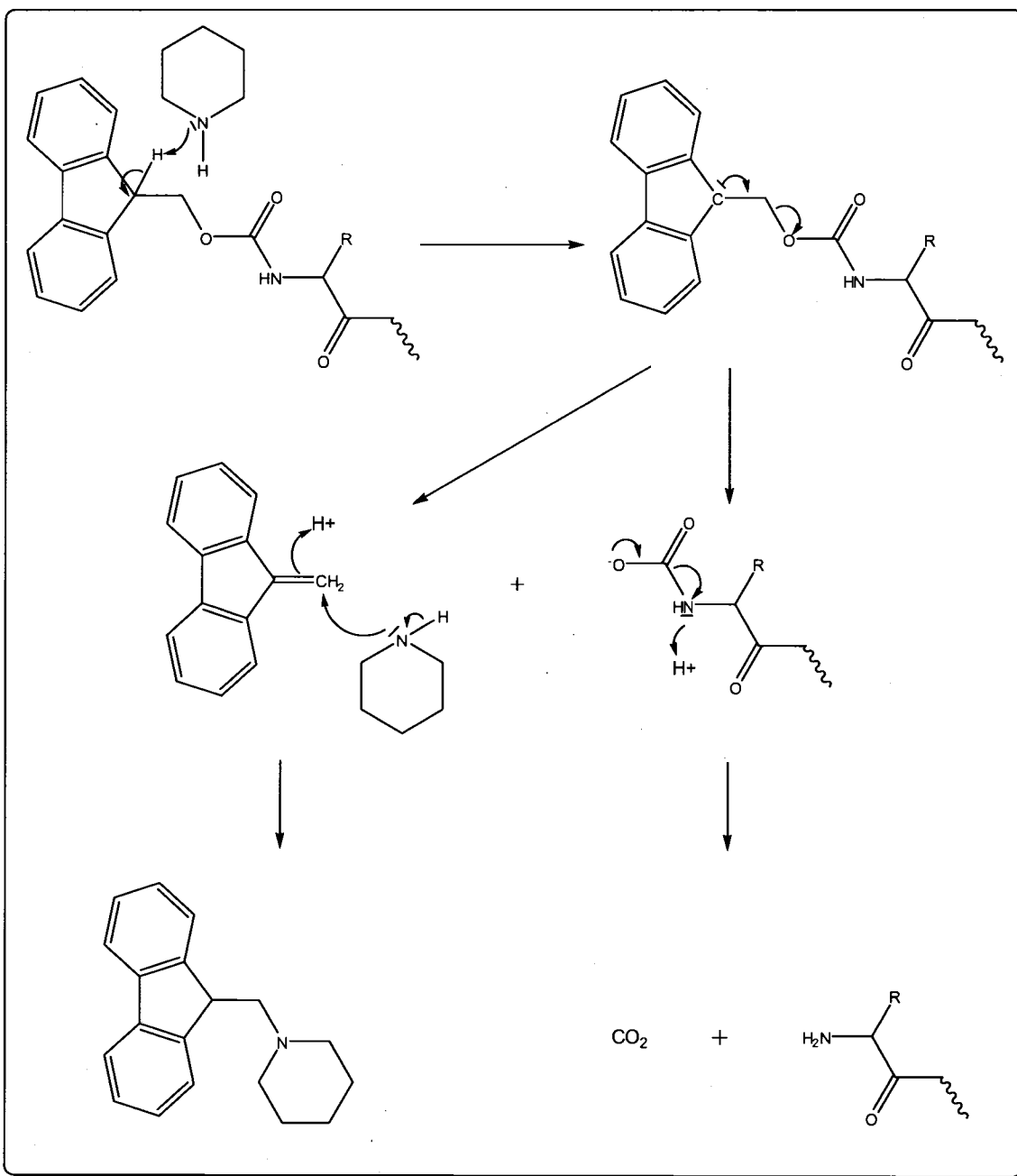


Figure 45: Scheme for Fmoc cleavage.

The Fmoc protected lysine was chosen for the easy removal of the protective group. Traditionally a mild base such as piperidine is used to knock off

the Fmoc. Piperidine is used at 30 % in DCM or chloroform, for a few minutes. Excellent yields are obtained but recovery of the deprotected PLA provided us with some challenge. Obviously it is necessary to remove the piperidine since it could interfere with the macroamine and preferentially open the NCA in the next step. One of the issues is that piperidine seems to help solubilizing the polymer in several solvents traditionally used for precipitation of PLA. Therefore, the solid cannot be filtered. Piperidine is not removed easily, by any mean (rotovapored...).

In order to overcome this problem, we looked at other possibilities for the deprotection of Fmoc. Another widely used technique is the TriFluoroAcetic acid (TFA) acidolysis, with an ion scavenger. We chose not to use this method in order to avoid using TFA. The second possibility that we preferred was to look for a somewhat stronger base than piperidine that we could use in smaller amount (vs. 30% v/v). Among several candidates we came up with the use of a tertiary amine: 1,8-Diazabicyclo[5.4.0]undec-7-ene, or more commonly DBU.

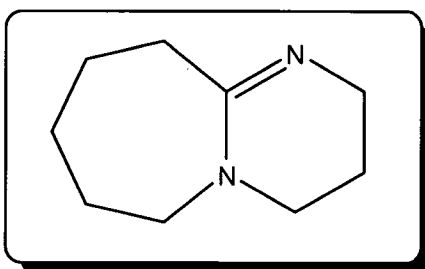


Figure 46: 1, 8-Diazabicyclo[5. 4. 0]undec-7ene.

This amine was used at 1% in CHCl_3 . The reason we chose DBU is that it is a tertiary amine. These compounds can still compete in the ring opening of

NCA but they are much less reactive toward NCA than piperidine, and obviously than the macroamine we intend to use.

2. 4. 4. NCA polymerization with PLA-NH₂

A few examples of NCA polymerization with macroamines have been reported. Modified PLA-NH₂ macroamines were reported to polymerize NCA under mild conditions (room temperature during 48h). As an example Gotsche et. al.⁶² obtained PLA homopolymers functionalized with NH₂ using both a modified Zinc alcoholate catalyst and the coupling/deprotection approach used in this work.

So far, we tried to polymerize NCA with our macroamine in different solvents with varying reaction times.

Table 7: NCA polymerizations with macroamine initiator PEG-PLA(NH₂)₂.

ID	Initiator	T	t	solvent	M/I	[initiator] mol/L	Quencher
EC156	PEG-PLA(NH ₂) ₂	RT	3 h	DCM	100	9.056E-07	MeOH
EC178	PEG-PLA(NH ₂) ₂	RT	48 h	Chloroform	100	0.00000101	Ether
EC181	PEG-PLA(NH ₂) ₂	RT	3 h	NMP	100	0.0000032	MeOH

The polymerization was followed by ¹H NMR and GPC. The reaction in NMP at room temperature during 3 hours, i. e. the condition we are using to ring open NCA with a conventional primary amine, did not yield any polymer as shown on GPC traces. The second 3 hours reaction in DCM did not work either.

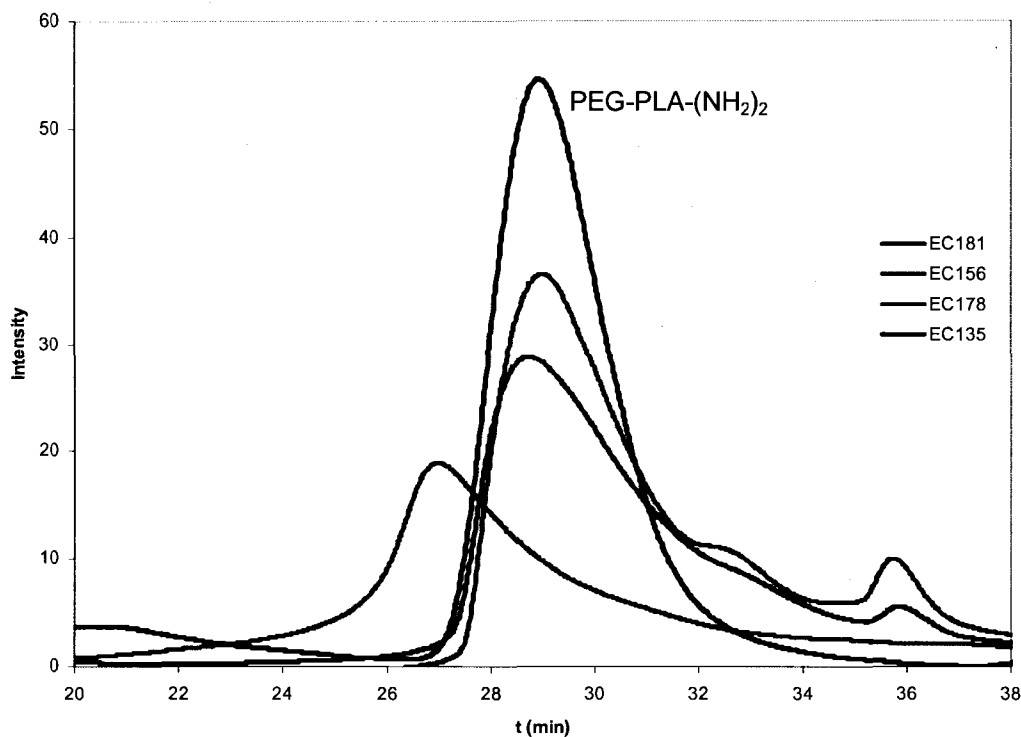


Figure 47: GPC traces of PEG-PLA-(NH₂)₂ macroamine initiator (EC177) and PEG-PLA-PGluBn copolymers.

According to the GPC traces, the polymerization in chloroform held for 48h at room temperature (EC178) did work and yielded a polymer with a broad polydispersity of 1.9. Using ¹H NMR, we calculated that the chains grown on the PEG-PLA macrodiamine were a bit shorter than the targeted molecular weight, in the order of 59 units versus 100.

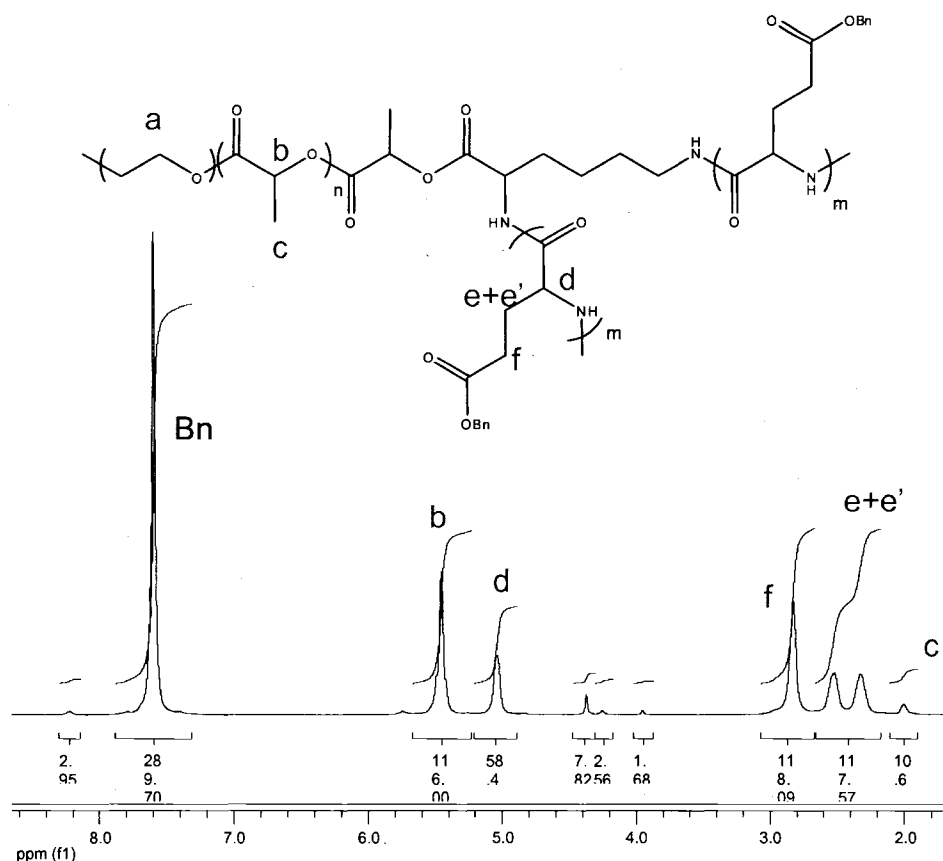
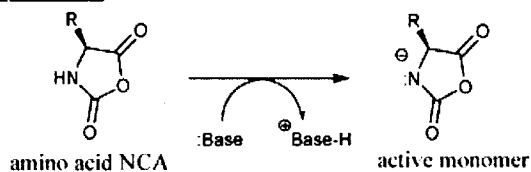


Figure 48: d-TFA ¹H NMR of PEG-PLA-PGLuBn initiated by PEG-PLA(NH₂)₂ macroamine.

This estimation is based on the integral of either e+e' or f, counting for 2H respectively, and the peak of the methine of PLA, b. It is possible that the washes from the precedent step were not efficient enough, leaving some DBU in solution. As we saw before, DBU is a tertiary amine. Even though those amines are not the preferential compounds employed for the opening of NCAs, they have been found to be potential catalysts. The amine abstracts the proton on the nitrogen atom, creating a very reactive anion. The anion can attack the carbon atom of the cyclic carbonyl ring opening the NCA.

Initiation



Propagation

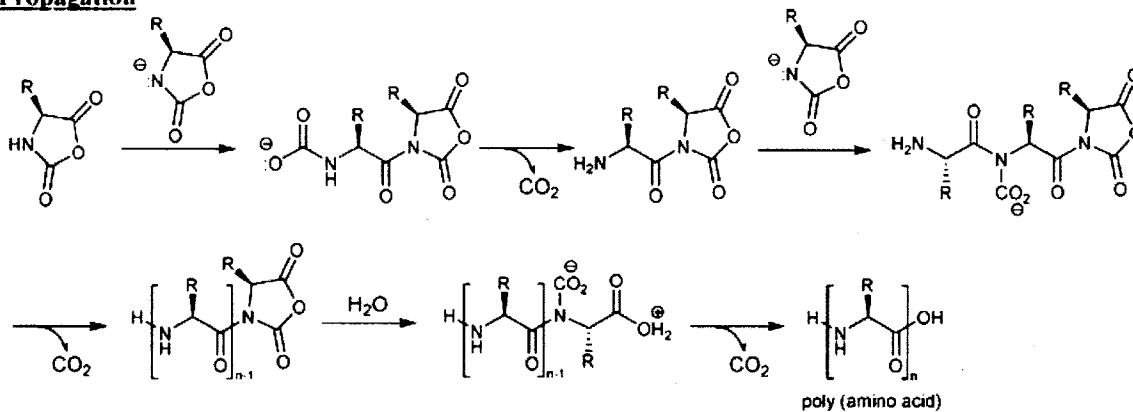


Figure 49: Initiation of NCA polymerization with tertiary amine.⁶⁴

If DBU is present in solution it can eventually compete with the macroamine. The formation of the reactive ion was found to be extremely slow, but it is likely to happen in the timescale of the reaction. This side reaction could explain the very low molecular weight polymer fraction that we can observe on the figure 43, corresponding to the bumps around 36 minutes of elution.

The yield off the reaction was also found to be quite low (<50%). We think it could be the result of a significant fraction of the poly(lactic acid) that was not functionalized in the previous step, and therefore it was not able to ring open the NCA.

Both this later observation and the occurrence of two distinct amine initiators (namely the macroamine and DBU) in the same batch yielding two types of PGLu could explain the wide distribution characterized by a PDI of 1.9.

There are many candidates that could be used as the multifunctional link between PLA and PGLu. We used lysine for its interesting diamine functionality, and its commercial availability in the Fmoc-protected form. Again there are many different protection/deprotection chemistries that we could explore. Moreover, this technique would open numerous possibilities in terms of architecture control.

CHAPTER III

SELF-ASSEMBLY OF THE COPOLYMERS AND INSULIN LOADING

3. 1. Purification and storage

3. 1. 1. Formation of the vesicles

As we saw, our amphiphilic copolymer is designed to self assemble in water. The first self assembly is obtained after synthesis by a precipitation in water with one equivalent of NaOH per COOH of the PGlu chains, in order to obtain the ionized form of the carboxylic acid, COO⁻.

In order to encapsulate insulin, the polymer solution is mixed with an insulin solution at pH 9, and sonicated for 3 minutes (amplitude 100%, 2 seconds on 2 seconds off). We use ultrasound energy as a mean of disrupting the polymeric membranes. Once the membrane is broken and the ultrasound stopped, the polymer chains reassemble, this time allowing the insulin to be trapped inside the vesicles or inside the membrane.

Obviously, a significant part of the energy we provide with ultrasound in order to disrupt the self assembly is actually heating the solution. In the higher range, we are limited by the denaturation of the insulin, and in the lower range, by the freezing of water. According to a temperature study described hereafter, we chose to work at 35°C.

This formulation is later referred to as “In&Out” since insulin is potentially present inside and out of the vesicles. It is contrasted to another formulation where the insulin is simply mixed with the polymer solution without sonication: this formulation was called “Out”. If needed, the solutions can be cleaned by ultrafiltration in order to remove free insulin.

3. 1. 2. Purification

The vesicles suspension was ultrafiltered on regenerated cellulose membranes (molecular weight cut off 30kD and 100kD). This operation has two major goals: elimination of solvent, reactants (such as coupling agent) and uncoupled species (solvated PGluO^-), and concentration of the final vesicles.

As we explained before, the reaction mixture in NMP is precipitated in 5 volumes of water. At this point the vesicles are in water containing 20% of NMP. The presence of such an amount of solvent most likely influences the assembly of polymer chains and this explains why we need to eliminate it.

Five volumes of DI water at pH 9 (10^{-5} M in NaOH) are used to accomplish the ultrafiltration cleaning. A tangential filtration apparatus is used (Millipore cartridges, regenerated cellulose, 30 kDa). Several systems have been used prior to this one. Frontal filtration was abandoned since the membranes were rapidly plugged under the applied pressure. A small scale tangential filtration system was also tested.

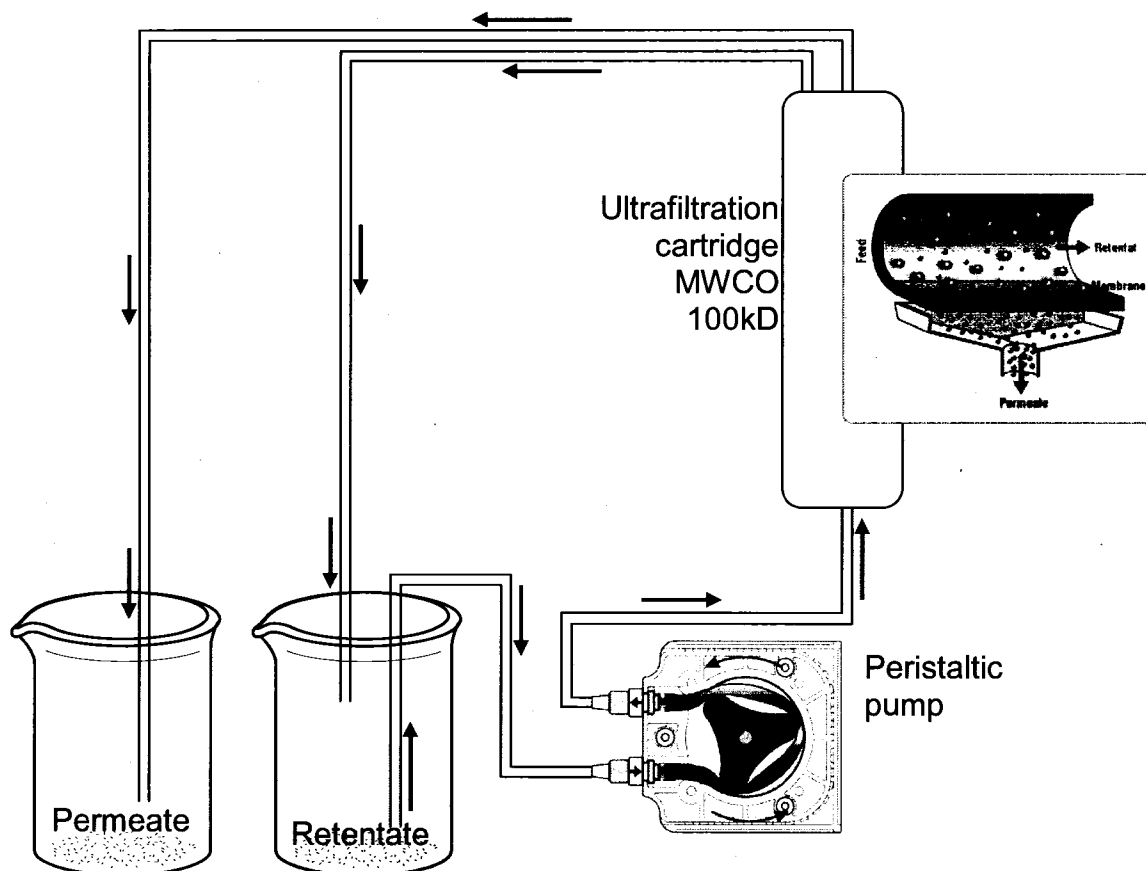


Figure 50: Ultrafiltration of the vesicles.

It was later replaced by a large scale cartridge allowing shorter operation times. The instrument set up is described in figure 50. The disadvantage of the system is due to the important volume of the cartridge. This retained volume containing vesicles must be cleaned out of the cartridge. Since it cannot be pushed out with air (it would dry the polymer inside), the polymer must be removed by running water through the cartridge. Therefore, part of the product has to be recovered as a very dilute solution due to the volume used for of the cleaning of the cartridge.

3. 1. 3. Storage

The storage of the nanovesicles is of great importance. One way to control the integrity of our self assemblies is to check if objects can reform after any kind of storage, leading to vesicles with the same diameter, and with colloidal stability that we have directly after the first assembly. The diameters were measured by DLS.

The drug delivery system is designed to biodegrade *in vivo*. Especially the polyester part is susceptible to hydrolysis in slightly acidic media. In order to avoid hydrolysis, either water could be removed by freeze-drying, or alternatively the formulations could be kept at temperatures well below 0°C.

Drying the vesicles was first investigated. We used a freeze drying apparatus to remove water from the clean vesicles suspension. This technique has a great advantage in terms of storage (dry powder) and handling. However the dry vesicles must be redispersed in solution after liophylization. We observed some issues when redispersing the polymer in aqueous media since we were unable to break aggregates and obtain reasonable colloidal stability, even after strong sonication. We believe that aside from reversible interactions between the particles resulting from concentration and some melting, we have formation of anhydrides of carboxylic acid as a result of total dehydration, leading to irreversible aggregates linked by covalent bonds.

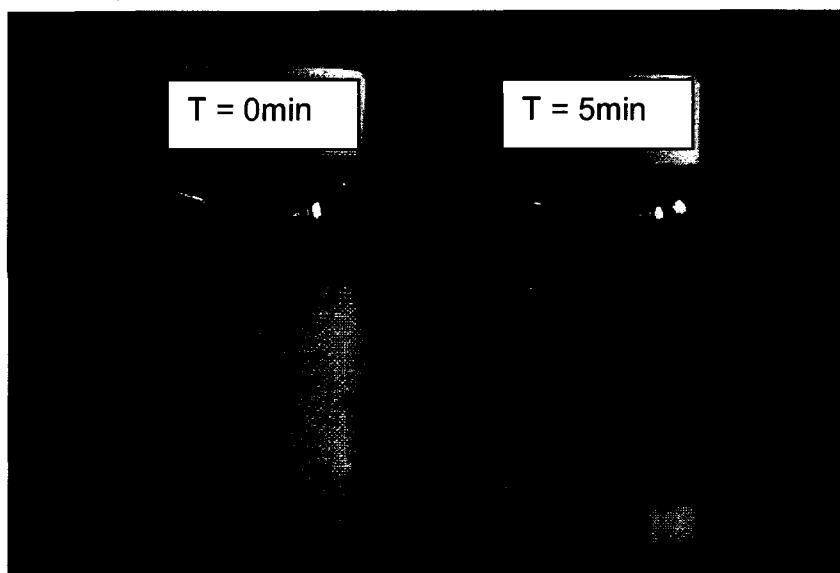


Figure 51: Stability of polymer redispersed in water after liophylization.

To prevent aggregations, we investigated the possibility of cold storage at -80°C in water. This technique is more demanding in terms of storage. Several cryoprotective agents (polyalcohols and sugars for instance) can be used to stabilize nanoparticles. Saez *et al.* reported a freeze-thaw study on PCL and PGLA nanoparticles evaluating the impact of these compounds on the nanoparticles size. They found that the use of a cryoprotective agent was important to keep the integrity of their system.⁶⁵ They observed the formation of irreversible aggregates in the absence of additives.

The goal of a cryoprotective agent is to induce a non-regular packing of the molecules, leading to an increased interstitial space. The density is lower than the packing induced by ice crystals and therefore it provides better protection to nanoparticles. Aggregation and pressure exerted by growing ice crystals is less likely to happen and damage the particles.

Since our particles are slightly different, we performed our own freeze-thawing study. A cycle of freeze-thawing at -80°C was repeated 5 times on the same sample of $\text{PLA}_{137}\text{PGlu}_{72}$ at 0.51% solid. Thawing was done at 35°C for about 2 hours. Sonication was performed with a Branson sonifier with settings of 2 seconds on 2 seconds off, 100% amplitude, for 5 minutes.

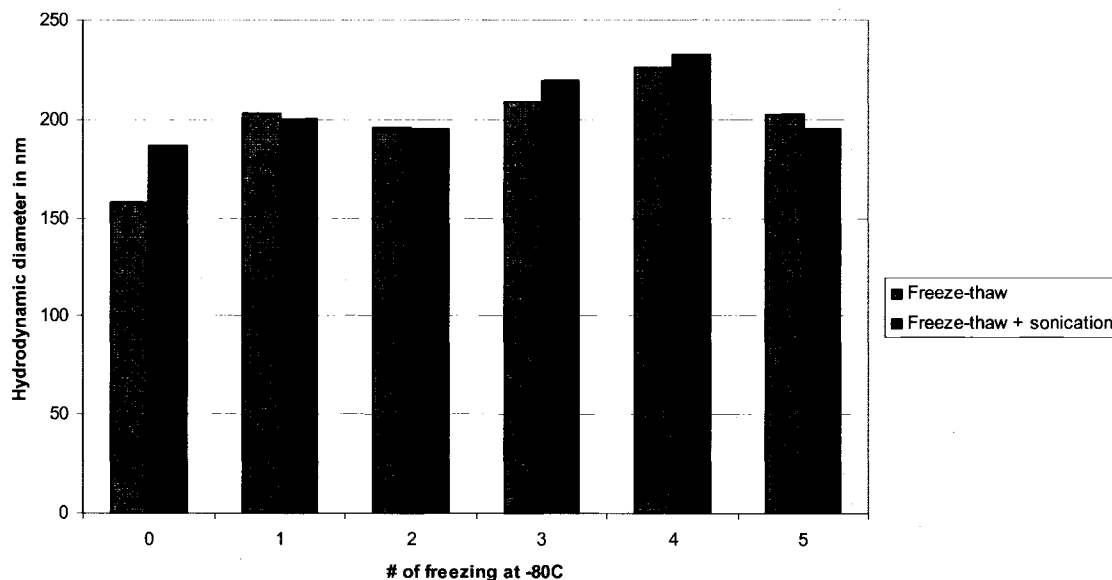


Figure 52: Freeze-thaw study on EC160, $\text{PLA}_{137}\text{PGlu}_{72}$.

Figure 52 shows two interesting results. We can see that the first self assembly, i. e. prior to freezing and sonication, has a significantly smaller average diameter than frozen samples. The second observation shows us a trend from the 2nd to the 4th freezing. The diameter seems to rise regularly, an indication of change in the assembly morphology. At this point, one important thing needs to be noticed. From the first sample (no freezing) to the sample number 4, the pH dropped from 9.3 to 7.7. As we said before, this can be an indication of degradation of the PLA, since it produces lactic acid. But it can also

affect the protonation of the PGlu. Before the 5th freezing the pH was adjusted to 9 again, and the diameter was found to be smaller. The behavior of the vesicles toward external stimuli is detailed in the next part.

As we said, these observations are to be interpreted carefully. On average the variations of size from sample #1 to #5 are not particularly significant. Therefore we think our vesicles are not irreversibly affected upon freezing and thawing. The drop in pH is not likely due to freezing, but is more likely due to the slow degradation of PLA during several thawing. There is no mechanical damage due to freezing, since our vesicles are easily reconstituted.

3. 2. Characterization of the self assemblies

3. 2. 1. Morphology and size characterization of crude vesicles

In the next pages, we briefly describe the panel of techniques used for the characterization of the objects formed by self assembly, and the results for each technique are discussed. A compilation of experimental observations and theory is proposed in paragraph 3. 3.

3. 2. 1. 1. Dynamic Light Scattering (DLS)

Dynamic Light Scattering was the primary technique used to determine the size of our nanoobjects. We used a Nanotracs 250 probe system (Microtrac Inc., PA).

The theory behind this experiment is based on two different assumptions: first the objects must be small enough to undergo Brownian motion in a resting fluid. The motion of such particles can be related to their sizes and this more easily if they can be considered as spherical and of large size compared to molecular level.

Technically speaking, monochromatic light is emitted through the suspension, and it is eventually scattered back with a difference in intensity, due interference between moving neighbor particles. The time dependence of these intensity fluctuations can yield the diffusion coefficient of the particles from which, via the Stokes Einstein equation, the hydrodynamic radius or diameter of the particles can be calculated. The Stokes-Einstein equation:

$$R_H = kT/(6\pi\eta D) \quad (6)$$

where R_H is the hydrodynamic radius, T the temperature, k is the effective interaction parameter, D is the diffusion coefficient and η is the viscosity.

The simplicity of DLS probe allows the live modification of many parameters during measurements. Some parameters give critical information about the self assembly, such as the response toward ionic strength, pH, temperature and solvent content. A typical size distribution obtained for a PLA-PGluOH assembly is provided below:

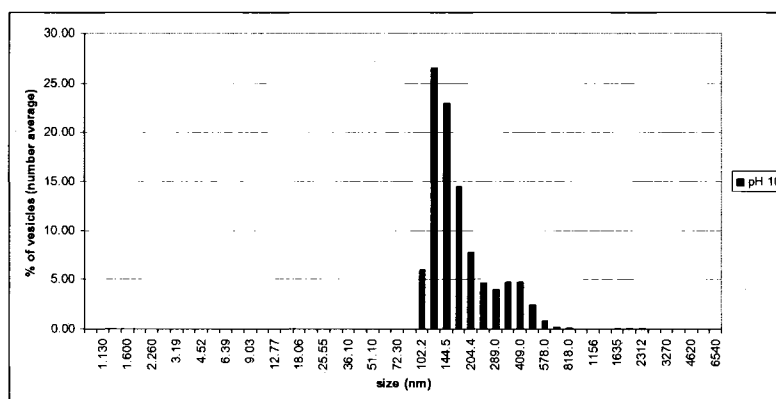


Figure 53: Diameter of vesicles from the self assembly of PLA-PGlu diblock in water.

Influence of pH

We measured the diameter of vesicles at different pHs. To the initial polymer solution in basic water (10^{-5} M NaOH), we slowly added dilute HCl to lower the pH. We found that the mean diameter of the objects was dependent on pH. Larger objects are obtained at acidic pH compared to basic pH.

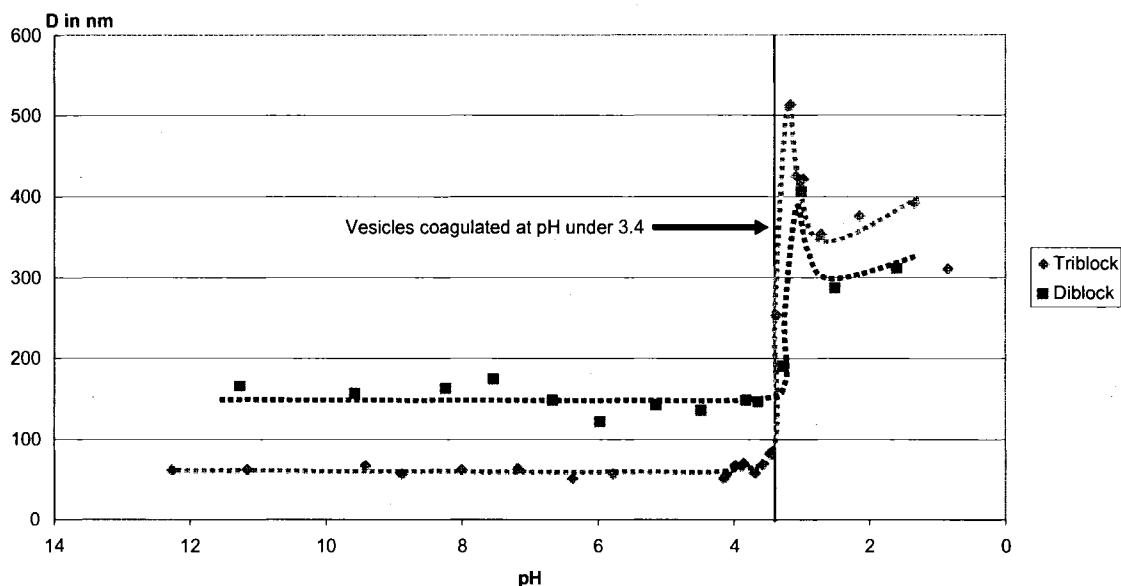


Figure 54: Diameter of diblock and triblock self assembly as a function of pH.

Figure 54 illustrates the evolution of size versus pH. For both diblock and triblock copolymers, there is a very clear threshold at pH 3.5, where vesicles lose colloidal stability. After this pH value, one should be careful about interpretation of the DLS values since the suspension is not stable anymore.

Ionic strength

The ionic strength was increased using NaCl crystals dissolved in the solution. Though the effect was less obvious than it is for pH, the ionic strength seems to induce a slightly comparable response. We observed on a sample that the diameter of vesicles decreased with salt concentration, until the assembly was disrupted at very high salt content, i. e. 1.85 mol/L.

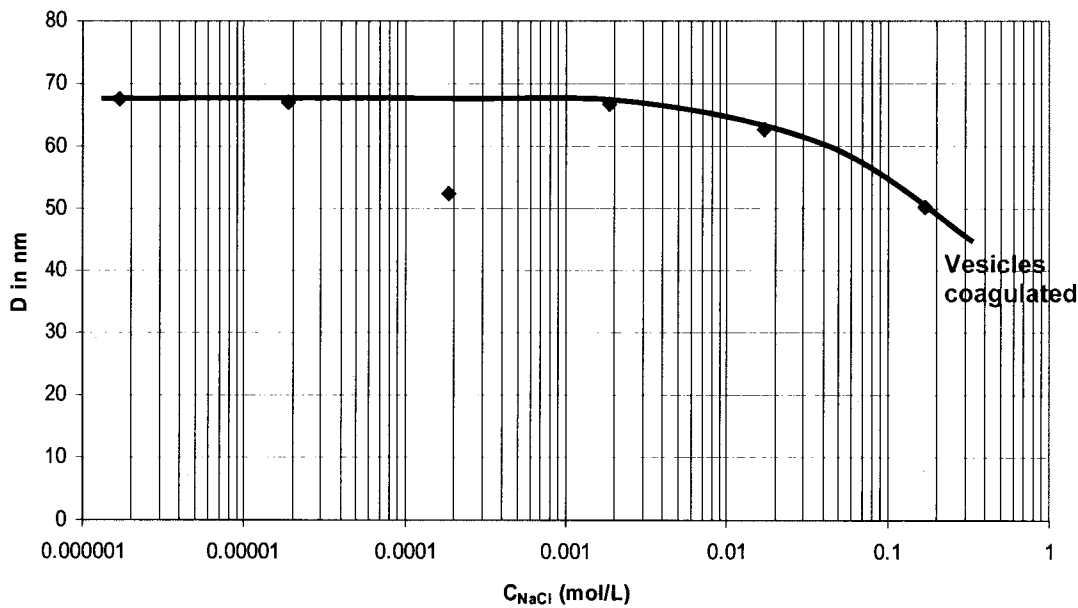


Figure 55: Influence of ionic strength on triblock vesicles diameter at constant pH (7.4).

The C_{salt} concentration values indicated in Figure 55 only refer to the NaCl concentration. It is possible that the salt content is slightly higher due to small amounts of NaOH.

Temperature

We performed a size measurement on the vesicles in water at different temperatures using DLS. The temperature window for the instrument ranged from 10 to 82°C. We observed an interesting trend: there is a significant change of slope in the curve around 25°C for the triblock size, whereas no obvious trend can be identified for the diblock in the temperature range of the experiment.

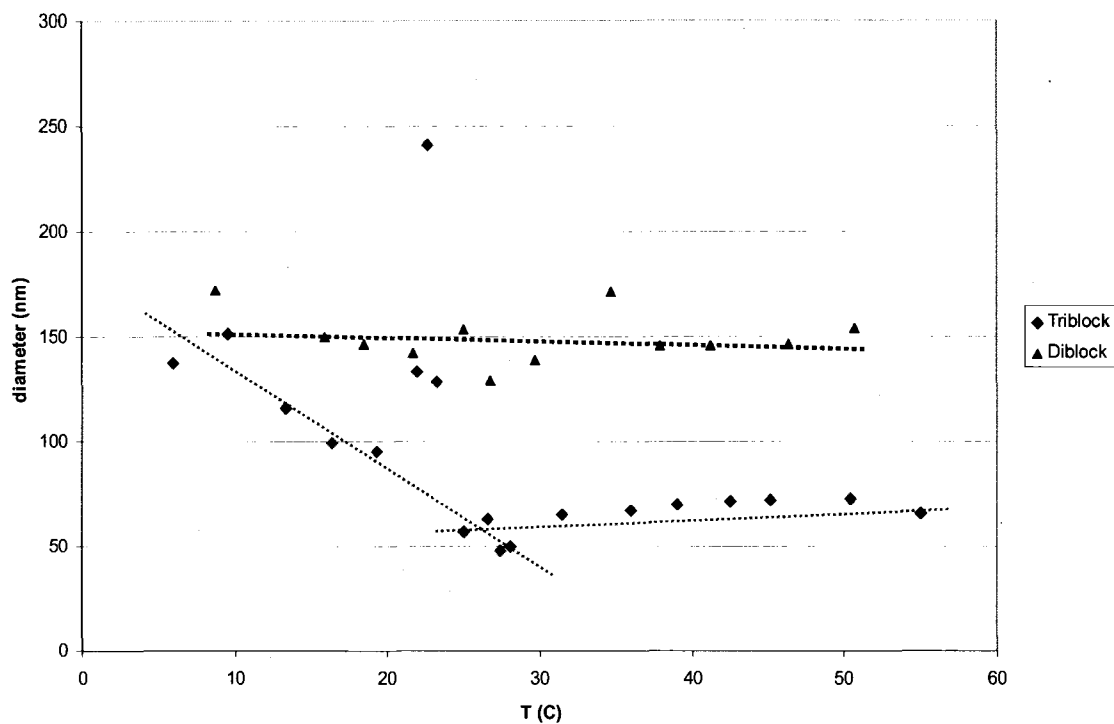


Figure 56: diameter of vesicles as a function of temperature.

The temperature at which the change of slope is observed can be related to another specific temperature: the T_g of the diblock PEG-PLA. According to the Fox equation, and assuming that our diblock is not phase separated in the assembly, the calculated T_g of the diblock used in this experiment ($PEG_{45}PLA_{112}$) is around 33°C (using a PLA T_g of 57°C , and a PEG T_g of -40°C). This observation leads us to think that the triblock copolymer assembly is kinetically trapped in a specific configuration, and it needs to be heated in order to find its equilibrium shape.

Solvent content

In this experiment, NMP was slowly added to the polymer solution up to 65% NMP. At 65 % NMP in water (volume ratio), the solution was clear and DLS could not measure any size, indicating that the polymer chains were in solution and not assembled.

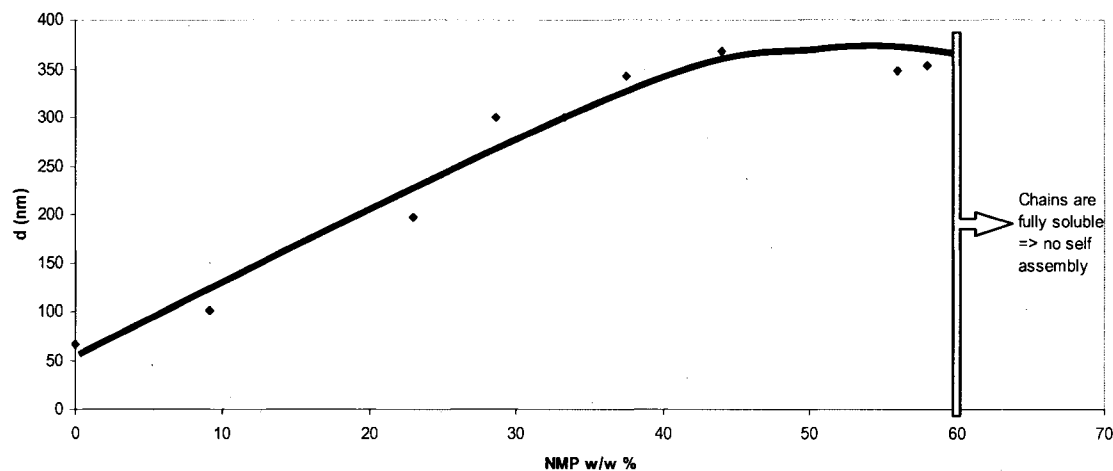


Figure 57: Evolution of vesicles diameter with increasing solvent concentration.

The increase in diameter is more surprising. The polymer chains are perfectly soluble in NMP, and there is no reason they would go into aqueous solution. This means that the interfacial tension decreases with the addition of NMP to the water suspension. Therefore, the vesicles could have a lower diameter without an energy penalty and we observe the contrary.

Diblock vs. triblock

On average, we found that using DLS at room temperature, the self assemblies of diblock PLA-PGlu are spherical nanoobjects with a diameter

around 200 nm, whereas the self assemblies of triblock copolymer have diameters around 80 nm. These discrepancies clearly indicate a difference in morphology.

Table 8: Size of self assemblies.

ID	Polymer	Size (nm)
EC46	PEG ₄₅ PLA ₁₂₃ PGLu ₁₀₀	80
EC120	PEG ₄₅ PLA ₁₀₄ PGLu ₁₀₀	95
EC150	PEG ₄₅ PLA ₁₁₂ PGLu ₁₀₀	100
EC186	PEG ₄₅ PLA ₁₁₂ PGLu ₉₅	70
EC126	PLA ₁₅₀ PGLu ₁₀₀	200
EC151	PLA ₁₉ PGLu ₁₀₀	220
EC160	PLA ₁₃₇ PGLu ₇₂	170

From this table, one can also notice that the sizes change might be consistent with the PGLu MW. The formulations with slightly smaller PGLu lengths have lower diameters.

3. 2. 1. 2. AFM

AFM studies were realized by Jun-Fu Liu on the diblock PLA-PGluOH at different pH. A precedent study by Collette was done on triblock vesicles in the wet state.⁴¹ The sample preparation was quite difficult and the results mitigated. We developed a technique in the dry state focusing on the persistence of the vesicles shape through the whole process. A drop of polymer solution was deposited on a muscovite mica sheet (V-1 quality) seating on liquid nitrogen to obtain instant freezing, and then was lyophilized. The measurements were done on tapping mode.

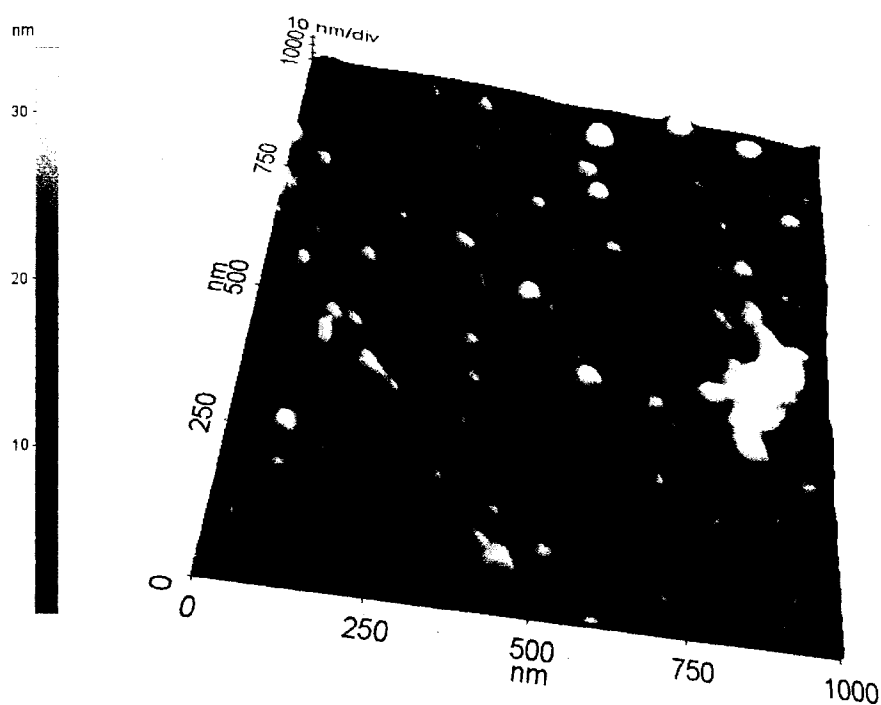


Figure 58: AFM 3D imaging of PEG-PLA-PGlu self-assembled vesicles at pH 10.

According to the pH of the initial solution, the average diameter of the particles is hugely different. It is found to be around at 0.5 μm at pH 3 and 90 nm

at pH 10 (complete reports are given in appendices). In all cases, we noticed that the height of the vesicles is around 10 nm. Most likely, it is due to vesicles flattening. When the water is removed by freeze-drying, nothing prevents the vesicles from collapsing, and therefore, the objects analyzed in AFM are comparable to flat pancakes or discs rather than hollow spheres.

3. 2. 1. 3. Small Angle X-Ray Scattering (SAXS)

The SAXS experiments were done at the University of Pennsylvania by Amelie Roset. Using this technique, a membrane thickness of about 12 nm was found. A further detailed report is provided in [66].

3. 2. 1. 4. Field Flow Fractionation (FFF)

Field Flow Fractionation is a separation technique with the ability to separate molecules, particles or cells with a wide range of molecular weight. The method is at the crossing of chromatography, electrophoresis and centrifuge. A solvent running through a well defined channel geometry is submitted to an external perpendicular field or gradient (hydraulic, thermal, electrical...). Differential flow occurs, separating components into several laminar flows. According to its response toward the external gradient, an object travels in a specific flow, i. e. a specific velocity.

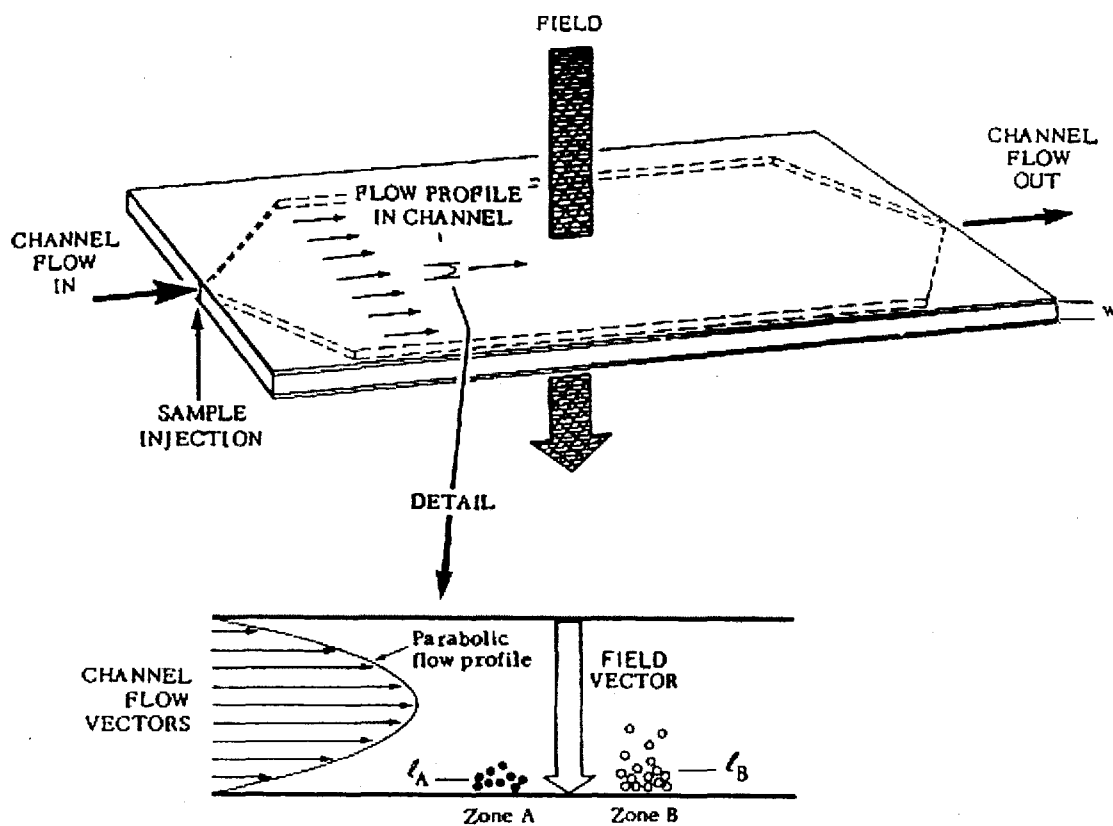


Figure 59: Field-flow fractionation channel showing laminar flow profile and field perpendicular to flow.⁶⁷

From the FFF coupled with MALS detector, we can have two pieces of information: size and absolute MW of the objects. The experiment and data were processed by John Champagne at Wyatt Technology Corporation (Milford, MA).

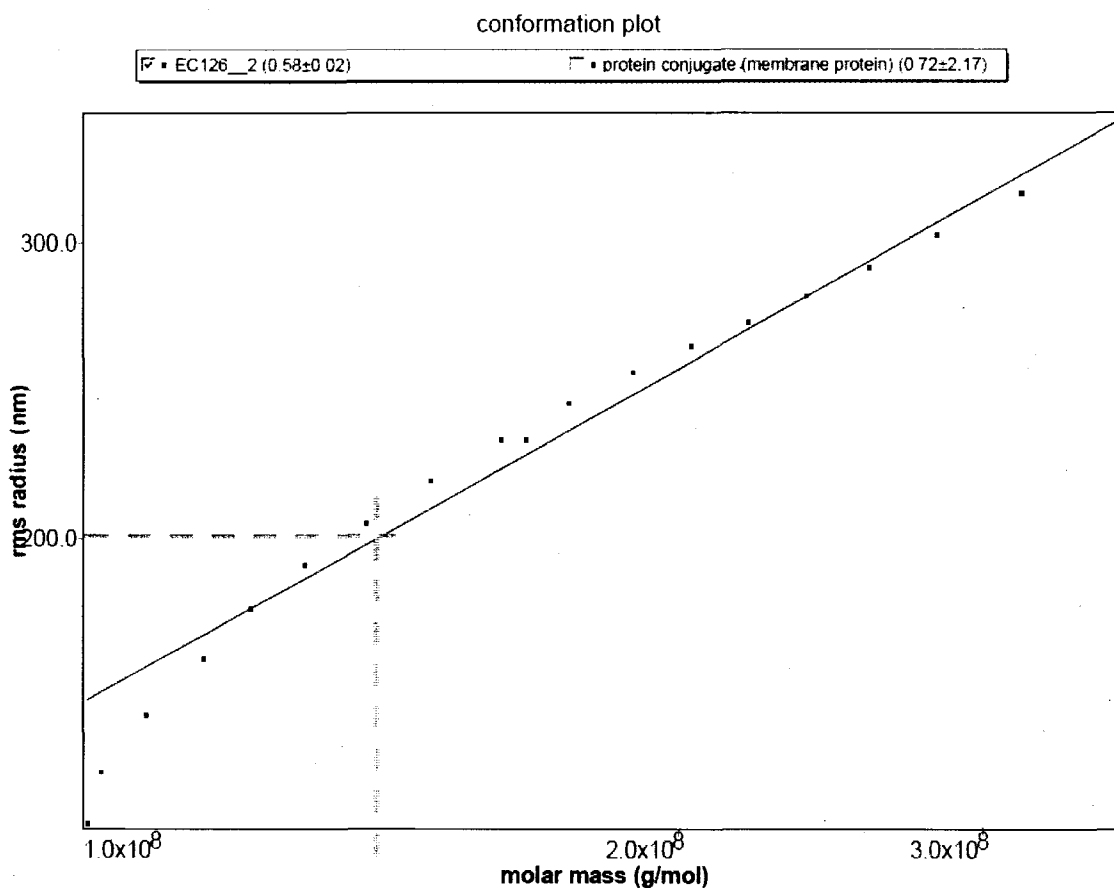


Figure 60: Root Mean Square radius (RMS radius) as a function of the molar mass.

The conformation plot obtained does not give a distribution of size (which has to be determined by DLS for instance), but it gives the molecular weight of self assemblies as a function of the particle size. This is a precious piece of information that can allow us to determine the number of chains involved in one vesicle also called aggregation number. The copolymer used for this study, EC126 is a diblock of PLA-PGlu with a total molecular weight of 23700 g/mol. Therefore, if we take 200nm as the size (consistent with DLS measurements) we can assume that we have $(1.5 \cdot 10^8) / 23700 = 6329$ chains constituting the bilayer membrane of one vesicle. One example of aggregation number calculation was

reported by Shen, for a PS₃₁₀-PAA₅₂ copolymer forming 100nm diameter vesicles.⁶⁸ According to his findings these vesicles were constituted of about 5000 chains. Although the two systems are not really comparable in nature, it is consistent with our results being in an acceptable range.

Using the data provided in Figure 60, a plot of thickness d versus radius was plotted according to equation (5):

$$d = R_1 - R_2 = R_1 - \sqrt[3]{R_1^3 - \frac{3m}{4\rho\pi}} \quad (7)$$

where m is the mass of the vesicle, ρ is the density of the polymer and R_1 is the radius of the vesicle.

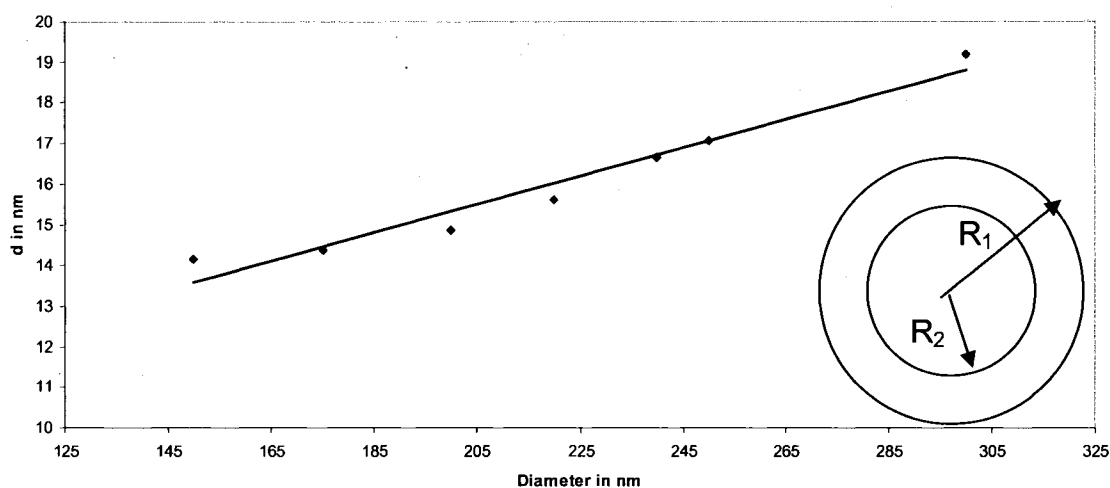


Figure 61: Thickness of membrane as a function of vesicle mass (number of chains).

This plot gives a thickness of about 15nm for our vesicles. The increase of thickness with radius is surprising as this could mean that the structure of the membrane, i. e. the organization of the chains constituting the membrane, is affected by the size of the vesicle. However, the effect is very weak. Interestingly,

the height given by AFM, corresponding to two dry bilayers is very consistent with the measure of thickness obtained by either SAXS or indirectly by FFF.

3. 2. 1. 5. Scanning Electron Microscopic (SEM)

A few attempts were made with Scanning Electron Microscopy to image the vesicles. One of the major issues we encountered was to keep the integrity of the vesicles in the dry state. The sample preparation was made with this aim. A drop of the polymer solution was deposited on a stub covered by a glass sheet held at negative temperature in order to obtain instant freezing. The frozen water was removed by sublimation in high vacuum. The sample was then coated with carbon.

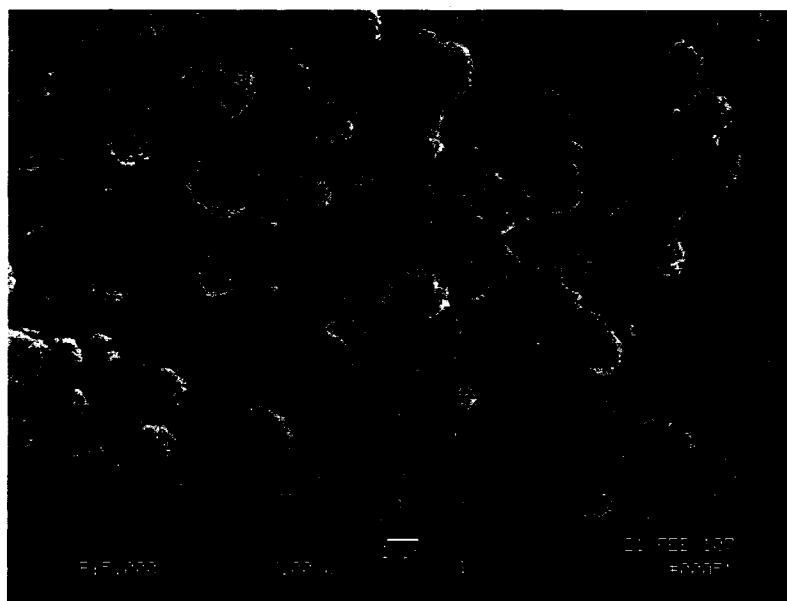


Figure 62: SEM picture of triblock copolymer PEG₄₅PLA₁₁₂PGluOH₁₀₀.

A few results were obtained, showing aggregated large objects, with a diameter around 1 μm . Most likely, the vesicles coagulated while drying. This

technique was found to be very difficult to perform and its results are only a poor repeat of the AFM study.

3. 2. 1. 6. Cryogenic Transmission Electron Microscopy (Cryo TEM)

Some Cryo-TEM experiments were run in order to confirm the presence of vesicles. Cryo TEM could also give us information on size distribution and thickness of the polymer shell. The reason cryo technology was used is to avoid collapse of our self-assemblies in the dry state under high vacuum.

We took several pictures, some of them showing nanoobjects. Spherical objects with diameters around 100 nm are shown on Figure 63.

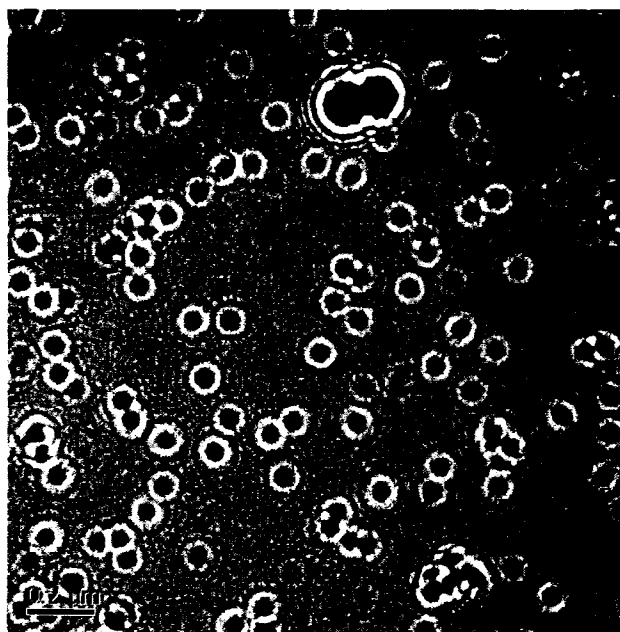


Figure 63: Cryo-TEM picture of nanoobjects formed by self-assembly of linear PEG₄₅PLA₄₇PGlu₁₀₀.

However, it is difficult to conclude. The technique is very difficult to perform (due to sample melting), costly, and had to be performed at Yale University. Therefore, we did not explore much further this direction.

3. 2. 2. Evaluation of the loaded system

One important parameter for the evaluation of our system is the percentage of insulin encapsulated or associated with the vesicles. In order to evaluate this amount of retained insulin a simple experiment was designed. A typical encapsulation process was used (as described in III. 1. 1. 1.). Then the free insulin (i. e. not associated and not encapsulated) was removed by ultrafiltration (Frontal ultrafiltration on Biomax regenerated cellulose, MWCO 100kD). The amount of free insulin, in the filtrate was determined by HPLC, monitoring the insulin UV peak at 280 nm. We used a Zorbax C8 column with a solvent gradient water/TFA and Acetonitrile/TFA, at 1ml/min and 30°C. A typical chromatogram obtained for insulin is given below:

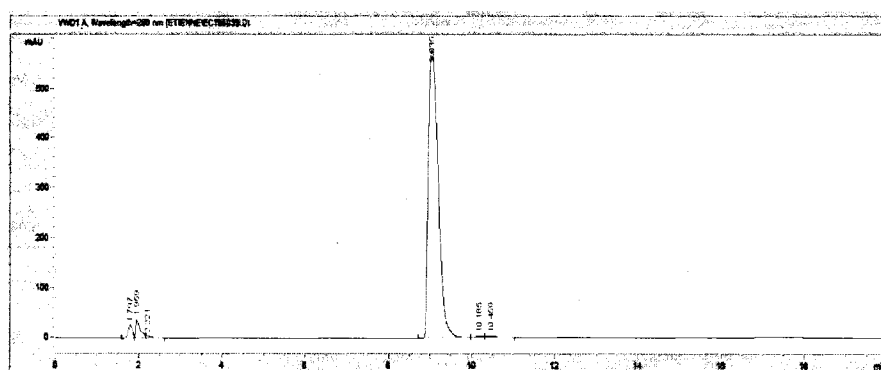


Figure 64: Chromatogram of insulin.

Knowing the amount of free insulin, a simple subtraction gave us the amount of insulin retained by our system. The filtration technique was later improved to reduce the experimental time. The solution of loaded insulin was placed in Centricon centrifuge tubes equipped with a 100kD MWCO regenerated cellulose filter, and a retentate bottom part. The tubes are centrifuged for 30 minutes at 3220 RCF. Since insulin is too small to sediment when centrifuged, an equilibrium is reached between the concentration of free insulin in the retentate and the filtrate.

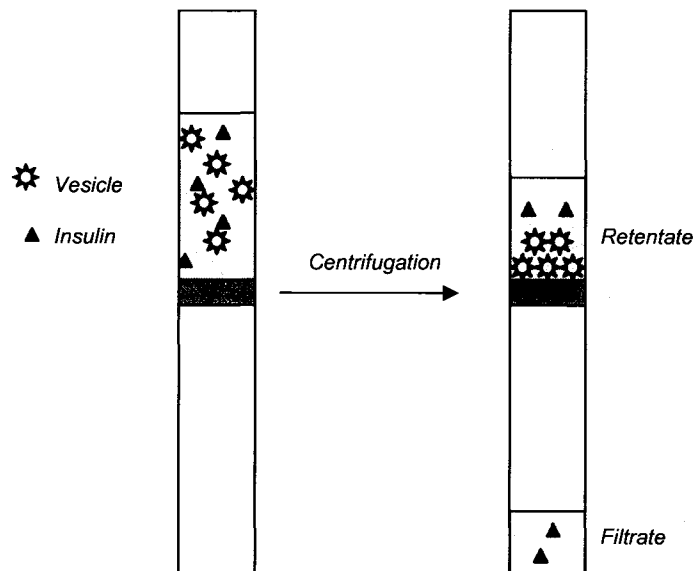


Figure 65: Separation of free insulin from loaded vesicles.

This filtered part is analyzed in HPLC. From the insulin concentration in the filtrate, the total free insulin and the ratio of insulin retained by the particles is easily deduced. As an example, the data shown on Figure 66 were obtained:

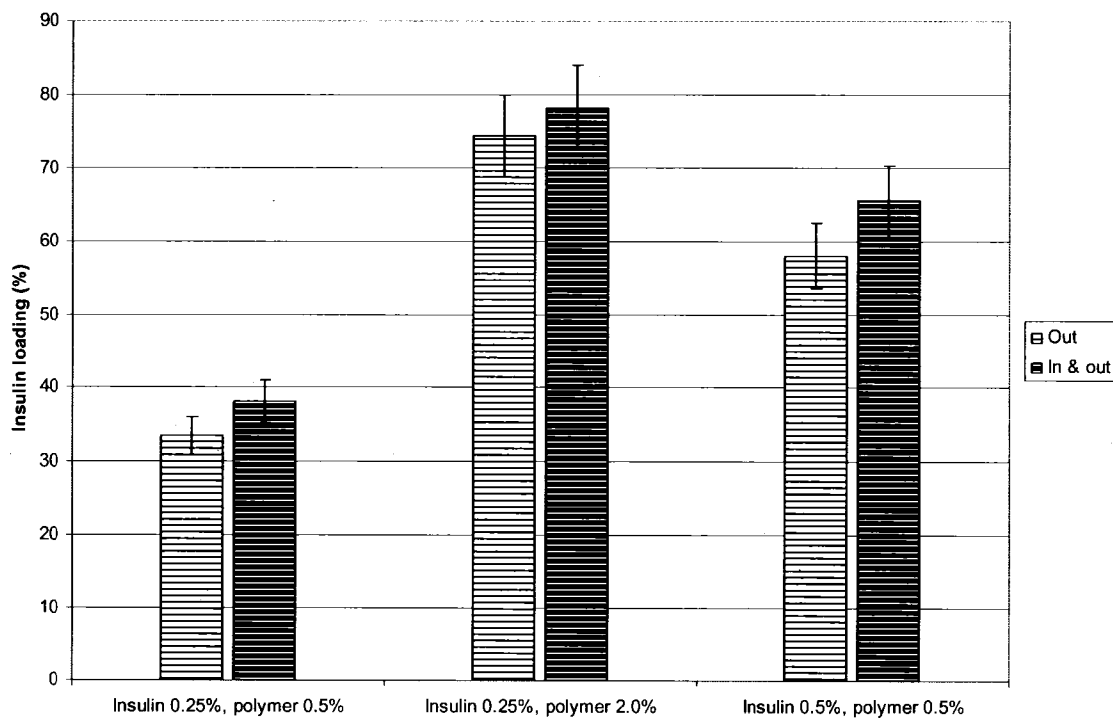


Figure 66: Typical data for the evaluation of encapsulation efficiency.

On this graph we can see the percentage of insulin retained by the system as a function of different parameters, such as insulin and polymer concentration. The detailed report of these loading studies is given and discussed further.

3. 3. Discussion

3. 3. 1. Understanding the self assembly

3. 3.1. 1. Bending of flat bilayers – the Helmutz surface free energy

In this paragraph we report a compilation of our calculations on the theoretical model describing the bending of a bilayer composed by amphiphiles into a vesicular shape. The model does not describe the formation of the bilayer itself, an organization driven by the ability of the hydrophobic blocks to segregate away from the hydrophilic solvent (water). As we saw before, such an assembly is only possible if the ratio between the hydrophilic and the hydrophobic fractions is asymmetric.

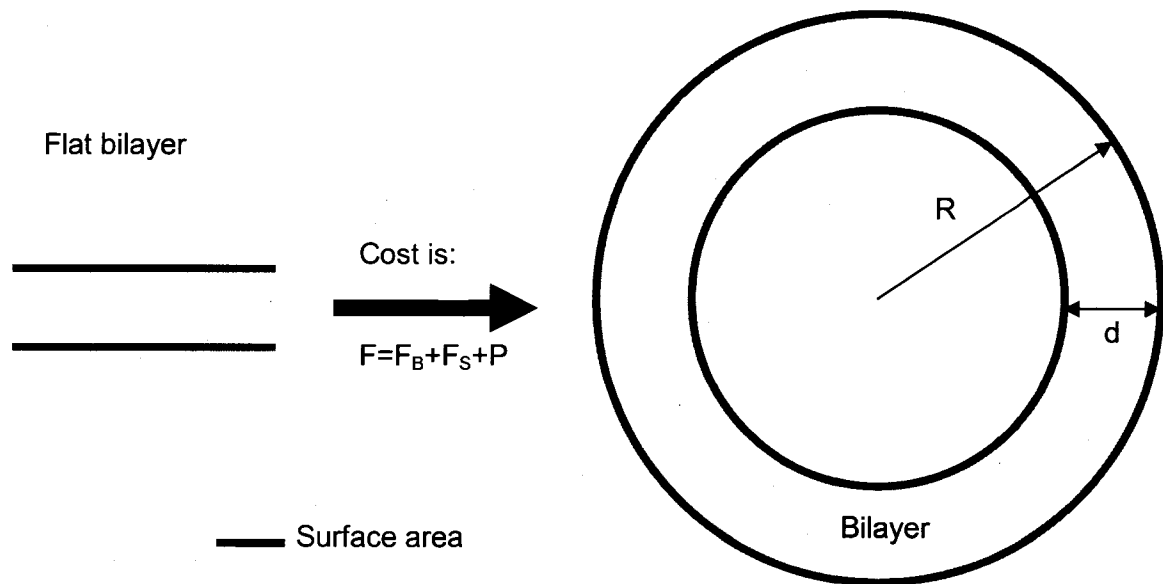


Figure 67: Bending of a flat bilayer into a spherical shape.

The cost of creating a curved bilayer was first described by Helfrich using the Helmutz surface free energy.⁶⁹ Helfrich, who was trying to understand the

particular biconcave disk shape of red blood cells, proposed the following equation (the Helfrich equation):

$$F = F_B + F_S + P \quad (8)$$

where F is called the Helmholtz surface free energy, F_B is the bending free energy, F_S is the interfacial free energy, and P is the osmotic pressure. P and F_S take in account the constraints of constant area and volume when the morphology is given by F_B . The above equation can be written as follows, for any kind of morphology:

$$F = \frac{1}{2} \oint \left[k_c \left(\frac{1}{R_1} + \frac{1}{R_2} - \frac{1}{R_0} \right)^2 + \frac{\bar{k}}{R_1 R_2} \right] dS + \Delta p \int dV + \gamma \oint dS \quad (9)$$

In this equation adapted from [70] the bending energy is given by:

$$F_B = \frac{1}{2} \oint \left[k_c \left(\frac{1}{R_1} + \frac{1}{R_2} - \frac{1}{R_0} \right)^2 + \frac{\bar{k}}{R_1 R_2} \right] dS \quad (10)$$

Here k_c is known as the bending modulus (or bending rigidity), R_1 and R_2 are the two principal radius of curvature, R_0 is the spontaneous radius of curvature, and \bar{k} is the Gaussian modulus.

The spontaneous curvature (defined as $1/R_0$) describes the tendency of the flat bilayer to bend either towards or away from the water phase. It is positive in the later case. The natural or spontaneous curvature arises from the competition between packing areas of the hydrophilic and hydrophobic blocks.

k_c is of the order of $K_B T$, the thermal energy, and represents the energy cost of deviating from the spontaneous curvature. \bar{k} is the energy associated with the deformation of the bilayer membrane. According to Goetz and Lipowsky,⁷¹ it is directly related to k_c and to the thickness d of the membrane by the following relation:

$$k_c = \bar{k} * d^2 * \beta \quad (11)$$

where β is a coefficient taking in account the fluidity of the membrane (β is taken as 1/48 for fluid bilayers, 1/12 for rigid bilayers). However, \bar{k} was also shown to be dependent on chemical properties.⁷²

For a sphere, we have $R_1 = R_2 = R$. Equation (10) integrated over the whole sphere yields the following solution:⁷⁰

$$F_B = 4\pi R^2 n_p \left[2k_c \left(\frac{1}{R} - \frac{1}{R_0} \right)^2 + \frac{\bar{k}}{R^2} \right] = 8\pi k_c n_p \left(1 - \frac{R}{R_0} \right)^2 + 4\pi \bar{k} n_p \quad (12)$$

with n_p the number of particles.

The second term in equation (8) is the interfacial energy. Its expression is given below:

$$F_S = 4\pi \gamma n_p \left[R^2 + (R - d)^2 \right] \quad (13)$$

here γ is the interfacial tension between the hydrophobic polymer (PLA) and water, R is the radius of the vesicle, d is the thickness of the membrane, and n_p is the number of particles. n_p is obtained with the following equation:

$$n_p = \frac{SC * V_T}{\frac{4}{3} \rho \pi (R^3 - (R-d)^3)} \quad (14)$$

where SC is the solid content, ρ is the density of the polymer and V_T the total volume.

From equation (13) and (14), we can reformulate F_s as:

$$F_s = \frac{\gamma^* SC * V_T}{\rho} \left[\frac{R^2 + (R-d)^2}{R^3 - (R-d)^3} \right] \quad (15)$$

We used the model assuming our vesicles were spherical, and assuming no osmotically induced tension, i. e. $P = 0$. We end up with the developed form of equation (8):

$$F = n_p \left[8\pi k_c \left(1 - \frac{R}{R_0} \right)^2 + 4\pi \bar{k} \right] + \frac{\gamma^* SC * V_T}{\rho} \left[\frac{R^2 + (R-d)^2}{R^3 - (R-d)^3} \right] \quad (16)$$

Using this equation we plotted the Helmutz surface free energy as a function of the radius. Theoretically, the preferential size for our vesicles can be found by minimizing equation (16) with respect to R , i. e. corresponding to a minimum in the curve. Note that the calculation is based on the number of vesicles in a 1ml sample with a 2% solid content.

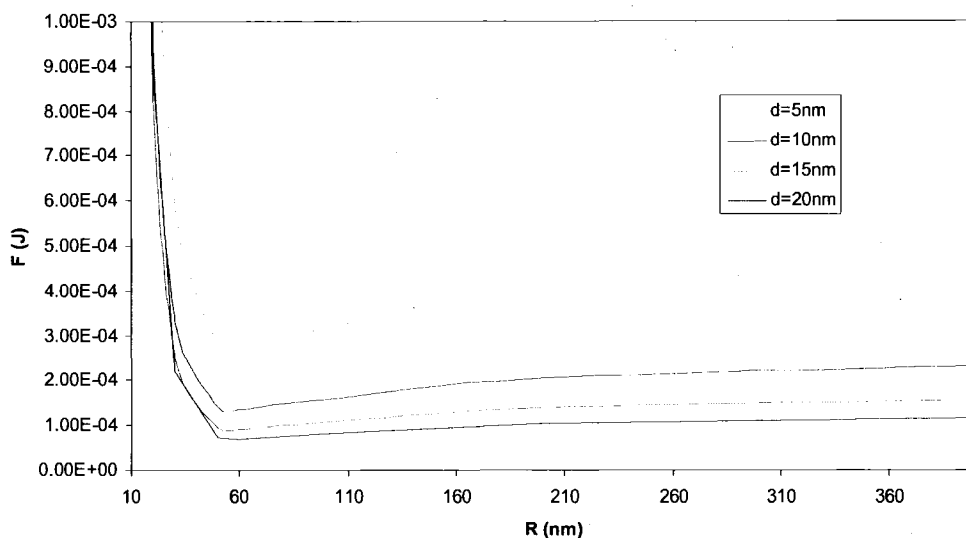


Figure 68: The Helmholtz surface free energy for bending a flat bilayer into a spherical membrane.

The constants used in this calculation are listed in table 9. d and R are the variables. \bar{k} is not in the table since it is calculated with equation (11).

Table 9: Constants for the Helmholtz free energy calculation.

Constant	Formula	Value	Units
k_c	$\sim 12 \cdot K_B T$	6.17983E-20	Joules
R_0	$\sim R$	6.00E-08	m
γ	n/a	0.052	N/m
ρ	n/a	1000	Kg/m ³
V_T	n/a	2.00E-06	m
SC	n/a	0.02	n/a

According to DLS size measurements, the triblock assemblies have diameters around 80nm and diblock assemblies have average diameters around 160nm. Both values seem to be reasonably close to the model prediction. However, if this model gives a value for radius around 60nm for the most stable

vesicle, one should be careful not to take it as face value. In order to obtain the final plot representing equation (16), we made several assumptions, and we approximated some of the constants. Most of the values were adapted from the work of Jung et. al.⁷³ who are studying surfactant assemblies.

In order to have a better comprehension of the influence of key parameters, we derived equation (16) with respect to R , and we solved the equation $dF/dR = 0$. The solution of this equation, R_c , is the critical radius adopted by the curved bilayer to minimize its energy. In the following plots, we can appreciate the influence of the spontaneous curvature $1/R_0$, the thickness d , the interfacial tension γ , and the bending modulus k_c , on the preferred size R_c .

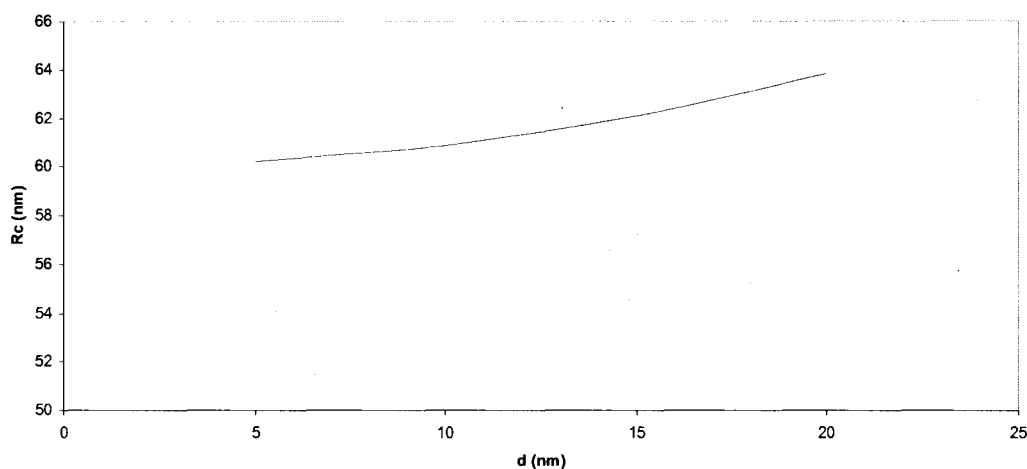


Figure 69: Favored critical radius as a function of membrane thickness.

In Figure 69, it is interesting to note that the thickness has a very weak influence on the equilibrium size. This result is in good agreement with the experimental data obtained by FFF-MALS (see Figure 61). Therefore both theory

and experiment show that the size of a vesicle is independent of the membrane's thickness. For this plot, we used the values of R_0 , k_c and γ reported in Table 9.

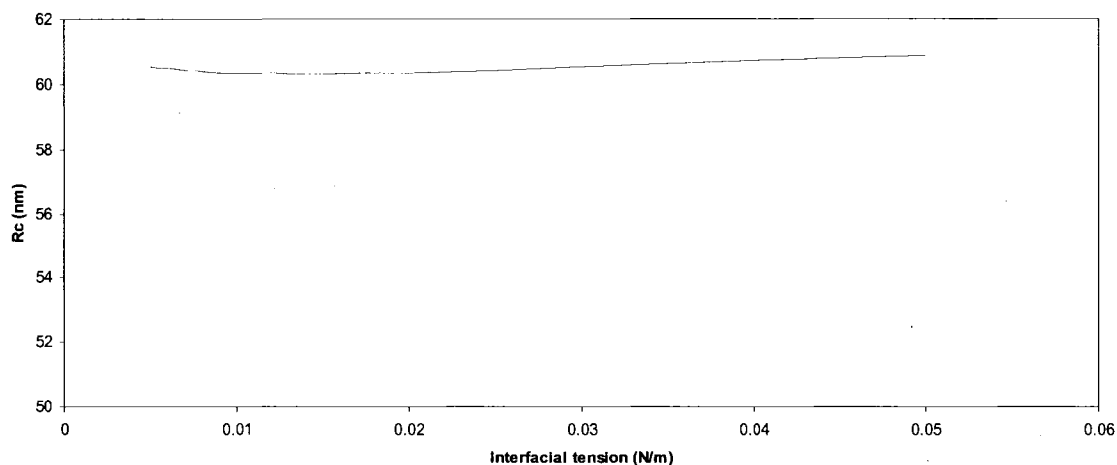


Figure 70: Preferred radius R_c as a function of the interfacial tension between water and the hydrophobic block. k_c and R_0 from Table 9, $d = 10\text{nm}$.

Figure 70 shows that the preferred size of the vesicle is also very weakly dependent on the interfacial tension. This result is not really surprising, since the interfacial tension is related to the surface area: the surface area change upon formation of a curved bilayer corresponds to the diminution of the inner surface, and is very small. The interfacial energy minimization is mostly involved in the formation of the bilayer, whereas this model describes the bending of a flat bilayer.

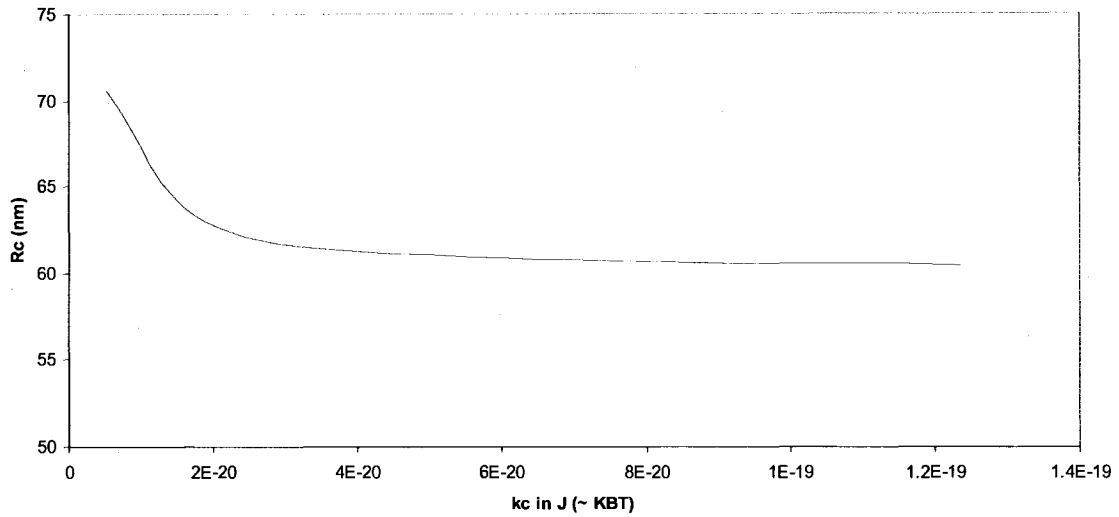


Figure 71: Influence of the bending modulus on the preferred size of vesicles. R_0 and γ from Table 9, $d = 10\text{nm}$.

According to Figure 71, the critical radius is significantly decreasing with the bending modulus decreasing. We know that k_c is homogeneous to an energy ($k_c \sim K_B T$). This plot suggests that it requires more energy to form a smaller vesicle. This is understandable since a smaller vesicle as a higher curvature, and therefore needs more bending when starting from a flat bilayer.

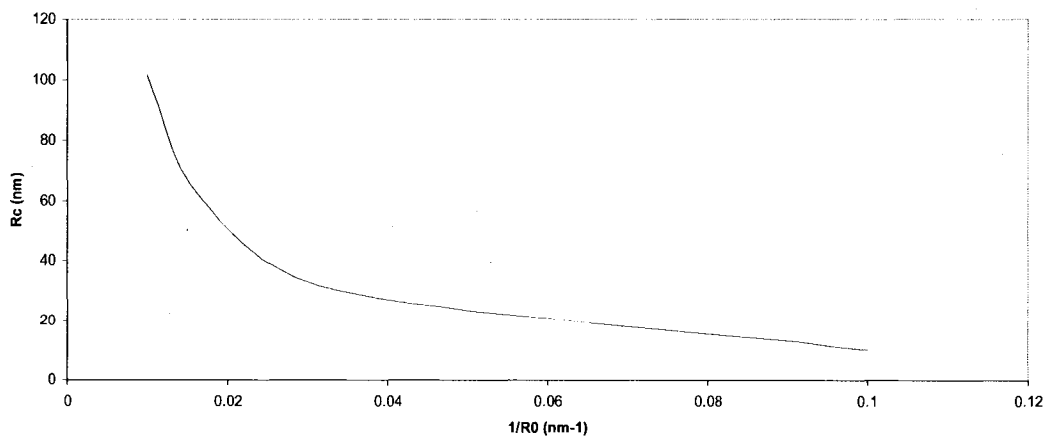


Figure 72: Preferred vesicle's size as a function of spontaneous curvature, γ and k_c from Table 9, and $d = 10\text{nm}$.

On Figure 72, we observe a very significant influence of the spontaneous curvature. As we said before, the spontaneous curvature describes the natural trend of a “flat” bilayer to bend slightly. When the spontaneous curvature is important, i. e. R_0 is small and $1/R_0$ is large, the preferred size is very small. When the spontaneous curvature is small, the preferred size is large. The spontaneous curvature is a result of a mismatch between the two leaflets of the bilayer. Such a mismatch is induced by small differences between polymer chains, most likely due to polydispersity of the chains. Moreover, we believe that our polymer architecture is not well controlled. The different architecture might also induce part of the spontaneous curvature.

3. 3. 1. 2. Considerations of key characteristics

Due to the high molecular weight and the polydispersity of polymer chains as well as their functionalities, polymeric self assemblies are not as simple as lipids self assemblies.

Thickness of the membrane

As we mentioned earlier, the thickness is an important parameter in the formation of curved bilayers. So far we did not describe what is influencing d . According to the literature,^{21, 72, 74} there is a commonly accepted empiric power-law relating d to the molecular weight of the hydrophobic polymer: $d \sim (MW)^\zeta$. The exponent is thought to be dependent on the interfacial tension and the

entropy of the chains. As an indication, for an ideal random coil configuration, $\zeta = 0.5$. It is unity for a fully stretched chain, and $\zeta = 2/3$ when the configuration is balanced between interfacial tension and entropy.

Using a thickness of 12nm that we found according to SAXS, and a molecular weight of 10000 g/mol we can roughly estimate ζ at 0.3 for our system. This value indicates that our chains are packed and entangled in the core of the membrane.

Membrane organization

The partitioning of polymer blocks in polymeric membranes is not well understood. Many conformations are possible, and these combinations are even complicated with the type of copolymer used. For instance, Disher and Eisenberg²¹ make the hypothesis that, unlike lipid assemblies forming a bilayer with a well defined midplane, AB type copolymers tend to form interdigitated structures due to chain entanglement and intrinsic polydispersity.

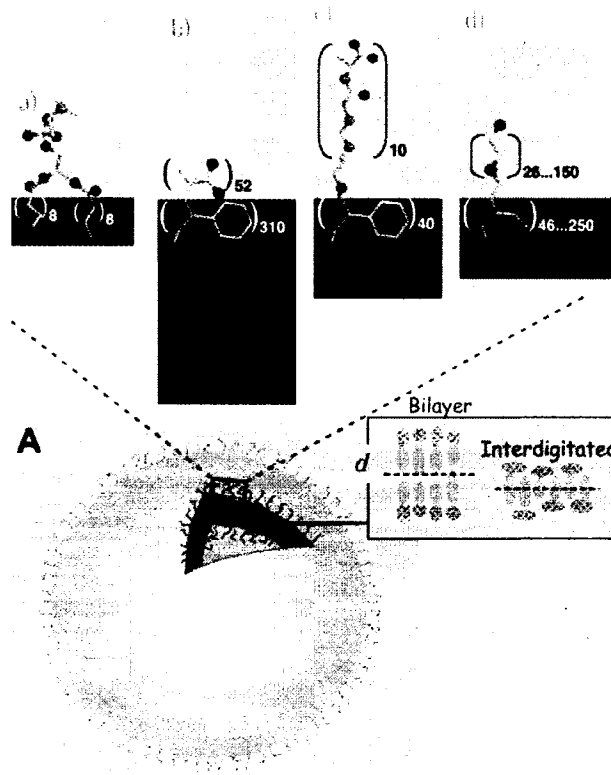


Figure 73: Well defined versus interdigitated organization. a) a phosphatidylcholine lipid; b) a diblock copolymer of poly(acrylic acid-polystyrene) (PAA-PS); c) PS-poly(isocyanate-L-alanine-L-alanine); and d) poly(ethyleneoxide-polybutadiene) (PEO-PBD).²¹

According to Meier and coworkers,⁷² triblocks can form two types of assemblies: the chains can either adopt a looped confirmation, or stretch across the width of the membrane (figure 74).

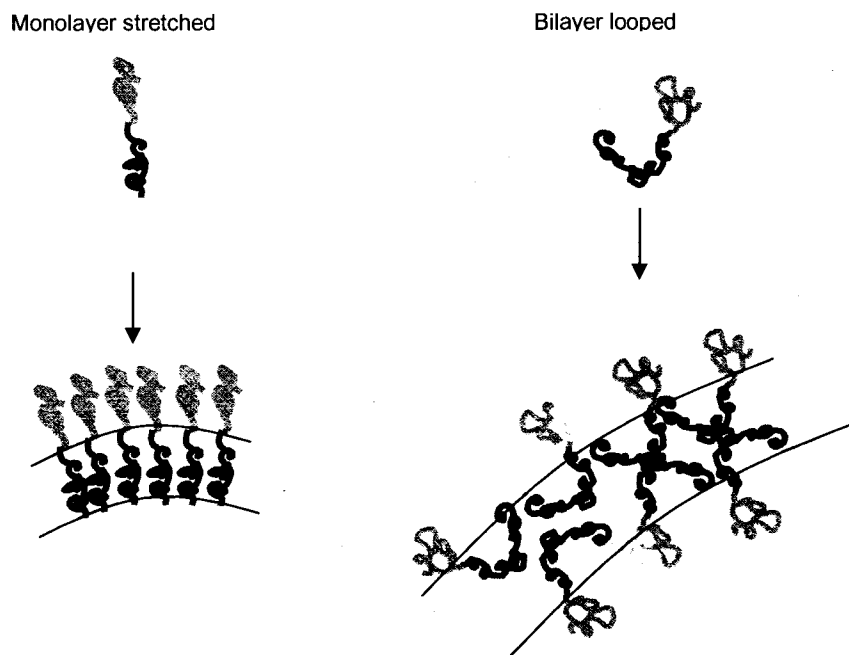


Figure 74: two possible configurations of triblock membranes.

In their work, they also mention that ABA symmetric triblocks are more prone to have looped configuration while ABC asymmetric triblocks tend to adopt the stretched configuration. Though our system is an asymmetric triblock and according to the results for the estimation of ζ , it seems that our polymer could adopt the looped confirmation were chains are entangled as opposed to the stretched model. With the goal to support this hypothesis, we did a DSC measurement on the wet triblock copolymer (0 to 75°C, ramp was 3°C/min is modulated mode, 1°C every 60sec.). The purpose of this experiment was to observe the glass transition of the PEG and PLA blocks in the copolymer.

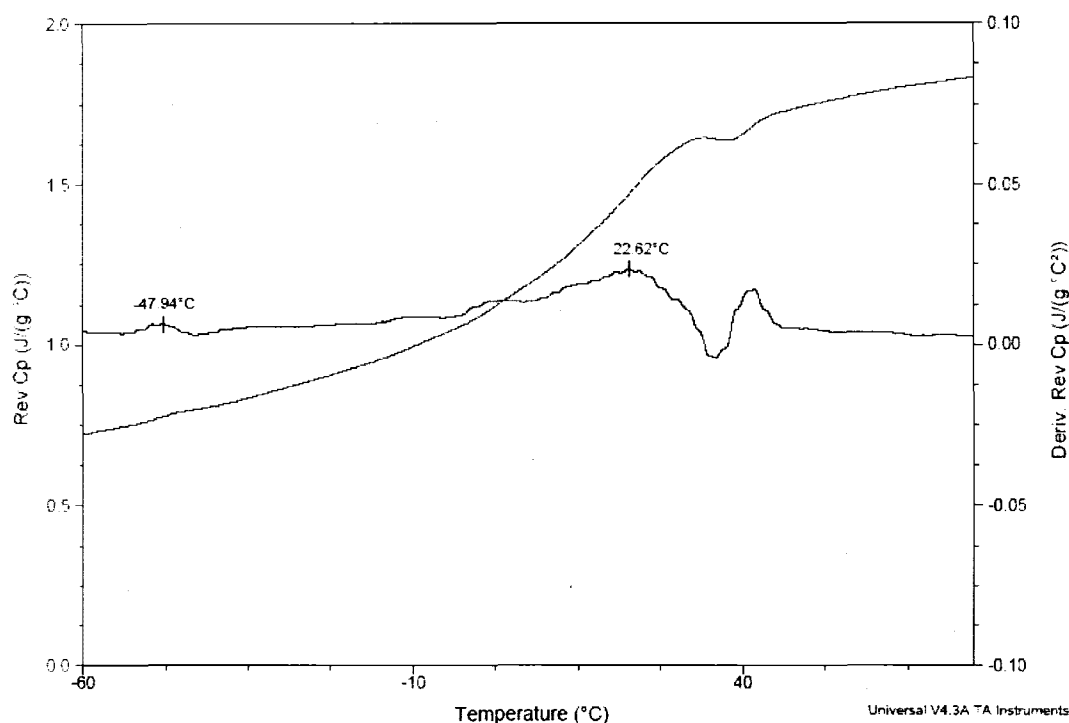


Figure 75: DSC trace of PEG-PLA-PGlu in water.

As we can see on the DSC trace, there is one transition around 22 °C, which does not correspond to a pure PLA block, and potentially a very small transition at -48°C which could be the PEG.

This means that PEG and PLA are probably not well separated in the self assembly, and it confirms that they could be entangled. On this topic, Bermudez and co workers ⁷⁴ suggest that in a PEG-PBD bilayer structure in water, a fraction of the PEG is collapsing toward its interface with PBD, shielding the hydrophobic polymer from water. Due to this phenomenon, they observe a decrease in membrane thickness and therefore a lower value for ζ (around 0.5 when they expected 2/3). It is possible that we have a similar phenomenon in our PEG-PLA domain that would explain such a low ζ value.

Segregation and flip-flop phenomenon

Several authors^{22, 75} are proposing that polymer chains having different length due to their polydispersity, rearrange in order to segregate chains in regions of a membrane. Although the mechanism is not well understood yet, it is most likely that the low Mw chains are oriented toward the inside leaflet of a bilayer. This mechanism is due to the ability of shorter chains to move into high curvature areas and allow for relaxing of the strain due to steric hindrance and electrostatic repulsions in the case of charged polymers.⁷² If the phenomenon helps stabilization of curvature, it can be limited by the thickness of the hydrophobic layer.

In our system, two arguments are in favor of such a mechanism. The PGlu is a charged polymer, therefore there are electrostatic repulsions, and its Y shape or structure is also a factor of large steric hindrance. In the case of the diblock, the curvature of the bilayer is most likely influenced by the segregation of the low MW PGlu chains on the inside, in order to minimize strain.

In the case of the triblock, knowing that a PGluO⁻ chain is much larger than a PEG₂₀₀₀ chain (MW is about 5 times bigger), and that PGluO⁻ is charged, it obviously requires more space to self assemble than PEG does. Therefore, curvature of the membrane forming vesicles is influenced by the lower MW PEG chains segregating in the inner part of the vesicle, and large charged PGluO⁻ pointing on the outside. Though it is tempting to describe the triblock assembly as PGlu on the outside, PLA in the midplane and PEG in the inside, it is not

excluded that some PGlu with low MW (due to polydispersity) would be on the inside too.

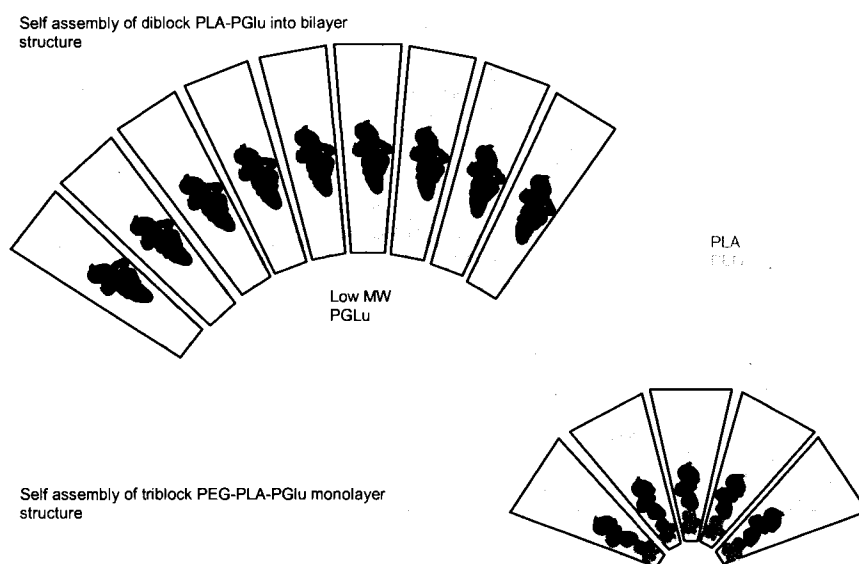


Figure 76: Self assembly of diblock and triblock copolymers, curvature is influenced by space filling.

As a conclusion, we think that the diblock copolymer is forming a bilayer, with PGlu on the outside and in the inside and the hydrophobic mid-plane formed by the PLA. Theoretically, the triblock was designed to form a monolayer due to its asymmetrical design, with PGlu on the outside, PLA as the hydrophobic “core” and PEG in the inside. However, we have several arguments ruling against this conformation since PLA does not seem to be stretched, and there is no phase separation between PEG and PLA.

On the other hand, we observe a very significant difference in size between the PEG-PLA-PGlu assemblies versus the PLA-PGlu ones. According to this result, and as sketched in figure 76, it could be explained as follows: the size of the vesicle is directly related to the amount of curvature. If the curvature of

the membrane is less important in the PLA-PGlu assembly (larger vesicles) than in the PEG-PLA-PGlu, it means that the chains might be in the stretched configuration, where PEG is inside, taking less space than the PGlu.

Response to environment

From the set of experiments described previously, we can draw a first straightforward conclusion: our system does form nanoobjects responsive to different external stimuli (pH, temperature...). The formation of such objects is not a random phenomenon.

Both DLS and AFM results show that the average size of the nanovesicles is strongly dependent on the pH of the solution. It is well known that poly(glutamic acid) can adopt different conformations through an α -helix to random coil transition. According to literature [76], this transition occurs below pH 4, and corresponds to the protonation of the acids.

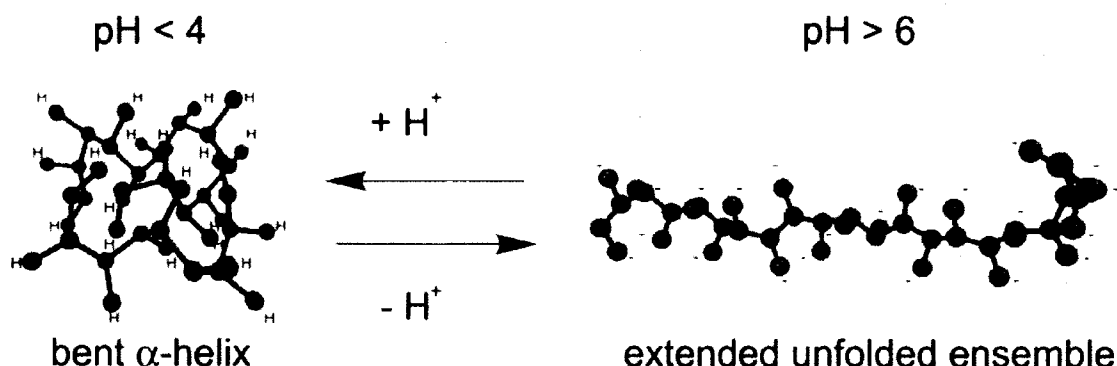


Figure 77: Representation of the helix to extended equilibrium structures of PGlu under acid or base titration.⁷⁶

In its helix shape, the poly(glutamic acid) folds in order to exclude water and therefore the space occupied by the PGLu chains shrinks. On the other hand, the extended chain conformation found at more basic pH imposed by electrostatic repulsions is characterized by a higher hydrodynamic radius.

A titration study of the carboxylic acids from the PGLuOH by NaOH was made by Zakaria Boukhal, in order to measure its pKa. According to his work, at acidic pH, the PGLuOH is in its protonated form, and the pKa is 4.5 which is in agreement with other values found in literature for the helix to coil transition.⁷⁶ Since it forms the external layer of the vesicle, aggregation is more likely to happen by hydrogen bonding between COOH groups of distinct particles. The average size of a cluster constituted by several vesicles has obviously a higher diameter than a single vesicle.

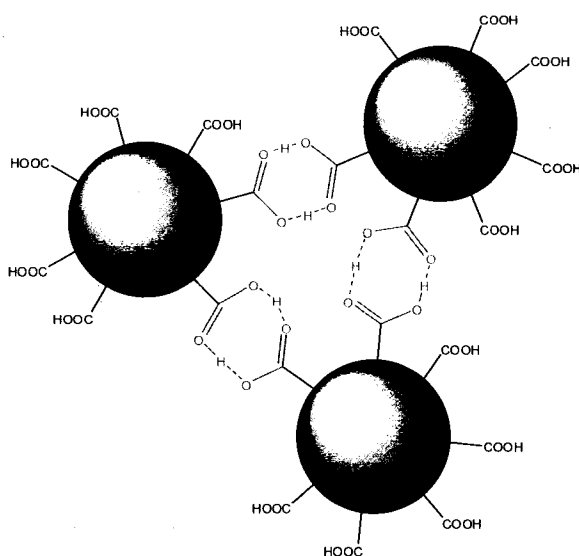


Figure 78: Hydrogen bonds between COOH at acidic pH. Formation of aggregates, and colloidal instability.

At basic pH, when most of the COOH are deprotonated, the electrostatic repulsion between negative charges on the freely extended P_{Glu} chains help stabilization, lowering aggregation and the average diameter of vesicles is smaller. The same behavior was observed for self-assemblies of diblock copolymer poly(aspartic acid-co lactic acid), where the pK_a of poly(aspartic acid) segments was measured to be around 7.³¹

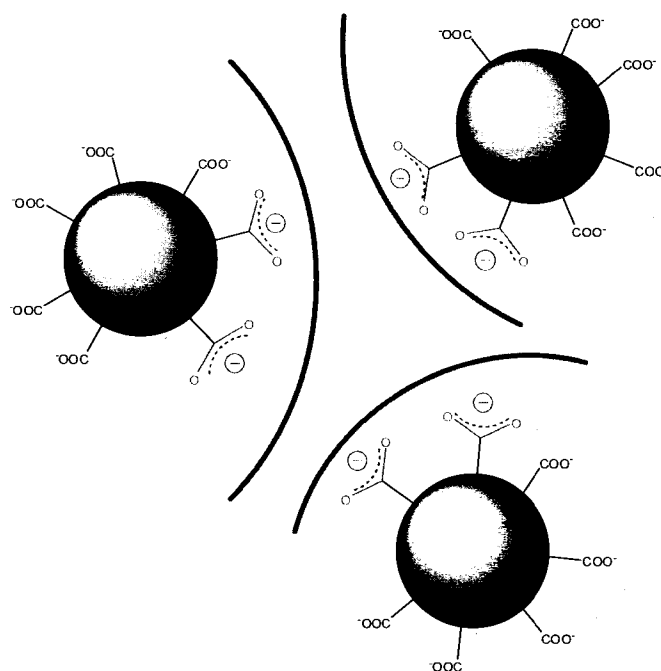


Figure 79: Electrostatic repulsion between vesicles in basic water.

Obviously, aggregation is not helping the encapsulation of insulin, since less material is available to reform vesicles. Therefore, all our products are formulated in water at pH 9, preventing aggregation. The phenomenon was found to be reversible, without the help of sonication, which we can see as a proof that our system forms well defined self assemblies.

This behavior toward pH environment change was also observed with the ionic strength. The more salt, i. e. ions, present in the solution, the smaller the diameter (see Figure 55).

Meier and coworkers observed a similar behavior with vesicle having a poly(acrylic acid) ionizable external layer.⁷⁷ One explanation for this behavior is that, with decreasing salt concentration (i. e. lower ionic strength), the electrostatic shielding between vesicles also decreases, allowing more swelling of the vesicles, and therefore a higher hydrodynamic radius is observed.

3. 3. 2. Protein solubilization

The word “solubilization” is here used to emphasize the multiple ways insulin can be loaded in our system. We make the hypothesis that one part is encapsulated inside the hollow vesicles during the self assembly, a secondary load is due to adsorption of the insulin on the external ionized PGluONa layer. The later can be explained by the obvious electrostatic affinity between an ionized protein and an ionized polypeptide. The third load is due to insulin trapped in the bilayer membrane of the vesicle during the self assembly process.

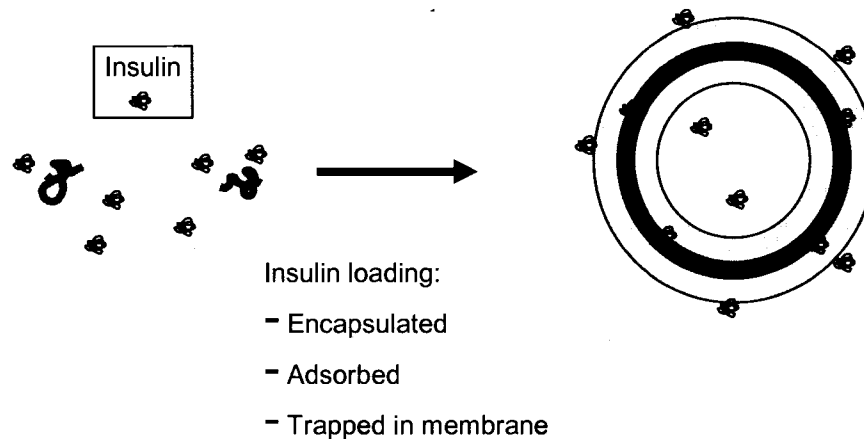


Figure 80: Insulin loading in vesicles.

Concerning the third hypothesis, it is obviously tempting to relate the trapping of insulin in polymeric membrane to transmembrane proteins found in cell membranes. So far, very few studies have been done on this topic. It is worth citing the work of Meier and co-workers, who managed to incorporate membrane proteins such as β -lactamase in their PMOXA-PDMS-PMOXA triblock and observed that the protein was fully functional.⁷⁸ Recently Pata *et al.* worked on the modeling of the integration of proteins into synthetic polymer membranes.⁷⁹ What they found supports the idea that even non-transmembrane proteins can be incorporated in polymeric membranes, as long as they have both hydrophilic and hydrophobic regions on their surface. In this case, they can sit at the interface between two regions.

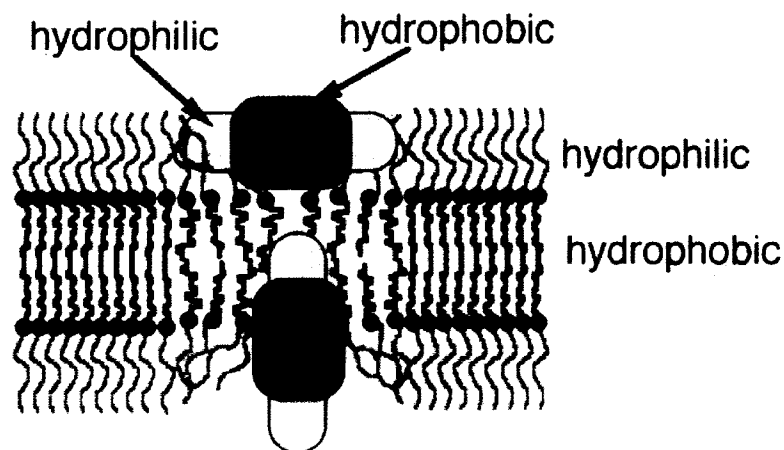


Figure 81: A schematic of bilayer perturbation by nonincorporated transmembrane proteins.⁷⁹

According to their work, the perturbation of the membrane assembly is due both to thickness mismatch between protein and membrane, and surface tension between hydrophobic and hydrophilic regions. Interestingly, the authors propose that polydispersity of the polymer chains can actually favor the incorporation of proteins in the membrane, by a local segregation: shorter chains arrange closely to the protein, matching its dimensions.

The results discussed in this part provide a study of the efficiency of insulin loading in the polymeric vesicles, while adjusting a number of parameters. We were interested in measuring the effect of insulin concentration, polymer concentration, and pH.

In a first experiment, formulation In&Out was tested. Figure 82 shows the percentage of insulin retained (the ratio retained insulin/total insulin) by the vesicles as a function of the cleaning buffer volumes used for filtration. After 5

volumes, the amount of free insulin present in the filtrate was almost negligible, meaning that most of the free insulin was removed from the retentate.

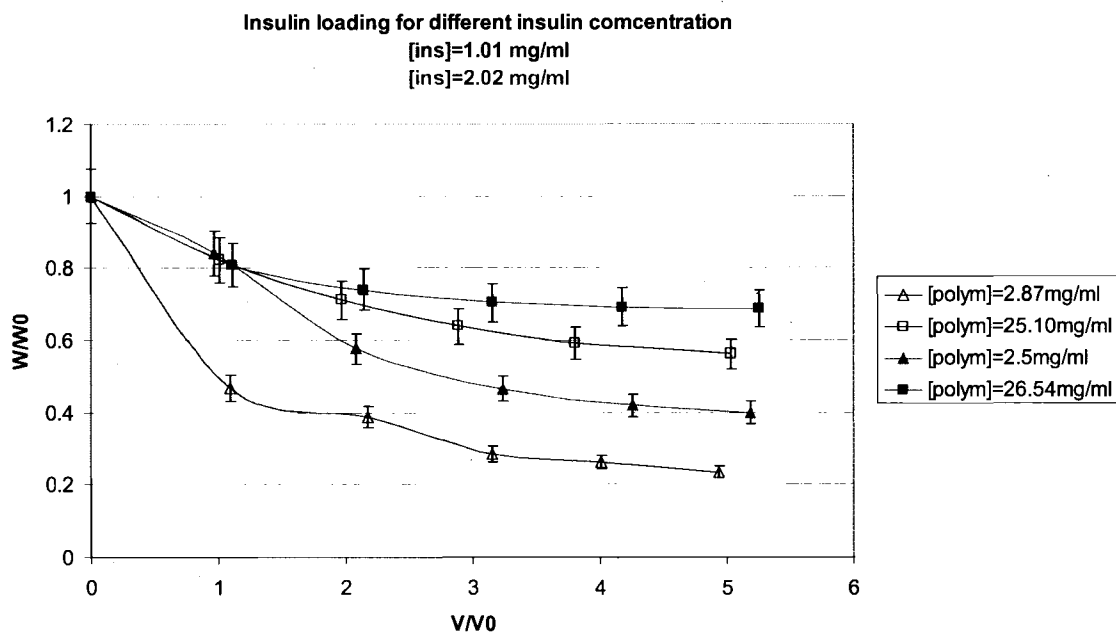


Figure 82: Insulin loading of triblock vesicles for different polymer concentration and insulin concentration.

The first observation we can see from this chart is that if we increase the polymer concentration, then the available material for insulin loading is increased too, and more insulin is associated in our system. What is more intriguing is to observe that the encapsulation efficiency increases with insulin concentration. The encapsulation efficiency is defined as the ratio between loaded and initial insulin. This proves that we do not have an equilibrium between free and loaded insulin. If we had an equilibrium the ratio between free and associated insulin should be constant at constant polymer concentration and this with no effect of insulin concentration.

In a second study using the improved technique described in paragraph 3. 2. 3., those results were confirmed, and other pieces of information were found.

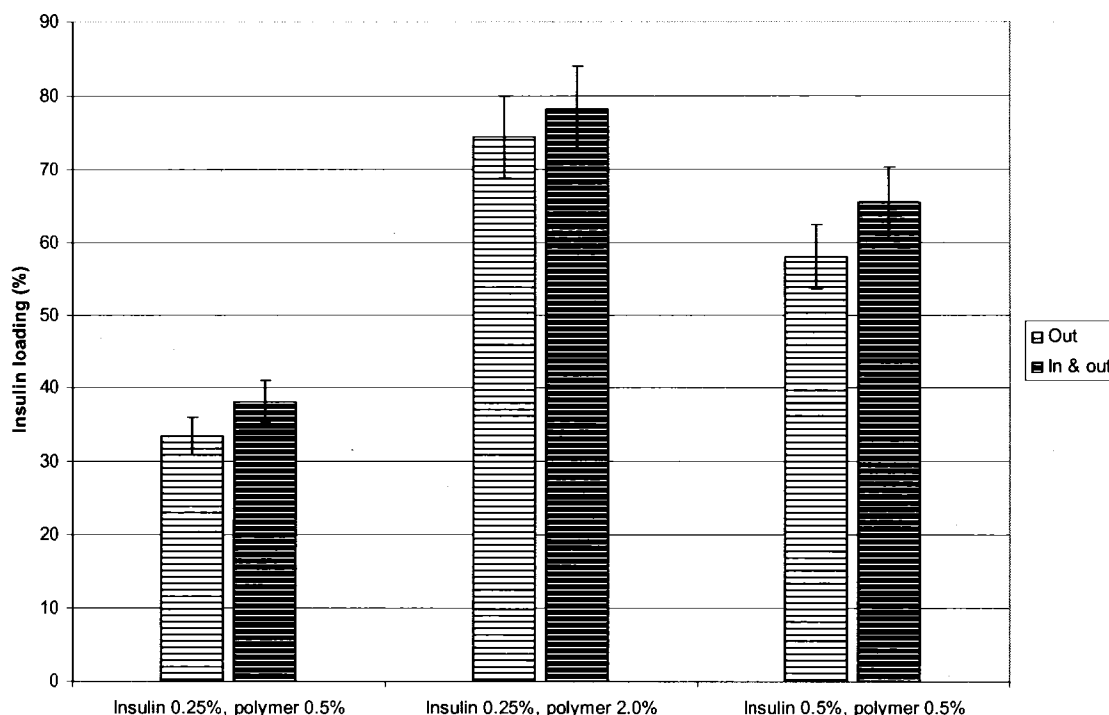


Figure 83: Insulin loading of triblock PEG₄₅PLA₁₁₂PGlu₉₅ at pH 9.

Again, we observe on Figure 83 an important increase, by a factor of 1.5, in loading efficiency when the insulin concentration is doubled. However, the most striking result is that the Out formulation is almost as efficient to retain insulin than the In&Out formulation. From this figure, even if we clearly see that the “In&Out” formulation is slightly more efficient than the “Out” formulation, due to the encapsulation and trapping of insulin in the membrane, we can already make the assumption that the major part of the load is not due to encapsulation.

This figure also confirms the findings of the first study concerning the polymer concentration: the loading is twice as efficient when the polymer content

is multiplied by 4. This trend was observed for the triblock copolymer and was confirmed for diblock copolymers (see Figure 84).

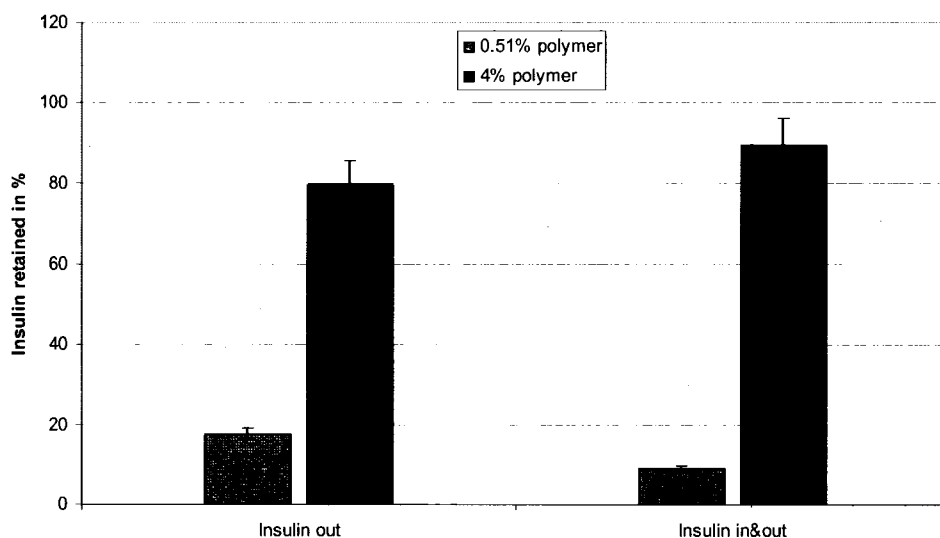


Figure 84: Diblock PLA₁₃₇PGlu₇₂ copolymer at different concentration loaded with insulin (pH 9).

A third study gave us some information on the loading efficiency of diblock versus triblock copolymers. The experiment was done at pH 9, with 0.25% of insulin and 0.5% of polymer in both cases. Interestingly, we found that more insulin is retained by the triblock self assembly.

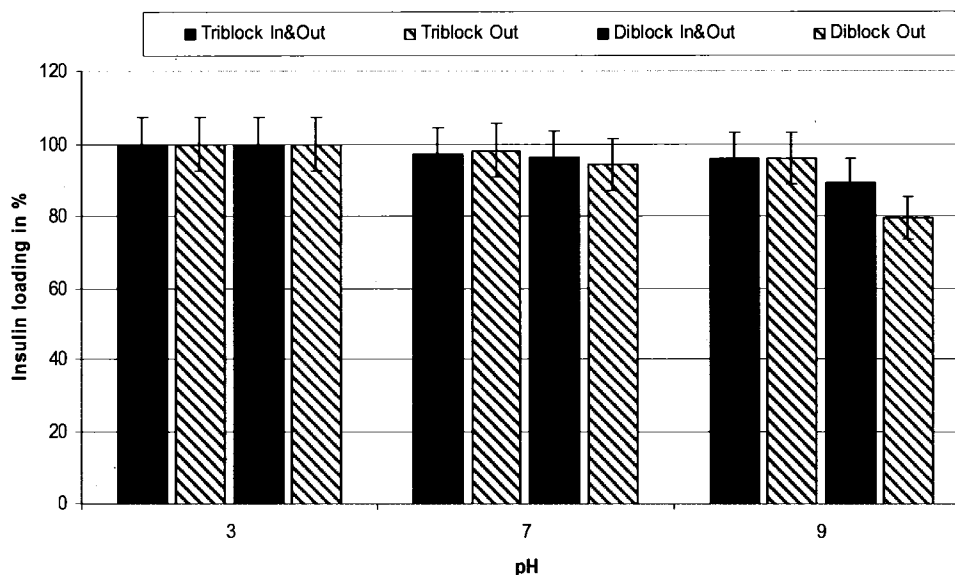


Figure 85: Insulin loading, triblock vs. diblock and pH study.

This result is actually easily explained. From the previous experiment, we found out that insulin was essentially associated with the vesicles according to a mechanism different than encapsulation. If we assume that this mechanism is related to the affinity between insulin and charged PGlu, then it means that the more PGlu is available, the more insulin is associated with it. Since triblock vesicles are twice as smaller as diblock vesicles, they offer more surface area, i. e. potentially more insulin can be associated with PGlu.

In the same study, we designed an experiment to explore the pH influence on loading. Different materials were used, all polymers at 0.5% solid and insulin at 0.25%. The first observation to make is that the encapsulation values at pH 3 are most likely erroneous. From the pH stability studies we know that the colloidal stability of our objects is lost under pH 3.5. In this case, the fraction of polymer involved in the formation of large micron size aggregates is quite large,

and most likely the filter was quickly plugged upon centrifugation and did not let any molecules, save water molecules go through. Additionally, insulin is not solubilized at such a low pH value.

Another argument that could explain the high value of insulin retained in this particular experiment is that we used 30kD MWCO filters instead of 100kD MWCO. This is a problem when considering that the hexameric form of insulin, 6 insulin molecules coordinated around a Zinc atom, has a molecular weight of 6 insulins, i. e. $6 \times 5808 = 34848 \text{ g.mol}^{-1}$.

In order to have a better understanding of the repartition between encapsulation, association and entrapment of insulin, a theoretical calculation was done, determining the amount of insulin that can effectively end up in the internal volume of the vesicles. The encapsulated insulin is obtained as follows: Amount of insulin encapsulated = (Total internal volume) x [Insulin]. The total internal volume is given by $V_i = n_p \times 4\pi(R_1^3 - (R_1 - d)^3)$ where n_p is the number of particles (given by equation (14)), and R_1 is the radius of the sphere and d is the thickness.

These calculations were done on a spherical model, with a monolithic layer of density 1.4 (combination between PLA and polyaminoacid densities). The insulin concentration is set at 0.25 % w/w, and the vesicle diameter, the thickness of the membrane and the polymer concentration (or solid content SC) are variables. The results show that, according to the choice of parameters, the insulin loading varies from 1 to more than 35 %.

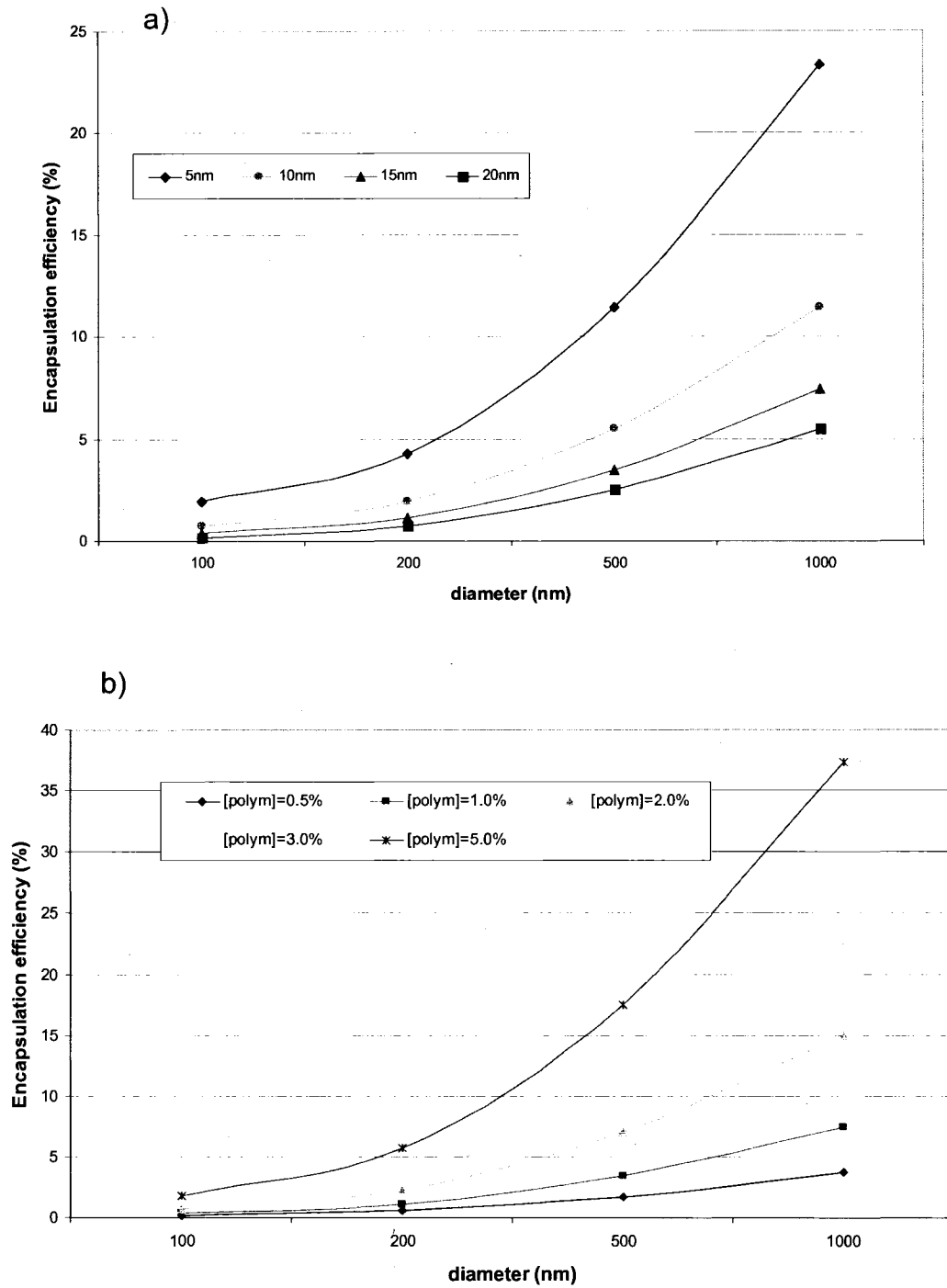


Figure 86: Theoretical encapsulation of insulin as a function of: a) vesicle diameter and membrane thickness (calculations made for [polym] = 1%), and b) vesicle diameter and polymer concentration (calculations made with a 15 nm membrane thickness).

According to our experimental observations, the best parameters to use in the model is to consider that we have vesicles of diameter between 100 and 200 nm, and a membrane thickness ranging somewhere between 10 and 20 nm. With these values, it is clear from the plots, that only a very small fraction of the insulin, in no case higher than 5%, is encapsulated.

Since we have a lot more retention of insulin than 5% (minima around 20%) the only acceptable hypothesis is that some of the initial insulin is retained, but not by encapsulation (and the hypothesis of experimental error such as insulin retention by filtration membrane is weak since we performed a control experiment before). It confirms that a significant amount of insulin associated with the $\text{PGluO}^-\text{Na}^+$ external part of the polymersomes, and some may also be “solubilized” in the membrane, like transmembrane proteins are. The assumption of insulin associated with ionized PGlu is quite straight forward. The transmembrane like insertion is an hypothesis. As we said, very little is known on this topic, and proving this issue would require the design of a nice experiment, involving labelization of the protein and confocal microscopy, or CryoTEM.

If, as we are stating, insulin gets associated with the PGlu, we can have an indirect proof that some polymer chains are arranged in such a way that part of the PGlu is on the inside. In this particular case we should have a very significant difference of loading efficiency between the two formulations In&Out and Out. The PGlu sitting on the inside of the membrane is exposed to insulin upon sonication, it can then “bind” more of the protein before reforming the self assembly.

As we saw, there is a small difference in loading efficiency that is not due to the insulin encapsulated in the internal volume of the vesicle. A quick calculation using the results shown on figure 83 and the theoretical calculations above gives interesting confirmation of this hypothesis. Both the model and the experiment are based on a 1ml solution with an insulin concentration of 0.25% and a polymer concentration of 0.5%. For the theoretical calculations, we used a membrane thickness of 15nm and a vesicle diameter of 100nm consistent with our findings on the triblock assemblies. In the following table we compared the difference in the amount of insulin associated with our system in the two formulations: Out and In&Out.

Table 10: Amounts of insulin associated with the vesicles: experiment vs. theory.

	Formulation	Insulin retained in %	Insulin retained in mg	Amount of insulin inside (mg)
Experiment	OUT	33.51	0.83775	0*
	IN&OUT	38.11	0.95275	0.115
Theory	IN	0.5	0.0125	0.0125

* by design

As we can see, the difference is quite large in the experiment when the theory says it should be much less significant. From this calculation, we conclude that the In&Out formulation is retaining more insulin according to two phenomenons: encapsulation in the internal volume of the vesicles, and another part is associated with the PGlu chains pointing toward the inside of the vesicle. From the calculations, we can say that there is a factor of almost 10 between the two.

In this paragraph, we showed that we load about 75 % of the initial insulin in our systems, whether we use diblock assemblies or triblock assemblies. We believe that the major part of the loading (about 80%) is due to electrostatic interactions between the insulin and the charged PGlu. The insulin may sit on the outside or deeper in the PGlu hairy layer. A second load, representing about 10% of the total loaded insulin, is most likely due to the entrapment of insulin inside the polymeric membrane, at the interface between hydrophilic PGlu and hydrophobic PLA. The third load corresponds to insulin effectively encapsulated in the available volume inside vesicles. This load counts for 0.5 to 2% according to the size of the vesicles. The missing insulin is retained in the filter during the centrifugation.

Assuming the important loading due to interactions between insulin and PGlu, we hypothesized that the loading efficiency of the In&Out should be superior to the Out formulation. Upon opening of the vesicles, the inner PGlu could theoretically pick up a lot of insulin. Not only should we observe a large difference in efficiency between the two formulations, but we should also reach a higher total efficiency. We do not observe this in the experiments, and we tried to understand why the insulin is not more present in the inside.

Using some simple calculations, we found an explanation to this issue. An example of the calculation is given below, for a triblock assembly assuming a stretched configuration for the chains. A schematic of the vesicle is given below, in Figure 87:

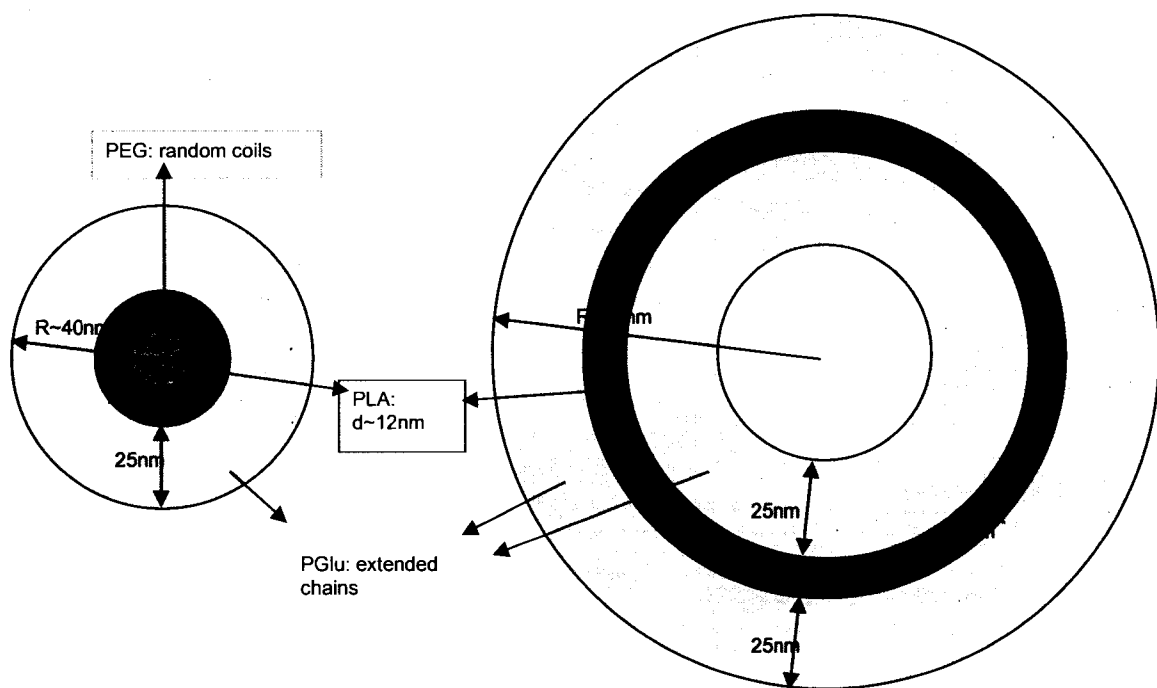


Figure 87: Schematic of triblock and diblock vesicles showing scaled membrane thickness and diameters.

According to our size measurements, the PGlu is in an extended chain configuration at pH above 6. In this case, and using 100 repeat units (common PGlu chains used in self assembly), we can have a rough estimation of the size of the external PGlu layer. We assume that we have a Y shaped triblock, meaning that only 50 units of the PGlu are actually counted in the thickness calculation. Using a monomer length of 5 Å or 0.5nm, $d_{\text{PGlu}} = 0.5 \cdot 50 = 25 \text{ nm}$. We know that the PLA layer is about 12 nm thick. Note that the calculation of the PLA_{120} radius of gyration gives $R_g = 0.5 \cdot \sqrt{120} = 5.5 \text{ nm}$. This gives a PLA layer of 11nm ($2 R_g$). Finally, assuming a random coil configuration for the PEG_{45} block in the inside, we have $d_{\text{PEG}} = 0.5 \cdot \sqrt{45} \sim 3.5 \text{ nm}$. The total thickness of the membrane is therefore given by $d = d_{\text{PGlu}} + d_{\text{PLA}} + d_{\text{PEG}} = 25 + 12 + 2 \cdot 3.5 = 44 \text{ nm}$.

Knowing that the average diameter for our triblock assemblies is 80nm, this means that our system looks more like a micelle, and there is no space in the inside for insulin.

This calculation applied on a diblock assembly indicates that the thickness of the membrane in the hydrated form is about 60nm. Since we have an average diameter of 180nm for our diblock vesicles, there is more space available inside the diblock assemblies. A schematic representation is given in figure 87.

3. 3. 3. Some considerations on the behavior of the polymer in the GIT

We prepared a formulation in basic water, where the external layer of our vesicles is mostly $\text{PGluO}^-\text{Na}^+$. We made the hypothesis that, if the PGlu can be formulated as PGluONa , it could probably “bind” other ions, such as ions found in the body. Zakaria Boukhal made an experiment to confirm this hypothesis. A triblock copolymer was mixed with a solution of known concentration of Ca^{2+} . This concentration was recorded with a Ca^{2+} electrode and plotted (Figure 88).

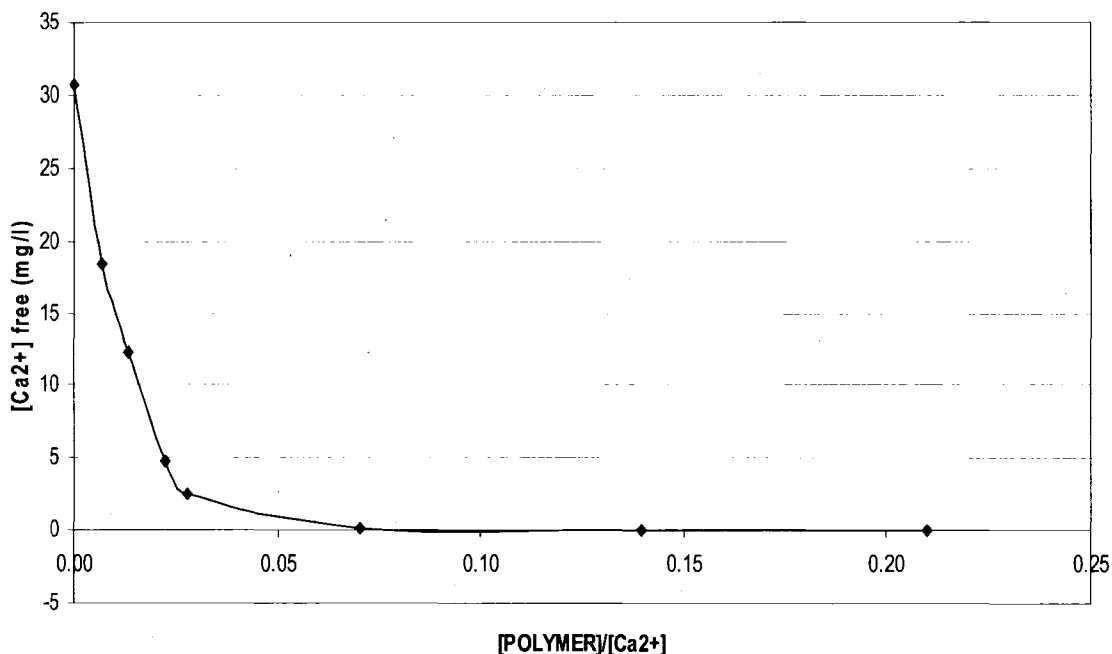


Figure 88: Evolution of Ca²⁺ concentration upon addition of triblock copolymer.

From this plot it is clear that the concentration is dropping scaling with the polymer concentration, proving that two COO⁻ from the PGLu may actually form a complex with a Ca atom. According to these preliminary results, we could say that this polyanion might have an inhibitory effect on some of the metalloproteases present in the GI tract. Several publications, as early as 1962, report the inhibitory effect of polyanions on proteins and enzymes. Many natural and synthetic systems can be used. As an example, Heparin is a natural highly sulfonated polysaccharide found in the human body with a molecular weight ranging from 6 to 40 kDa. It is one of the most negatively charged biomolecules.⁸⁰

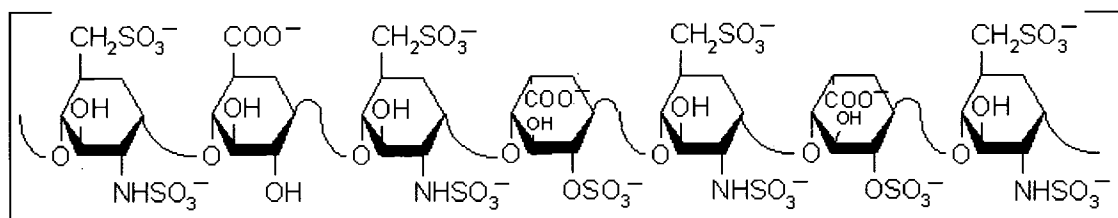


Figure 89: Structure of Heparin.⁸¹

Heparin is commonly injected and used as an anticoagulant. It is a co-factor of antithrombin, the protease responsible for thrombin and factor IX inhibition. Heparin complexes with antithrombin due to its electronegativity and changes the conformation of antithrombin, speeding the inhibition.¹²

PGluONa is thought to compete with proteases through the binding of cations, especially Zn^{2+} and Ca^{2+} . This competition is likely to lower the global proteases activity, when a significant amount of the enzymes are deprived from cations that are essential to their activity/organization. As an example Carboxypeptidase A is a metalloenzyme using Zn^{2+} in its active site.

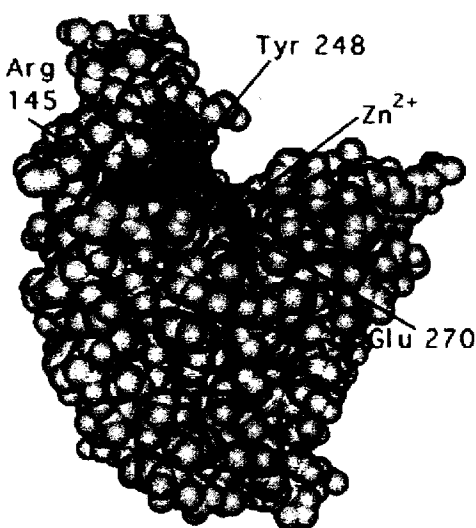


Figure 90: molecular model of the unbound carboxypeptidase A enzyme.⁸²

Eventually, the PGlu is saturated with cations (two COO^- for one cation) and the enzymes are no longer deprived from cations. The saturation of the PGlu by cations has another effect, the diminution of its hydrophilicity. Another hypothesis is to view the PGluO^- as a polymer having potential mucoadhesive properties.

CONCLUSIONS

In this work, we report the synthesis and purification of fully biodegradable and biocompatible amphiphilic copolymers with both synthetic and semi-synthetic blocks. PEG-PLA-PGlu, PEG-PCL-PGlu and PLA-PGlu were synthesized in three steps: first PLA (or PCL) synthesis, then PGlu synthesis and finally coupling between those two entities. Lactide was polymerized in bulk using an organic catalyst, DMAP, and an alcohol as initiator. The polymerization times are extremely short, and the polymerization was living, allowing full control of MW with relatively low PDI. PCL was obtained from the ROP of its monomer in toluene, using $\text{Al}(\text{Et})_3$ as a catalyst. Again, the polymerization is controlled. PGluBn was synthesized by ROP of the benzylglutamate NCA in NMP. The PGluOH was obtained after cleavage of the Bn group. The NCA polymerization is living. We refined the conditions of the deprotection step due to side reactions we encountered. The coupling between the OH terminated PLA and a COOH of PGlu was optimized to reach high yields and diminish side reactions. We also performed preliminary work on a new synthetic pathway in order to avoid this last coupling by modifying the end group of PLA from an OH to a NH_2 . This new polymer is then used as the amine for ROP of NCA. The preliminary experiments were encouraging, and it should be further explored. It has the potential to allow many different polymer architectures.

These polymer amphiphiles did assemble in water to form nanoobjects identified as vesicles, using a variety of analytic techniques. Since size is a major characteristic of those self assemblies, DLS proved to be extremely useful for the characterization of the vesicles. AFM, SAXS, FFF-MALS, were also powerful techniques. They all gave us a piece of the puzzle, respectively size and shape, thickness of the membrane, number of chains in one assembly.

Using these results and with the help of simple models, we found out that according to the copolymers used, we could form different types of membranes, leading to different sizes of vesicles. Diblocks tend to form well defined bilayers with diameters around 160nm, when triblocks are most likely forming membranes with a mix of stretched chains and entangled chains, with vesicle diameters around 70nm. In both cases, the external layer consists of PGlu.

Since those nanovesicles are made of biocompatible and biodegradable components they are potential candidates for drug carriage. Insulin was successfully loaded in those vesicles with high efficiency. The system was initially designed to be used in oral administration due to its gastrointestinal resistant properties, i. e. the polymer was supposed to protect the encapsulated protein against enzymes. Our research lead us to think that the loading of the protein is actually the result of several mechanisms. Most of the loading seems to be due to associated insulin with the charged external PGlu. This means that the protein is poorly protected in these systems. A second load (about 10% of the total) seems to be due to insulin trapped in the membrane or on the inside of the

membrane. Finally, the volume available for effective encapsulation is so small that this loading counts for less than one percent.

Recommendations

We have several options to improve the bioavailability of the insulin without rethinking the whole concept. We could either propose a larger inside volume to encapsulate more insulin, i. e. make larger nanovesicles, or we need to protect the system polymer/protein through the first region of the GIT, the stomach, typically with an enteric coating such as Eudragit. This has already been done, using Eudragit S100 for the delivery of insulin.⁸³ The third possibility would be to find a way to optimize the fraction of insulin entrapped in the membrane. It would be interesting to study the maximum amount of protein that can be solubilized in the membrane with a minimum perturbations. In that regard, the effect of membrane thickness and MW of the chains is probably of great importance.

In order to choose the best research direction, we need to do more work on the interactions between insulin and poly(glutamic acid), using Isothermal Titration Calorimetry (ITC), and understand the location of the insulin inside the membrane. This could probably be observed by confocal microscopy with insulin labeling. Several parameters of our system are tunable. For instance it would be of great interest to explore the influence of the PGluOH MW on the morphology. We already now it is increasing the hydrodynamic radius, but we do not know what its effect on loading efficiency is.

Also, in the case that we are interested by the membrane thickness approach, the synthesis of a symmetric triblock PGlu-PLA-PGlu could probably give us some certitude about the organization of the chains in the membrane. Another idea would be to synthesize a poly(amino acid) using glutamic acid as the first monomer and a hydrophobic amino acid such as isoleucine for the second block. With such a polymer it is possible that the interactions between protein and polymer would increase, allowing for more solubilization.

LIST OF ABBREVIATIONS

CDI: carbodiimidazole
DCC: Dicyclohexylcarbodiimide
DCM: Dichloromethane
DMAP: 4-Dimethylaminopyridine
GIT: gastrointestinal tract
mPEG: poly(ethylene glycol)
MSA: Methane sulfonic acid
NCA: N-carboxyanhydride
NMP: N-MethylPyrolidone
PAA: poly(acrylic acid)
PBD: polybutadiene
PCL: poly(ϵ -caprolactone)
PDMAI: Poly(5-(N,N-dimethylamino)isoprene)
PDMS: poly(dimethylsilane)
PEE: poly(ether ester)
PEG: poly(ethylene glycol)
PEO: poly(ethylene oxide)
PGlu: poly(glutamic acid)
PGluBn: poly(benzyl glutamate)
PLA: poly(lactic acid)
PMOXA: poly(2 methyloxazoline)
PS: poly(styrene)
ROP: ring opening polymerization

EXPERIMENTAL SECTION

Synthesis of PEG-PLA

The lactide was polymerized by ROP using alcohols as initiator, and DMAP as a catalyst. A typical preparation of PEG₄₅-PLA₁₄₀ diblock is described below.

The lactide (25.09 g, 0.1742 mol) and PEG (6.33 g, 0.00316 mol) were mixed in a in a three-necked RBF equipped with gas purging adaptors and a magnetic stir bar. Once the monomer and initiator are placed in the RBF, it is purged 3 times with vacuum and filled with argon, while heating to 135°C. After everything is melted, DMAP (0.7703 g, 0.0063 mol) is added through the third neck to the reaction media. The reaction is held for 35 minutes under argon atmosphere and agitation at 135°C to reach high conversion. When polymerization is complete, the flask is placed in liquid nitrogen and rapidly cooled to stop the reaction. The solid polymer is then dissolved in 250 ml of THF under agitation, and precipitated in a beaker containing 1L of cold ether. The sticky solid is recovered and dried under vacuum at 60°C for 12 hours. Yield 90%. Note that the PLA homopolymer is obtained with the same reaction using a small alcohol instead of mPEG.

Table 11: Synthesis of PEG-PLA.

T°C	t(min)	m PEG (g)	n PEG (mol)	m lactide (g)	n lactide (mol)	m DMAP (g)	n DMAP (mol)
135	40	6.46	0.00323	25.09	0.1742	0.77	0.00630

Synthesis of PGluBn

PGluBn is obtained by ROP of benzyl-glutamate NCA. NCA was purchased from Isochem (France). The NCA (101 g, 0.384 mol) is dissolved at room temperature in 700 ml of N-MethylPyrolidone ([NCA] = 0.143 g/ml) using a 1000 ml RBF, and ring opened by a primary amine, benzylamine (421 μ l, 0.00384 mol). After 3 hours of reaction at 40°C, the reaction mixture is poured in a beaker of 5 volumes (3.5 L) of neutral DI water under agitation. The precipitate is washed over a coarse fritted glass with 2.5 volumes of basic water at pH 10, 2.5 volumes of acidic water at pH 3, 2.5 volumes of neutral water, then a mixture of THF and isopropanol (2:1 v/v) and finally ether. The polymer is dried under vacuum for 12 hours. Yields are about 80%.

Table 12: NCA polymerization.

T	t (min)	m NCA (g)	n NCA (mol)	m benzylamine (g)	n benzylamine (mol)	V NMP (ml)
40	180	101	0.38403042	0.412	0.00383256	700

Deprotection of PGluBn

The PGluBn (29.99 g, 0.1369 mol) is placed in a RBF and dissolved in 300 ml of TriFluoroAcetic acid at room temperature. It is cooled down to 10°C using a cooling water exchanger. Then MSA (300 ml, 4.655 mol) and anisole (74.22 ml, 0.6847 mol) are slowly added to the polymer solution. After 45 minutes of reaction at 10°C, the polymer is precipitated in 5 volumes of ether (3 L), filtered over a coarse fritted glass and thoroughly washed with 5 volumes of ether. The polymer is dried under vacuum for 12 hours at room temperature. The yield of this reaction is 95%.

Table 13: PGluBn deprotection.

T	t (min)	m PGluBn (g)	n PGluBn (mol)	V MSA (ml)	V TFA (ml)	V anisole (ml)
10	45	29.99	0.13694064	300	300	74.7

Coupling

The triblock is obtained by coupling diblock PEG-PLA with PGlu. CarboDilmidazole CDI is used as an activator for COOH groups of PGlu, then the activated carboxylic acids react with the OH-terminated PEG-PLA. PGluOH (15.55 g, 0.001268 mol) is dissolved in 195 ml of NMP and then cooled down to 10°C using a water exchanger. A solution of CDI (0.2057 g, 0.001268 mol) in NMP (5 ml) is added to the PGluOH reaction and left to react for 15 minutes. After 15 minutes, a solution of PEG-PLA (5.116 g, 0.00063 mol) in NMP (50 ml) is added to the PGluOH/CDI solution. The reaction runs for 1 hour at 10°C. The polymer is recovered by precipitation in 5 volumes (1.25 L) of basic water containing 1.1 equivalents of NaOH (5.3 g, 0.1325 mol) per COOH, and the suspension is ultra filtered with another 5 volumes of basic water (at 10⁻⁵ M) to get rid of NMP, CDI, and unreacted PGluOH. Coupling yields range from 50 to 75 %.

Table 14: Coupling reaction.

T	t (min)	m PEG-PLA (g)	n PEG-PLA (mol)	m PGluOH (g)	n PGluOH (mol)	m CDI (g)	n CDI (mol)	V NMP (ml)
10	60	5.19	0.0005157	15.55	0.00126887	0.2079	0.0012821	250

Typical encapsulation experiment

0.025 g of dry human recombinant insulin (Biocon, provided by Bentley pharmaceuticals) are added to 10 ml of a polymer solution at 2% in DI water, pH

9. The pH is adjusted to 9 if needed with NaOH. According to the formulation needed, the solution is sonicated for 5 minutes using a sonication tip, at 100% amplitude, set on a period of 2 seconds ON, 2 seconds OFF. The temperature recorded with a thermocouple is maintained below 37°C with an ice bath. For the Out formulation, no sonication is needed.

BIBLIOGRAPHY

1. T. R. Shantha Kumar, K. Soppimath and Nachaegari, S.K., Novel Delivery Technologies for Protein and Peptide Therapeutics. *Current Pharmaceutical Biotechnology*, **2006**, 7(4), 261-276.
2. Salmaso, S., Bersani, S., Semenzato, A. and Caliceti, P., Nanotechnologies in Protein Delivery. *Journal of Nanoscience and Nanotechnology*, **2006**, 6, 2736-2753.
3. http://en.wikipedia.org/wiki/Gastrointestinal_tract
4. <http://www.colorado.edu/kines/Class/IPHY3430-200/image/villi.jpg>
5. Mustata, G. and Smith, S.M., Approaches to Oral Drug Delivery for Challenging Molecules. *Critical Reviews in Therapeutic Drug Carrier Systems*, **2006**, 23(2), 111-135.
6. Takada, K., Oral Delivery of Hematopoietic Factors: Progress with Gastrointestinal Mucoadhesive Patches, Microdevices, and Other Microfabrication Technologies. *American Journal of Drug Delivery*, **2006**, 4(2), 65-77.
7. Hiroyuki Asada, Douen, T., Waki, M., Adachi, S., Fujita, T., Yamamoto, A. and Muranishi, S., Absorption characteristics of chemically modified-insulin derivatives with various fatty acids in the small and large intestine. *Journal of Pharmaceutical Sciences*, **1995**, 84(6), 682-687.
8. Agarwal, V. and Khan, M.A., Current Status of the Oral Delivery of Insulin. *Pharmaceutical Technology*, **2001**, 25(10), 76-90.
9. Lueen, H.L., de Leeuw, B.J., Perard, D., Lehr, C.-M., de Boer, A.G., Verhoef, J.C. and Junginger, H.E., Mucoadhesive polymers in peroral peptide drug delivery. I. Influence of mucoadhesive excipients on the proteolytic activity of intestinal enzymes. *European Journal of Pharmaceutical Sciences*, **1996**, 4(2), 117-128.

10. Andreas Bernkop-Schnürch and Thaler, S.C., Polycarbophil-cysteine conjugates as platforms for oral polypeptide delivery systems. *Journal of Pharmaceutical Sciences*, **2000**, 89(7), 901-909.
11. Martien, R., Loretz, B. and Schnürch, A.B., Oral gene delivery: Design of polymeric carrier systems shielding toward intestinal enzymatic attack. *Biopolymers*, **2006**, 83(4), 327-336.
12. I. Björk and Lindahl, U., Mechanism of the anticoagulant action of heparin. *Molecular and Cellular Biochemistry*, **1982**, 48(3), 161-182.
13. Dharendra Kumar Malik, Sanjula Baboota, Alka Ahuja, Hasan, S. and Ali, J., Recent Advances in Protein and Peptide Drug Delivery Systems. *Current Drug Delivery*, **2007**, 4(2), 141-151.
14. Wu Z. H., Ping Q. N., Wei Y. and Lai J. M., Hypoglycemic efficacy of chitosan-coated insulin liposomes after oral administration in mice. *Acta Pharmacologica Sinica*, **2004**, 25(7).
15. Varshosaz, J., Pardakhty, A., Hajhashemi, V.I. and Najafabadi, A.R., Development and Physical Characterization of Sorbitan Monoester Niosomes for Insulin Oral Delivery. *Drug Delivery*, **2003**, 10, 251-262.
16. <http://www.who.int/mediacentre/factsheets/fs312/en/index.html>
17. IUBMB Enzyme Nomenclature, <http://www.chem.qmul.ac.uk/iubmb/enzyme/EC3/4/23/1.html>
18. <http://en.wikipedia.org/wiki/Insulin>
19. Stephan Förster and Plantenberg, T., From Self-Organizing Polymers to Nanohybrid and Biomaterials. *Angewandte Chemie International Edition*, **2002**, 41(5), 688-714.
20. Discher, D.E. and Ahmed, F., Polymersomes. *Annual Review of Biomedical Engineering*, **2006**, 8(1), 323-341.
21. Discher, D.E. and Eisenberg, A., Polymer Vesicles. *Science*, **2002**, 297(5583), 967-973.
22. Luo, L. and Eisenberg, A., Thermodynamic Size Control of Block Copolymer Vesicles in Solution. *Langmuir*, **2001**, 17(22), 6804-6811.

23. Patrick Lim Soo and Eisenberg, A., Preparation of block copolymer vesicles in solution. *Journal of Polymer Science Part B: Polymer Physics*, **2004**, 42(6), 923-938.
24. Dennis. E. Discher and Ahmed, F., Controlled Release Polymersomes, US 2005/0003016 A1, Jan. 6, 2005, **2005**.
25. Ahmed, F. and Discher, D.E., Self-porating polymersomes of PEG-PLA and PEG-PCL: hydrolysis-triggered controlled release vesicles. *Journal of Controlled Release*, **2004**, 96(1), 37-53.
26. Min-Hyo Seo and In-Ja-Choi, Polymeric composition for solubilizing poorly water soluble drugs and process for the preparation thereof, US 6616941 B1, Sep. 9, 2003, **2003**.
27. Ghoroghchian, P.P., Li, G., Levine, D.H., Davis, K.P., Bates, F.S., Hammer, D.A. and Therien, M.J., Bioresorbable Vesicles Formed through Spontaneous Self-Assembly of Amphiphilic Poly(ethylene oxide)-*block*-polycaprolactone. *Macromolecules*, **2006**, 39(5), 1673-1675.
28. Bhalchandra Shripad Lele and Leroux, J.C., Amphiphilic Diblock, Triblock and Star-Block Copolymers and their Pharmaceutical Compositions, US 2003/0181613 A1, Sep. 25, 2003, **2003**.
29. Najafi, F. and Sarbolouki, M.N., Biodegradable micelles/polymersomes from fumaric/sebacic acids and poly(ethylene glycol). *Biomaterials*, **2003**, 24(7), 1175-1182.
30. Yakai Feng, Doris Klee and Höcker, H., Biodegradable block copolymers with poly(ethylene oxide) and poly(glycolic acid-valine) blocks. *Journal of Applied Polymer Science*, **2002**, 86(11), 2916-2919.
31. Arimura, H., Ohya, Y. and Ouchi, T., Formation of Core-Shell Type Biodegradable Polymeric Micelles from Amphiphilic Poly(aspartic acid)-*block*-Polylactide Diblock Copolymer. *Biomacromolecules*, **2005**, 6(2), 720-725.
32. Chécot, F., Lecommandoux, S., Klok, H.A. and Gnanou, Y., From supramolecular polymersomes to stimuli-responsive nano-capsules based on poly(diene-b-peptide) diblock copolymers. *The European Physical Journal E - Soft Matter*, **2003**, 10(1), 25-35.

33. Lecommandoux, S., Achard, M.F., Langenwaller, J.F. and Klok, H.A., Self-Assembly of Rod-Coil Diblock Oligomers Based on α -Helical Peptides. *Macromolecules*, **2001**, 34(26), 9100-9111.
34. Jeong, Y.I., Sun, H.S., Shim, Y.H., Kim, C., Park, S.H., Choi, K.C. and Cho, C.S., Nifedipine encapsulated core-shell type nanoparticles based on poly(γ -benzyl L-glutamate)poly(ethylene glycol) diblock copolymers. *Journal of Microencapsulation*, **2004**, 21, 445-453.
35. Tatsuro Ouchi, Miyazaki, H., Arimura, H., Tasaka, F., Hamada, A. and Ohya, Y., Synthesis of biodegradable amphiphilic AB-type diblock copolymers of lactide and depsipeptide with pendant reactive groups. *Journal of Polymer Science Part A: Polymer Chemistry*, **2002**, 40(9), 1218-1225.
36. Tatsuro Ouchi, Miyazaki, H., Arimura, H., Tasaka, F., Hamada, A. and Ohya, Y., Formation of polymeric micelles with amino surfaces from amphiphilic AB-type diblock copolymers composed of poly(glycolic acid lysine) segments and polylactide segments. *Journal of Polymer Science Part A: Polymer Chemistry*, **2002**, 40(10), 1426-1432.
37. Floudas, G., Papadopoulos, P., Klok, H.A., Vandermeulen, G.W.M. and Rodriguez-Hernandez, J., Hierarchical Self-Assembly of Poly(γ -benzyl-L-glutamate)-Poly(ethylene glycol)-Poly(γ -benzyl-L-glutamate) Rod-Coil-Rod Triblock Copolymers. *Macromolecules*, **2003**, 36(10), 3673-3683.
38. Nardin, C., Hirt, T., Leukel, J. and Meier, W., Polymerized ABA Triblock Copolymer Vesicles. *Langmuir*, **2000**, 16(3), 1035-1041.
39. Stoenescu, R. and Meier, W., Asymmetric Membranes from Amphiphilic ABC Triblock Copolymers. *Molecular Crystals and Liquid Crystals*, **2004**, 417(1), 185 - 191.
40. Bieringer, R., Abetz, V. and Müller, A.H.E., Triblock copolyampholytes from 5-(N,N-dimethylamino)isoprene, styrene, and methacrylic acid: Synthesis and solution properties. *The European Physical Journal E - Soft Matter*, **2001**, 5(1), 5-12.
41. Collette, F., Supramolecular Engineering of Vesicles via Self-Assembly: Application to Drug Delivery, Master's Thesis in Chemistry, **2005**, University of New Hampshire, p. 1-159.
42. Kricheldorf, H.R., Berl, M. and Scharnagl, N., Poly(lactones). 9. Polymerization mechanism of metal alkoxide initiated polymerizations of lactide and various lactones. *Macromolecules*, **1988**, 21(2), 286-293.

43. Dubois, P., Jacobs, C., Jerome, R. and Teyssie, P., Macromolecular engineering of polylactones and polylactides. 4. Mechanism and kinetics of lactide homopolymerization by aluminum isopropoxide. *Macromolecules*, **1991**, 24(9), 2266-2270.
44. Nederberg, F., Connor, E.F., Möller, M., Glauser, T. and Hedrick, J.L., New Paradigms for Organic Catalysts: The First Organocatalytic Living Polymerization. *Angewandte Chemie International Edition*, **2001**, 40(14), 2712-2715.
45. Hao Feng and Dong, C.-M., Preparation and characterization of chitosan-graft-poly(ϵ -caprolactone) with an organic catalyst. *Journal of Polymer Science Part A: Polymer Chemistry*, **2006**, 44(18), 5353-5361.
46. Thomas Trimaille, Möller, M. and Gurny, R., Synthesis and ring-opening polymerization of new monoalkyl-substituted lactides. *Journal of Polymer Science Part A: Polymer Chemistry*, **2004**, 42(17), 4379-4391.
47. Collette, F., Supramolecular Engineering of Vesicles via Self-Assembly: Application to Drug Delivery, Master's Thesis in Chemistry, **2005**, University of New Hampshire, p. 66.
48. Shibasaki, Y., Sanada, H., Yokoi, M., Sanda, F. and Endo, T., Activated Monomer Cationic Polymerization of Lactones and the Application to Well-Defined Block Copolymer Synthesis with Seven-Membered Cyclic Carbonate. *Macromolecules*, **2000**, 33(12), 4316-4320.
49. Kim Moon, S., Seo Kwang, S., Khang, G., Cho Sun, H. and Lee Hai, B., Preparation of poly(ethylene glycol)-block-poly(caprolactone) copolymers and their applications as thermo-sensitive materials. *J Biomed Mater Res A*, **2004**, 70(1), 154-158.
50. Mingxiao Deng, Chen, X., Piao, L., Zhang, X., Dai, Z. and Jing, X., Synthesis of four-armed poly(ϵ -caprolactone)-block-poly(ethylene oxide) by diethylzinc catalyst. *Journal of Polymer Science Part A: Polymer Chemistry*, **2004**, 42(4), 950-959.
51. Changyong Choi, Chae, S.Y., Kim, T.-H., Kweon, J.K., Cho, C.S., Jang, M.-K. and Nah, J.-W., Synthesis and physicochemical characterization of amphiphilic block copolymer self-aggregates formed by poly(ethylene glycol)-block-poly(ϵ -caprolactone). *Journal of Applied Polymer Science*, **2006**, 99(6), 3520-3527.

52. Storey, R.F. and Sherman, J.W., Kinetics and Mechanism of the Stannous Octoate-Catalyzed Bulk Polymerization of ϵ -Caprolactone. *Macromolecules*, **2002**, 35(5), 1504-1512.
53. Dubois, P., Ropson, N., Jerome, R. and Teyssie, P., Macromolecular Engineering of Polylactones and Polylactides. 19. Kinetics of Ring-Opening Polymerization of ϵ -Caprolactone Initiated with Functional Aluminum Alkoxides. *Macromolecules*, **1996**, 29(6), 1965-1975.
54. Chen, C.T., Huang, C.A. and Huang, B.H., Aluminum Complexes Supported by Tridentate Aminophenoxide Ligand as Efficient Catalysts for Ring-Opening Polymerization of ϵ -Caprolactone. *Macromolecules*, **2004**, 37(21), 7968-7973.
55. Huang, C.H., Wang, F.C., Ko, B.T., Yu, T.L. and Lin, C.C., Ring-Opening Polymerization of ϵ -Caprolactone and L-Lactide Using Aluminum Thiolates as Initiator. *Macromolecules*, **2001**, 34(3), 356-361.
56. W. E. Hanby, S. G. Waley and Watson, J., Synthetic polypeptides. Part II. Polyglutamic acid. *Journal of the Chemical Society*, **1950**, 3239.
57. Collette, F., Supramolecular Engineering of Vesicles via Self-Assembly: Application to Drug Delivery, Master's Thesis in Chemistry, **2005**, University of New Hampshire, p. 68-77.
58. Kato, Y., Umemoto, N., Kayama, Y., Fukushima, H., Takeda, Y., Hara, T. and Tsukada, Y., A novel method of conjugation of daunomycin with antibody with a poly(L-glutamic acid) derivative as intermediate drug carrier. An anti- α -fetoprotein antibody-daunomycin conjugate. *J. Med. Chem.*, **1984**, 27(12), 1602-1607.
59. Roset, A., Nanoparticles for the Oral Delivery of Therapeutic Proteins. Internship report, University of New Hampshire, **2006**, 15-19.
60. Staab, H.A., New Methods of Preparative Organic Chemistry IV. Syntheses Using Heterocyclic Amides (Azolides). *Angewandte Chemie International Edition*, **1962**, 1(7), 351-367.
61. Heinz A. Staab, Martin Lüking and Dürr, F.H., Darstellung von Imidazoliden. Synthese von Amidinen, Hydraziden und Hydroxamsäuren nach der Imidazolidmethode. *Chemische Berichte*, **1962**, 95(5), 1275-1283.

62. Michael Gotsche, Helmut Keul and Höcker, H., Amino-terminated poly(L-lactide)s as initiators for the polymerization of N-carboxyanhydrides: synthesis of poly(L-lactide)-block-poly(α -amino acid)s. *Macromolecular Chemistry and Physics*, **1995**, 196(12), 3891-3903.
63. Xiongwei Yan, Kieran Curley and Lawrence, D.S., The specificity of the protein kinase C α , β II and γ isoforms as assessed by an unnatural alcohol-appended peptide library. *Biochemical Journal*, **2000**, 349, 709-715.
64. Honda, T., Miyazaki, M., Nakamura, H. and Maeda, H., Controllable polymerization of N-carboxy anhydrides in a microreaction system. *Lab on a Chip*, **2005**, 5(8), 812-818.
65. Saez, A., Guzman, M., Molpeceres, J. and Aberturas, M.R., Freeze-drying of polycaprolactone and poly(-lactic-glycolic) nanoparticles induce minor particle size changes affecting the oral pharmacokinetics of loaded drugs. *European Journal of Pharmaceutics and Biopharmaceutics*, **2000**, 50(3), 379-387.
66. Roset, A., Nanoparticles for the Oral Delivery of Therapeutic Proteins. Internship report, University of New Hampshire, **2006**, 24-28.
67. David J. Chittleborough, Soheyl Tadjiki, James F. Ranville, Finlay Shanks and Beckett, R., *Soil colloid analysis by Flow Field-Flow Fractionation*, in *SuperSoil 2004: 3rd Australian New Zealand Soils Conference*. 2004: University of Sydney, Australia.
68. Shen, H. and Eisenberg, A., Morphological Phase Diagram for a Ternary System of Block Copolymer PS₃₁₀-b-PAA₅₂/Dioxane/H₂O. *J. Phys. Chem. B*, **1999**, 103(44), 9473-9487.
69. Zhong-can, O.-Y. and Helfrich, W., Instability and Deformation of a Spherical Vesicle by Pressure. *Physical Review Letters*, **1987**, 59(21), 2486.
70. Tothova, J., Richterova, M. and Lisy, V., On two direct methods for measurement of interfacial tension at microdroplet surfaces. *ArXiv Condensed Matter e-prints*, **2004**, nov.
71. Goetz, R., Gompper, G. and Lipowsky, R., Mobility and Elasticity of Self-Assembled Membranes. *Physical Review Letters*, **1999**, 82(1), 221.
72. Almut Mecke, Christian Dittrich and Meier, W., Biomimetic membranes designed from amphiphilic block copolymers. *Soft Matter*, **2006**, 2, 751-759.

73. Jung, H.T., Lee, S.Y., Kaler, E.W., Coldren, B. and Zasadzinski, J.A., Gaussian curvature and the equilibrium among bilayer cylinders, spheres, and discs. *PNAS*, **2002**, 99(24), 15318-15322.
74. Bermudez, H., Brannan, A.K., Hammer, D.A., Bates, F.S. and Discher, D.E., Molecular Weight Dependence of Polymersome Membrane Structure, Elasticity, and Stability. *Macromolecules*, **2002**, 35(21), 8203-8208.
75. Katarzyna Kita-Tokarczyk, Julie Grumelard, Thomas Haefele and Meier, W., Block copolymer vesicles—using concepts from polymer chemistry to mimic biomembranes. *Polymer*, **2005**, 46(11), 3540-3563.
76. John M. Finke, Jennings, P.A., Lee, J.C., Onuchic, J.N. and Winkler, J.R., Equilibrium unfolding of the poly(glutamic acid)₂₀ helix. *Biopolymers*, **2007**, 86(3), 193-211.
77. Sauer, M. and Meier, W., Responsive nanocapsules. *Chemical Communications*, **2001**, (1), 55-56.
78. Wolfgang Meier, Corinne Nardin and Winterhalter, M., Reconstitution of Channel Proteins in (Polymerized) ABA Triblock Copolymer Membranes. *Angewandte Chemie International Edition*, **2000**, 39(24), 4599-4602.
79. Pata, V. and Dan, N., The Effect of Chain Length on Protein Solubilization in Polymer-Based Vesicles (Polymersomes). *Biophys. J.*, **2003**, 85(4), 2111-2118.
80. Silva, M.E. and Dietrich, C.P., Structure of Heparin. *The Journal of Biological Chemistry*, **1975**, 250(17), 6841-6846.
81. <http://www.people.vcu.edu/~urdesai/hep.htm>
82. <http://www.chemistry.wustl.edu/~edudev/LabTutorials/Carboxypeptidase/carboxypeptidase.html>
83. Deepti Jain, Amulya K. Panda and Majumdar, D.K., Eudragit S100 Entrapped Insulin Microspheres for Oral Delivery. *AAPS PharmSciTech.*, **2005**, 6(1), E100-E107.
84. http://en.wikipedia.org/wiki/Route_of_administration
85. <http://www.fda.gov/cder/dsm/DRG/drg00301.htm>

86. Rocca, J.G. and Park, K., Oral Drug Delivery: Prospects & Challenges. *Drug Delivery Technology*, **2004**, 4(4).
87. <http://en.wikipedia.org/wiki/Biodegradable>
88. Dorland, W.A.N., *Dorland's illustrated medical dictionary*. Saunders: Philadelphia, **2003**.
89. John C. Middleton and Tipton, A.J., Synthetic Biodegradable Polymers as Medical Devices. *Medical Plastics and Biomaterials*, **1998**, 5(2), 30-39.
90. Kang Moo Huh, Yong Woo Cho and Park, K., PLGA-PEG Block Copolymers for Drug Formulations. *Drug Delivery Technology*, **2003**, 3(5).
91. Pitt, G.G., Gratzl, M.M., Kimmel, G.L., Surles, J. and Sohindler, A., Aliphatic polyesters II. The degradation of poly (DL-lactide), poly (ϵ -caprolactone), and their copolymers in vivo. *Biomaterials*, **1981**, 2(4), 215-220.
92. Geng, Y. and Discher, D.E., Hydrolytic Degradation of Poly(ethylene oxide)-*block*-Polycaprolactone Worm Micelles. *J. Am. Chem. Soc.*, **2005**, 127(37), 12780-12781.

APPENDICES

APPENDIX A: ADMINISTRATION ROUTES

In drug delivery, the route of administration of a drug/protein defines the path by which a drug/protein is brought to contact with the human body. The transport of the drug from the site of entry to the targeted part of the body where its action is needed is far from being trivial. The pharmacokinetics of a particular drug (its uptake process, distribution and elimination) are hugely influenced by the route of administration. The FDA^{84, 85} broadly classifies routes of administration into:

- Topical: local effect, substance is applied directly where its action is desired,
- Enteral: desired effect is systemic (non-local), substance is given via the digestive tract,
- Parenteral: desired effect is systemic, substance is given by other routes than the digestive tract.

Sometimes it might be advantageous to use the body's own transport mechanism, but not all drugs and proteins can be delivered this way. For instance, a wide range of proteins are used in therapies, mainly as parenteral drugs (i. e. route of administration is done by injection, infusion or implantation). In most cases, the controlled delivery of the active principle is highly desirable. The goals of such a technology are diverse:

- Increase the duration of the effect of the drug by maintaining its concentration over the minimal effective concentration,
- Diminishing the toxicity of the product by reducing the amplitude of the concentration peak.

Provided by such a motivation, the search for drug delivery technologies throughout the last decades has significantly increased.

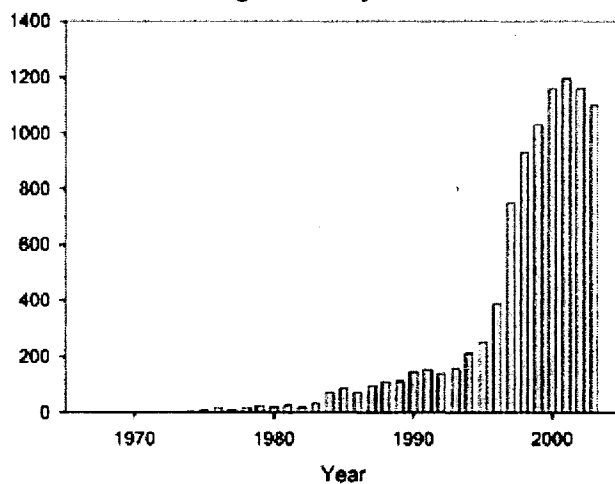


Figure 91: Number of publications on controlled drug delivery published since 1970.⁸⁶

Nowadays, controlled drug delivery of drugs can be done in many different ways, involving a variety of technologies targeting various parts of the body. Among these technologies, the use of synthetic polymers as drug carriers is

developing fast. The polymer carrier is combined with the drug, the predominant techniques being:

- Drug covalently attached to the polymer,
- Association of the drug with the polymer (adsorption or encapsulation).

The first technique is quite complicated, since it requires a full study of toxicity on the modified drug. In both approaches, the polymeric carriers must be biocompatible, eliminated, able to protect the load from enzymes, able to carry and deliver a significant amount of the drug to the target.

The biocompatible polymers used can be either biodegradable or inert and easily eliminated/excreted by the human body. Today the research in this area is focusing on biodegradable systems, trying to take advantage of some of the natural reactions and byproducts occurring while degrading.

These systems, usually small particles, are administered by subcutaneous injections or oral uptake.

The commercial interest in oral drug/protein delivery systems is real, since the most desirable administration form is by oral dosage: it allies ease of administration, patient compliance and low cost compared to other techniques such as transdermal delivery, pulmonary delivery, parenteral and mucosal delivery.

If oral delivery of drug and proteins is obviously the most convenient way of drug administration, it is unexpected to see that among the advances made over the last decades, few of them were made in this particular area. One of the reasons is the result of the limitations imposed by the transportation of the protein through the gastrointestinal tract (GIT).

APPENDIX B: BIODEGRADABLE POLYMERS

A plastic is considered as biodegradable if it can be broken down by living organisms.⁸⁷ Since our vesicles are designed to be drug carriers in the human body, not only they need to be biodegradable, but they must be biocompatible. The definition of biocompatibility is the quality of not having toxic or injurious effects on biological systems, such as the human body.⁸⁸

Our polymeric vesicles must be biodegradable and biocompatible: both the initial polymer chains and their degradation products must be biocompatible. There is a diversity of products available as medical plastics or biomaterials. They have different characteristics, such as mechanical properties or degradation time. Table 15 gives some characteristics of common biodegradable polymers.⁸⁹ Note that the degradation times reported are those of polymer chunks.

Table B15: Properties of common biodegradable polymers.

Polymer	Melting Point (°C)	Glass-Transition Temp (°C)	Modulus (Gpa) ^a	Degradation Time (months) ^b
PGA	225—230	35—40	7.0	6 to 12
LPLA	173—178	60—65	2.7	>24
DLPLA	Amorphous	55—60	1.9	12 to 16
PCL	58—63	(—65)— (—60)	0.4	>24
PDO	N/A	(—10)—0	1.5	6 to 12
PGA-TMC	N/A	N/A	2.4	6 to 12
85/15 DLPLG	Amorphous	50—55	2.0	5 to 6
75/25 DLPLG	Amorphous	50—55	2.0	4 to 5
65/35 DLPLG	Amorphous	45—50	2.0	3 to 4
50/50 DLPLG	Amorphous	45—50	2.0	1 to 2
A Tensile or flexural modulus.				
b Time to complete mass loss. Rate also depends on part geometry.				

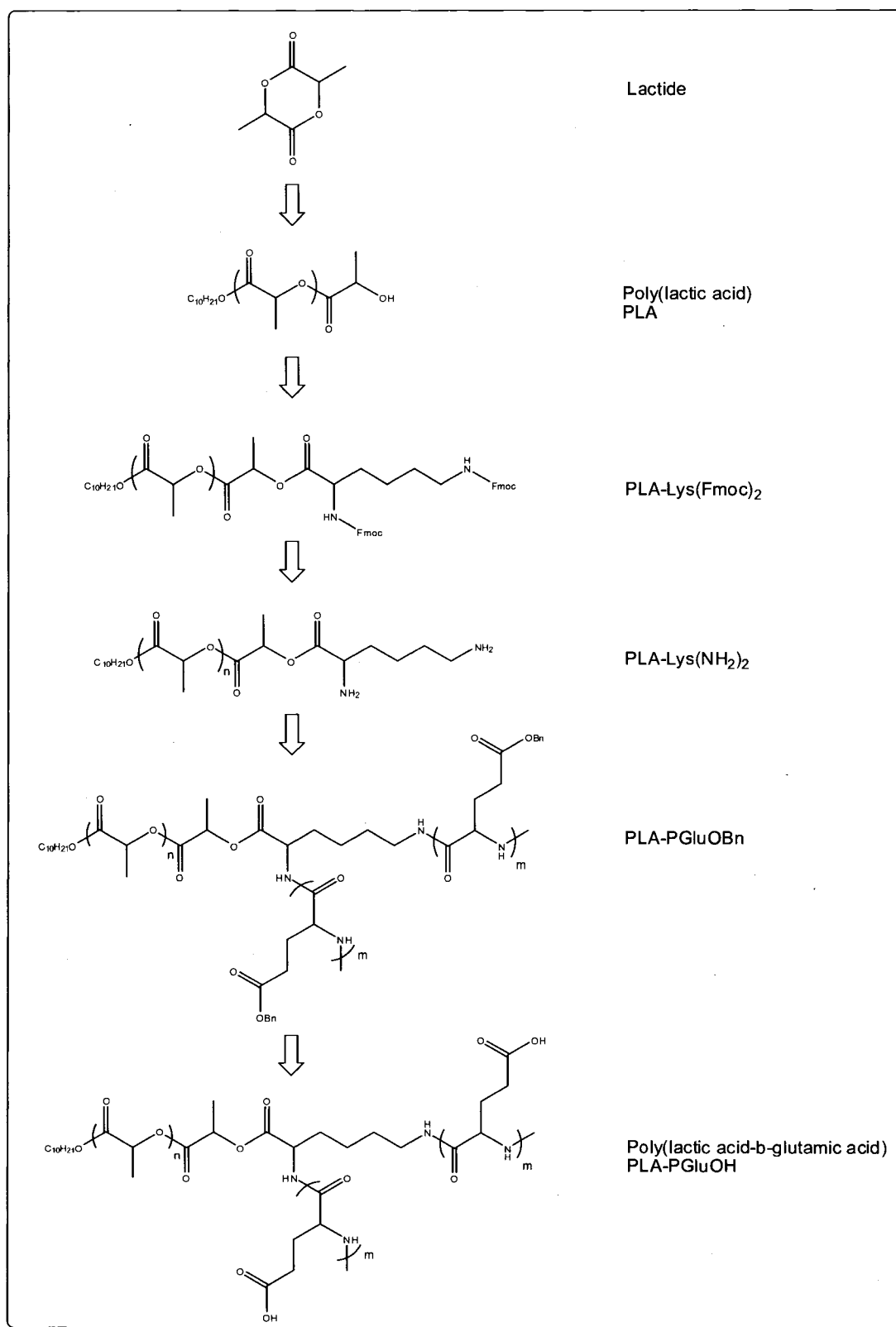
Poly(ethylene glycol), poly(lactic acid), poly(glycolic acid), poly(lactic acid-co-glycolic acid) and poly(ϵ -caprolactone) are common biomaterials. Low molecular weight PEGs (smaller than 10000 g/mol) are easily excreted by urine.⁹⁰

Biodegradation of the polyester polymers in vivo proceeds in two phases. First, water penetrates the bulk polymer and causes non-enzymatic random hydrolytic ester cleavage.⁹¹ Then eventually, the resulting water soluble fragments are metabolized and broken down into smaller molecules.⁸⁹ In the end, PLA is degraded in lactic acid in acidic pH water. PCL is predominantly degraded in 6-hydroxycaproic acid (6-HPA).⁹² PLA, PGA and PCL have different rates of degradation. Poly(D,L-LA) degrades faster.

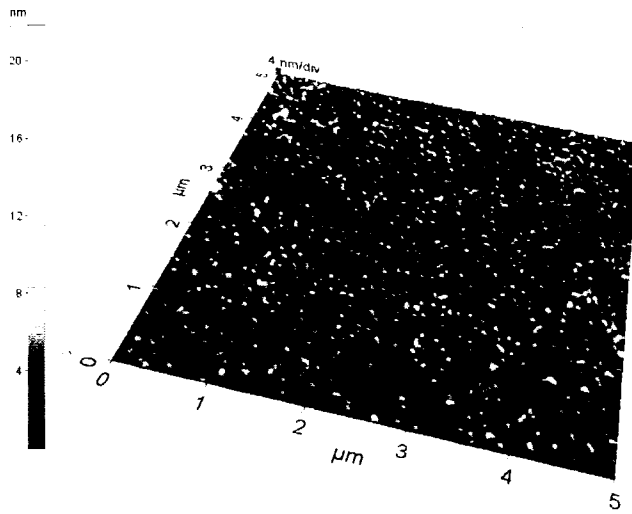
Several factors accelerate the degradation of polyesters. The more hydrophilic the backbone is, and the less crystalline the polymer is, the higher the degradation rate. Due to high crystallinity polycaprolactone and degrades slowly compared to PLA. The crystallinity reduces the accessibility of small molecules to ester linkages in PCL.⁹¹ In poly(D, L-lactide), the random distribution of isomeric forms prevents any long range organization and is yielding an amorphous polymer. Though glycolic acid yields a highly crystalline polymer, it degrades faster than PLA and PCL because PGA is the simplest polyester, with the most hydrophilic backbone. It is widely used as a co-monomer to tune the degradability of polyesters: since the lactic acid monomer disrupts the crystallinity of PGA,⁸⁹ their copolymers degrade even faster than the homopolymers.

Poly(glutamic acid) is a polypeptide. As a polyaminoacid, the peptide bonds of its backbone are degraded by proteases in the gastrointestinal tract yielding glutamic acid. These polymers are safe as long as their backbone contains a maximum of two different amino acids. Otherwise they can be assimilated as a protein by the immune system.

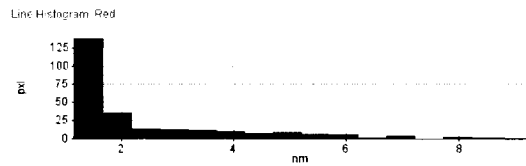
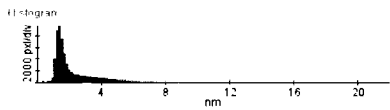
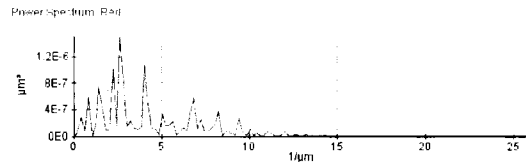
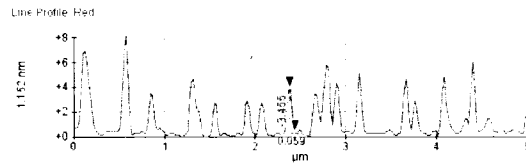
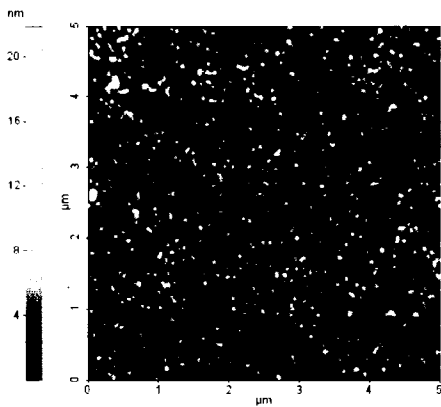
APPENDIX C: SYNTHESIS PATHWAY USING MACROAMINE



APPENDICE D: AFM IMAGING - TRIBLOCK AT PH 10



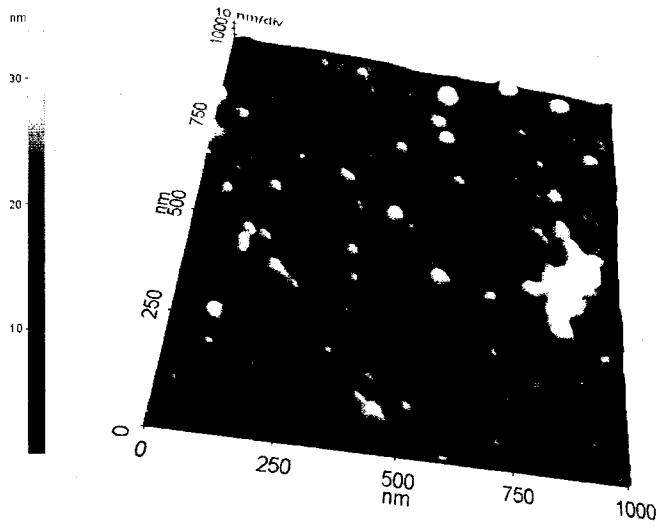
File Name G70221- hy008 copy.tif
 Head Mode HC-AFM
 Source Topography
 Data Width 256 (px)
 Data Height 256 (px)
 X Scan Size 5 (μm)
 Y Scan Size 5 (μm)
 Scan Rate 1 (Hz)
 Set Point -1.88 (μm)
 Data Gain -143.95E-6 (μm/step)



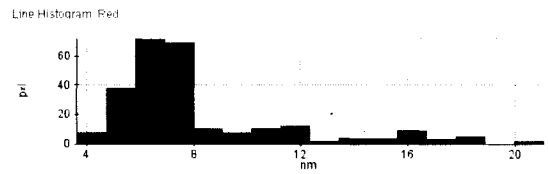
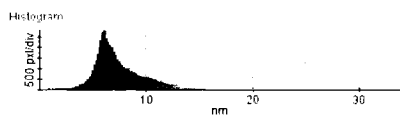
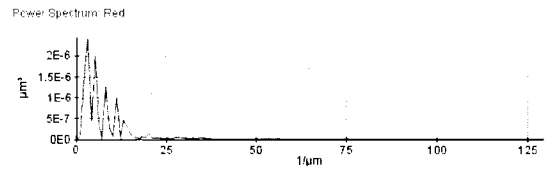
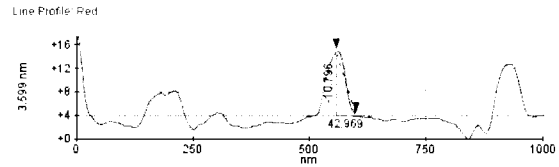
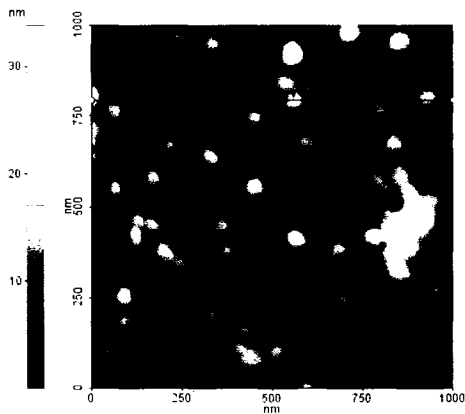
Statistics

Line	Min(nm)	Max(nm)	Mid(nm)	Mean(nm)	Rov(nm)	Rq(nm)	Ra(nm)	Rz(nm)	Rsk(μm)	Rku(μm)
Red	1.152	9.213	5.182	2.421	8.061	1.595	1.224	4.457	-258.489	827.082

APPENDICE E: AFM IMAGING – TRIBLOCK AT PH 10



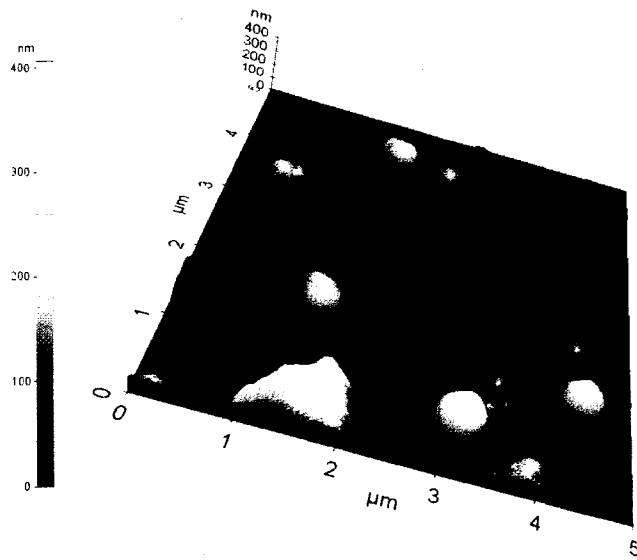
File Name 670221...hy016 copy.tif
 Head Mode NC-AFM
 Source Topography
 Data Width 256 (pxl)
 Data Height 256 (pxl)
 X Scan Size 1 (um)
 Y Scan Size 1 (um)
 Scan Rate 1 (Hz)
 Set Point -0.8 (um)
 Data Gain -143.95E-6 (um/step)



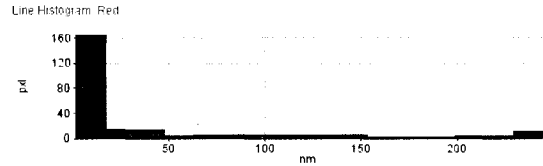
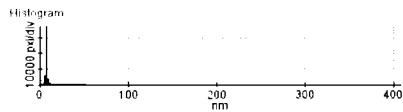
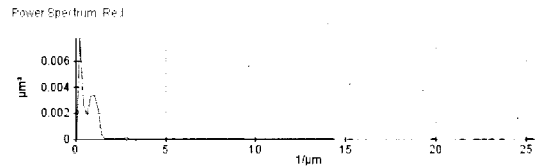
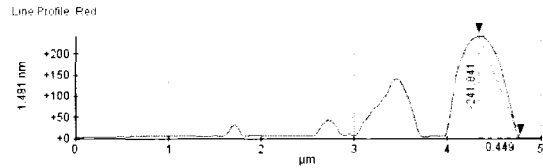
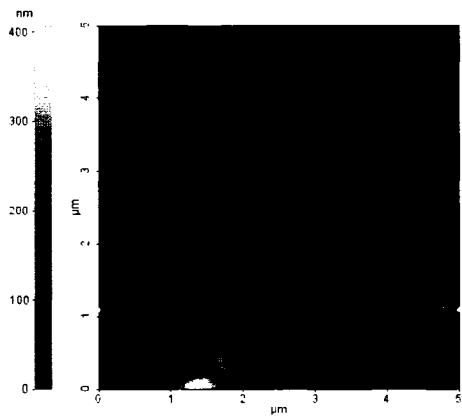
Statistics

Line	Min(nm)	Max(nm)	Mid(nm)	Mean(nm)	Rpy(nm)	Rq(nm)	Ra(nm)	Rz(nm)	Rsk(um)	Rku(um)
Red	3.599	21.017	12.308	8.139	17.418	3.400	2.493	7.128	-253.730	789.792

APPENDICE F: AFM IMAGING - TRIBLOCK AT PH 3



File Name 070222-hy014 copy.tif
 Head Mode NC-AFM
 Source Topography
 Data Width 256 (px)
 Data Height 256 (px)
 X Scan Size 5 (μm)
 Y Scan Size 5 (μm)
 Scan Rate 1 (Hz)
 Set Point -0.95 (μm)
 Data Gain -24.242E-6 (μm/step)



Statistics

Line	Min(nm)	Max(nm)	Mid(nm)	Mean(nm)	Rpv(nm)	Rq(nm)	Ra(nm)	Rz(nm)	Rsk(μm)	Rku(μm)
Red	1.481	243.332	122.407	43.124	241.851	66.371	49.656	157.809	-44.965	126.115